

# Influence of Anesthetics on the Nerve Membrane and the Nerve Pulse.

Kaare Græsbøll

December 19, 2008

# Contents

<b>Teaser</b>	<b>1</b>
<b>Abstract</b>	<b>1</b>
<b>Acknowledgements</b>	<b>2</b>
<b>Abbreviations</b>	<b>3</b>
<b>1 Introduction</b>	<b>4</b>
1.1 Anesthetic Action . . . . .	5
1.2 Nerves . . . . .	7
1.3 The Nerve Signal . . . . .	8
1.4 Simulating the Membrane . . . . .	10
<b>2 Theory</b>	<b>11</b>
2.1 Membrane properties . . . . .	12
2.1.1 Melting point depression . . . . .	14
2.1.2 Partition coefficient . . . . .	15
2.1.3 Pressure reversal . . . . .	17
2.1.4 The Meyer-Overton Relation . . . . .	18
2.2 The Hodgkin-Huxley model . . . . .	19
2.3 The Soliton Model . . . . .	22
2.3.1 The analytical solution . . . . .	23
2.3.2 A little soliton history . . . . .	25
2.4 Computer Simulations . . . . .	28
2.4.1 Monte Carlo Simulations . . . . .	29
2.4.2 Static grid Ising model . . . . .	32
2.4.3 The Bastard model . . . . .	35
<b>Interlude</b>	<b>42</b>
<b>3 Methods and Materials</b>	<b>43</b>
3.1 Differential Scanning Calorimetry . . . . .	44
3.1.1 DPPC vesicles . . . . .	44
3.1.2 Anesthetics . . . . .	46

3.1.3	Pressure cell	49
3.2	Photo-spectrometry	50
3.3	Simulations	51
3.4	Data processing	51
3.5	Visualization	52
<b>4</b>	<b>Results</b>	<b>53</b>
4.1	Calorimetry Data	54
4.1.1	DPPC	55
4.1.2	Anesthetics	57
4.1.3	Pressure	63
4.2	Simulation Data	66
4.2.1	Static grid Ising-model	66
4.2.2	Bastard results	70
4.3	Solitons	76
<b>5</b>	<b>Résumé, Discussion, and Conclusion</b>	<b>82</b>
5.1	Résumé	82
5.2	Discussion	82
5.3	Conclusion	88
<b>Bibliography</b>		<b>i</b>
<b>A</b>	<b>Appendix</b>	<b>vii</b>
A.1	Compressibility	viii
A.2	Spectrophotometry	x
A.3	Pressurized anesthetics	xi
A.3.1	Bupivacaine	xi
A.3.2	Lidocaine	xii
A.3.3	Pentobarbital	xiii
A.4	Symmetry of simulated phase transitions	xiv
A.5	Solitons of anesthetics	xv
A.5.1	Lidocaine	xv
A.5.2	Bupivacaine	xvi
A.5.3	Propofol	xviii
A.5.4	Pentobarbital	xix
<b>The End</b>		<b>xxi</b>

# Teaser

*If you are having your car fixed, you will expect the mechanic to know how your car functions in order to repair it. If you go through surgery, you would expect your surgeon to know how your body functions and the anesthesiologist to know how the anesthesia influence your nerve system. The latter, however, is not the case! While the auto mechanic knows every bolt and the surgeon every vein, the anesthesiologist cannot give you a definite answer. Why? - Science simply has not provided one yet.*

*This thesis investigates the properties of nerves under the influence of anesthetics, recaps theories of nerves and anesthetics, and tries to create a new simulation method to test it all.*

## Abstract

This master thesis investigates the heat capacity, the shift in melting point, the pressure relation, and compressibility of DPPC membranes under influence of anesthetics. The results are applied onto a new theory of nerves proposed by Heimburg and Jackson (2005) [1]. From this density waves in lipid membranes are shown theoretically possible. The Hodgkin-Huxley theory of nerves is also discussed within this context. And the experimental setup is proposed as method to determine partition coefficients of anesthetics into membranes.

Furthermore a new coarse-grain simulation model is developed to lay the foundation for better understanding key properties of membranes in the phase transition and influence of anesthetics herein. But more time must be invested to establish the parameters governing this computational model.

# Acknowledgements

First of all I would like to thank Heiko Seeger for a thorough introduction to the laboratory and good lab practice, and for always being ready to answer my questions. In the same spirit, I appreciate the assistance of Martin Gudmand who always had good advice particularly on cleaning standards. Also a big 'thank you' to the computer supervisor at NBI - Björn Nilsson. I would like to thank everybody from the Bio Membrane group at NBI for their interest and good discussions especially Andreas Blicher. I thank Andrew D. Jackson for advise on the numerical solution of solitons and how to give talks. And last, but most importantly, I would like to thank my supervisor -Thomas Heimburg- for supporting my ideas, no matter how crazy, and for always being ready to take the time for scientific as well as personal problems.

Thank you all!

*I dedicate this thesis to Von dü and Sandra  
- for jump starting my enthusiasm.  
With love to my family - who always believed in me.*

# Abbreviations

DPPC	di-palmitoyl-phosphatidyl-choline
DSC	Differential Scanning Calorimeter
EDTA	ethylene-diamine-tetra-acetic acid
GA	Glauber Algorithm
HE	Half Enthalpy
Hepes	4-(2-hydroxy-ethyl)-1-piperazine-ethane-sulfonic acid
HHM	Hodgkin-Huxley Model
HWHH	Half Width at Half Height
KdV	Korteweg-de Vries
LD	Liquid-Disordered
MA	Metropolis Algorithm
MCC	Monte Carlo Cycle
MCCT	Monte Carlo Cycles per Temperature-step
MCS	Monte Carlo Simulations
MDS	Molecular Dynamics Simulations
PT	Phase Transition
SM	Soliton Model
SO	Solid-Ordered
UPB	Upper Phase Boundary
UV/VIS	Ultra Violet / VISual

References in this thesis will often be done only by [placement in bibliography] and occasionally by main author(s). It is acknowledged that some references have many authors, who by this method is foregone their glory of being mentioned in this thesis. But it is of the opinion of the author of this thesis, that a full reference within the thesis text disturbs the read.

# Chapter 1

## Introduction

The use of anesthetics can be traced as far back as ancient Egypt and the old Chinese Dynasties, where lotus flowers, opium plant or cannabis were used. Up through history new types of drugs have been developed to improve strength, control, and fatality rate. Modern use of anesthetics is sophisticated to a degree that implies a deep understanding of the action of these medicaments – This is, however, not all true. Physicians may know a lot about when to use what in which doses, but little is known about the actual microscopic effects of the anesthetics – though much is speculated. The lack off a satisfactory model on anesthesia should be taken as a clue that the predominant model of nerve function, which is the scheme wherein anesthetics work, should be revised.

The incapability of the traditional nerve model to explain the action of anesthetics in a satisfactory way, and along with other contradictory findings, led Heimburg and Jackson [1] to suggest a new model for nerves in spring 2005. Their model is based on thermodynamical properties of the nerve membrane and assumes an adiabatic wave in the cell membrane – a soliton – to be the carrier of the nerve signal. The soliton is *a priori* dependent of the physical properties of the cell membrane in particular the sound speed and density. Mengel and Christiansen [2] have shown that anesthetics change properties of the cell membrane that will effect creation of solitons. It seems that the soliton model will easily incorporate the effects of anesthetics. If so the Heimburg-Jackson model will have to be accepted as a candidate for a new model on nerves.

The intend of this master thesis is to elaborate on the advantages of the Soliton model.

*Let's get this thesis going on...*

## 1.1 Anesthetic Action



Figure 1.1: Anesthetics are a very diverse group. (Left picture) Various inhalation anesthetics. (Right picture) Intravenous anesthetics. (Bottom picture) Atomic building blocks. By Urban [3].

Figure 1.1 displays a small collection of molecules. They vary from single atom to complex molecules, but despite their obvious differences they all act as anesthetics. The common properties of these drugs were discovered more than a hundred years ago by C.E. Overton [4]:

*The dose needed to induce general anesthesia, is proportional to the solubility of the anesthetic in oil.*

This is known as the Meyer-Overton relation. For his experiments Overton used tadpoles as test subjects. And for tadpoles the anesthetic dose,  $ED_{50}$ , were defined as the concentration at which 50% of tadpoles had lost the ability to right themselves after being tilted - the Loss of Righting Reflex (LRR). For gaseous anesthetics the definition were anesthetic pressure,  $EP_{50}$ , the partial pressure of an anesthetic above the water, which caused 50% LRR - as depicted in figure (1.2).

The broader implications of Overton's experiments were that: All substances dissolvable in oil, act as anesthetics proportional to their solubility. Since all living's cells' membranes are of oily substance, this finding were interpreted as:

*The anesthetic dose of a given substance is proportional to its solubility in the nerve membrane.*

Which was confirmed by various groups in the 60s along with some corrections and some limits [6]. One would assume that this old finding is easily incorporated in the modern understanding of how nerves work, since nerves are

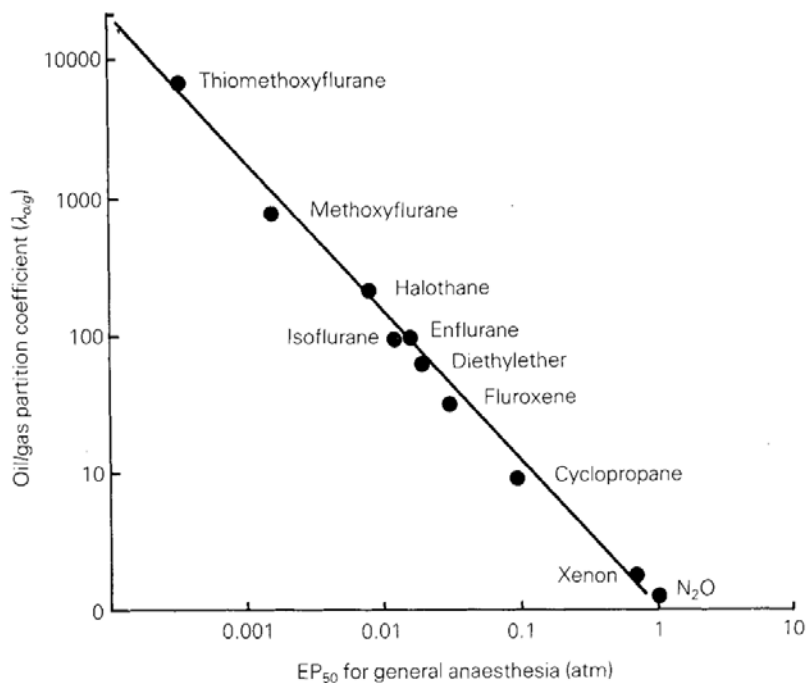


Figure 1.2: The oil/gas partition coefficients of inhalation anesthetics display correlation with anesthetic pressure,  $EP_{50}$ . This relationship was discovered by Meyer and Overton around year 1900. Data from republished book by Overton [5]

where anesthetics function. However, this is not the case!

## 1.2 Nerves

*Are you ticklish?*

The action of anesthetics is obviously closely connected to the function of nerves, since nerves are the *a priori* site of action for the anesthetic. So to understand how anesthesia function, it is important to have a clear idea of how nerves function.

Nerves are cells and as such share characteristics with other cells. Nerves have an outer membrane that confines the cell, inside are proteins, mitochondria, the nuclei which contains the DNA, and other organelles.<sup>1</sup>

Nerve models explain how nerves transmit a signal from one end to the other. For nerve models, the most important feature is the cell membrane which is made of a lipid bilayer with embedded and adhered proteins. The important question is, whether it is the membrane or the proteins embedded in the membrane, that are responsible for the function of nerves - the nerve signal.

The membrane bilayer is made of lipids. These lipids are characterized by a hydrophilic head group and two hydrophobic carbon chains. In vivo there is a large variety of head groups, and carbon chains can be found of lengths 14-24 that are saturated to various degrees. [7]

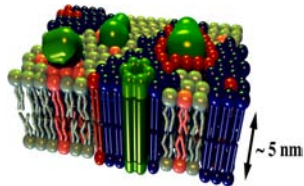
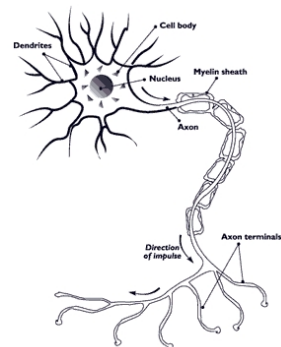
Membrane proteins are a large and diverse group of complex molecules, with a variety of functions from maintaining the cells interior levels of water, ions and molecules, to communicating with surrounding cells. Proteins in living cells make up for 10-50% of the mass of the cell membrane, depending on the type of cell.

There exist more than 10,000 different nerve types, ranging from meter long spinal nerves to micro meter size in the brain and sensory system.

(Include a little more history of nerves and membranes.)

<sup>1</sup>Picture of nerve from: Nerve Cells and Neurotransmission. Retrieved 12. October, 2006, from [http://teens.drugabuse.gov/mom/tg\\_nerves.asp](http://teens.drugabuse.gov/mom/tg_nerves.asp). Picture of membrane by T. Heimburg made with POV-Ray.

EXAMPLE OF NERVE



MEMBRANE BILAYER

### 1.3 The Nerve Signal

That the nerve signal is associated with electricity was discovered in 1791, and directly led to the creation of the first batteries by A. Volta and L. Galvani. They constructed these to perform experiments on frog nerves and electric eels.

The electric nerve pulse, which is often referred to as the 'action potential', was first measured by a German physicist Emil du Bois-Reymond in 1848. That same year, Helmholtz started to measure the thermodynamic properties of a stimulated nerve - he did so while he was still enlisted in the Prussian army [8]. It was also Helmholtz who two years later was the first to measure conductance velocities of the nerve signal. Today it is known that the nerve signal travels at speeds between 1 to 120 meters per second, depending on nerve type.

In the 1940s, measurements of ion concentration differences across the nerve membrane, lead Hodgkin and Huxley [9] to propose an electrical model of the nerve signal. This model of Huxley and Hodgkin was based on the electrical properties of the membrane and movements of ions through the membrane. In 1963 Hodgkin and Huxley earned the Nobel Prize in Medicine for this theory.

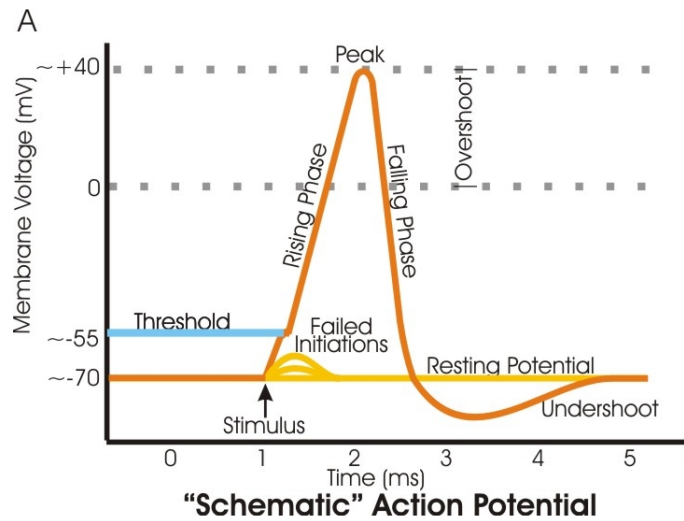


Figure 1.3: The action potential / electric nerve pulse is a measured change of electric potential across the membrane of approximately 100 mV. The 'threshold' value is the voltage it takes to initiate the pulse. If less than the threshold value is applied, it results in a 'failed initiation'. Figure from Wikimedia Commons reproduced under GNU License.

Today the Hodgkin-Huxley Model (HHM) is the predominant theory of the action potential.

In the 1970s Neher and Sakmann [10] developed the patch-clamp technique - which demonstrated 'single' events in the electric potential across the nerve

membrane. These measurements of so-called 'single' events were interpreted as membrane proteins acting like ion channels. The HHM relies on a mechanism that controls ion movement across the membrane, and so the results of Neher and Sakmann were received as conclusive evidence of the HHM.

The patch-clamp method has since been one of the most popular methods of measuring the activity of ion channels and the influence of different drugs on their action.

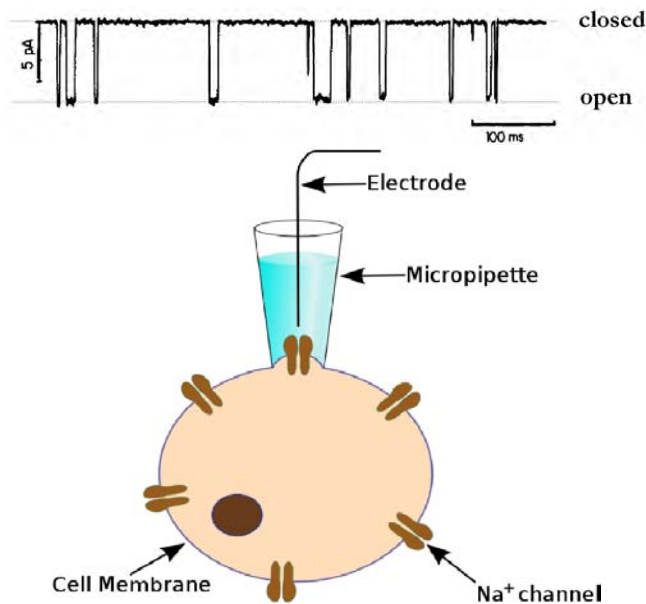


Figure 1.4: The patch clamp technique. (Top) Example of measured current during patch clamp experiment, can be interpreted as ion channels being open or closed. (bottom) Visualization of patch clamp technique – A micropipette with an electrode is attached by suction to a patch of membrane. However, measurements of similar results have been conducted on lipid membranes without protein channels. Figure created by Theresa Knott used under Creative Commons License.

The single events seen by Neher and Sakmann have later been reproduced in lipid membranes without channels [11, 12], leaving some scientists to speculate whether the correlated action of ion channels has been properly proven. Also, the HHM does not include parameters such as temperature or pressure, which has been shown to influence the action potential [13, 14]. These and other disadvantages of the HHM lead Heimburg and Jackson [1] to present a new model based on thermodynamic properties of nerves: The Soliton Model (SM).

In the Soliton model the nerve pulse is a density wave traveling along the nerve. With the change in density two effects generates the measured action potential: The first is that the membrane contains charged lipids, and chang-

ing the area of the membrane changes the charge density thereby changing the field across the membrane. Secondly - given that the inside and the outside of the nerve cell contains ions of different concentration, the membrane acts as a capacitor for these. Thus changing the thickness of the membrane changes the capacitive properties of the membrane.

The thermodynamic qualities of the nerve membrane will be thoroughly introduced in section (2.1), and the HHM and SM will be described in detailed in sections (2.2) and (2.3).

In conclusion: The goal of this master thesis is to introduce the Soliton model on nerve function. And experimentally test the influence of anesthetics on this model, in a way that will incorporate the Overton data.

## 1.4 Simulating the Membrane

Well into the experimental work of this thesis, a desire to visualize the membrane and the anesthetics was somehow forged into the mind of the author. The reason being that no detailed pictures can be obtained of membranes *in vivo*, simply because of the minuscule size of lipids and proteins. And assumptions were made on the behavior of the anesthetics, and arguments against the HHM presented with basis in small membrane events, which cannot be directly observed.

So it became an obsession to construct, a simulating environment that would allow to visualize key components of the experimental setup. The purpose was to further the intuitive understanding of this realm of ions and small molecules usually far beyond our daily visual horizon. To do so was a mighty castle to begin construction on, and it must be confessed that no towers will throne by the end of this thesis. However, a foundation has been cast, and some interesting initial results will be presented.

A more formal introduction to the simulation will be done in section 2.3.

*Now let's get ready to rumble, it's: Hodgkin-Huxley vs. the Soliton!*

# Chapter 2

# Theory

This section will go into detail with the properties of membranes and the action of anesthetics in these. The Hodgkin-Huxley model will be presented and the Soliton model derived. Furthermore, the new simulation model will be introduced.



Figure 2.1: (Picture left) Meyer and C.E. Overton, who established the Meyer-Overton relation. (Picture right) J.S. Russell, who discovered the solitary wave – which lead to the discovery of solitons.

## 2.1 Membrane properties

The Meyer-Overton rule establishes that the higher solubility of a drug into oil, the lower is the dose needed to induce anesthesia. Obviously, all lipid soluble drugs are miscible in the nerve membrane. The question is – what does this matter to the properties of the membrane? This will be tested in this thesis. And in this section, theoretical grounds to predict and explain the outcome of these experiments are presented.

As it will be shown in the data section, the most profound effect of anesthetic on the nerve membrane is a shift of melting temperature. In section (2.1.1), the theoretical basis of melting point depression will be explained, and in section (2.1.3) a simple way to reverse the anesthetic action is presented. But first an introduction to membrane properties.

The primary property of concern for this thesis is the phase transition of the membrane (PT). The lipid membrane phase can simplified be described by two parameters, with each two options:

**Membrane structure:** [*Solid / Liquid*] Below PT the lipids are arranged in a crystalline structure - The membrane is *solid*. Above the PT lipids diffuse around more freely in the membrane - They behave as a *liquid*.

**Lipid phase:** [*Ordered / Disordered*] Below PT the lipid chains are stretched out and immobile - They are *ordered*. Above PT the lipid chains fluctuate within the rotational phase space of the carbon bonds - They are *disordered*.

So below phase transition, the membrane is Solid-Ordered (SO) and above it is Liquid-Disordered (LD), as seen in figure (2.2). Throughout this thesis the SO phase will be referred to as the gel phase, and the LD phase as the fluid phase.

Now it is time to introduce the lipid of choice for this thesis: di-palmitoyl-phosphatidyl-choline referred to as DPPC.<sup>1</sup> This lipid was chosen, since it is one of the most common lipids found in nerve tissue [7]. It is easily attainable – even though it cost twice as much as gold. And it has a phase transition region at near human body temperature, which is a temperature regime that is easy to reach with not to sophisticated laboratory equipment.



The phase transition of lipid membranes does not happen at *one* temperature, rather it stretches across approximately 10 K. It is the mixture of different lipid

---

<sup>1</sup>Picture of DPPC taken from: [www.lce.hut.fi/research/polymer/membranes.shtml](http://www.lce.hut.fi/research/polymer/membranes.shtml)  
Blue balls are carbon, reds are oxygen, brown is phosphor, and dark blue is nitrogen.

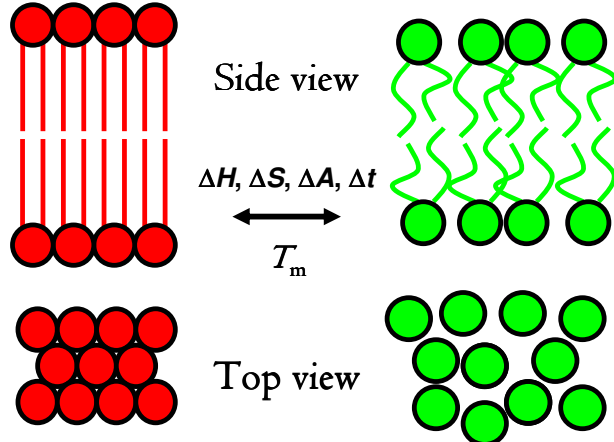


Figure 2.2: Phase transition of the lipid membrane is a shift from a Solid-Ordered state (left) to the Liquid-Disordered phase (right). The membrane shifts from a *solid* crystalline structure to a *liquid* like structure, where lipids diffuse around freely (bottom). The carbon chains of the lipids change from *ordered* structure to an *disordered* (top). The phase transition is associated by changes in enthalpy, entropy, area, and thickness.

types, that is the cause of this broad region of phase transition *in vivo* (Fig. 2.3). In the artificial DPPC membrane phase changes also occurs within a 10 K region, but these changes are related to conformal changes of the membrane structure. The precise mechanics of this has not been definitely determined. Nor whether the transition from Solid-Ordered to Liquid-Disordered are direct or via Solid-*Disordered* or Liquid-*Ordered*.

But there are properties of the phase transition that are easily measured or are deductible from measurements and therefore known. The primaries being the change of enthalpy,  $\Delta H$ , and change of volume and area,  $\Delta V$  and  $\Delta A$ , from these it is possible to deduct the change in entropy,  $\Delta S$ , heat capacity,  $\Delta c_P$ , density,  $\Delta \rho$ , and compressibility,  $\Delta \kappa$ , and some relations between these.

The phase transition is very broad but in this thesis it will be defined by one temperature,  $T_m$ . In the next section (2.1.1) 'regular solution theory' will be used to derive changes in the melting point of the membrane with anesthetic added. To be consistent with these calculations, the melting temperature,  $T_m$ , of all data obtained by calorimetry is defined by the 'upper phase boundary', which is the temperature where all lipids are of the fluid form. As an example, for the bovine lung surfactant (figure 2.3) the upper phase boundary is at 37°C.

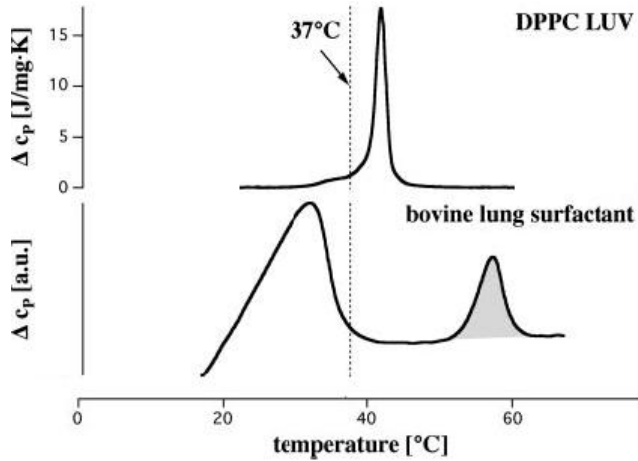


Figure 2.3: Heat capacity of DPPC and bovine lung surfactant, display phase transitions around body temperature. Grey area are protein unfolding. Picture from Heimburg [1].

### 2.1.1 Melting point depression

From the experiments later on, it is seen that anesthetics change the melting temperature of the lipid membrane. This is commonly referred to as a 'melting point depression'. To explain the melting point depression of the lipids with added anesthetics, one assumes a simple eutectic model of phase behavior. [15]

The eutectic model assumes that the lipids only exist in a gel and a fluid state, that the anesthetic does not have a phase-change, and that anesthetic is only miscible in the fluid phase. Then using the basic thermodynamic equation, which states that the chemical potential of a solution is dependent on concentration, the following equations appear:

For the anesthetic in the membrane there is only one phase:

$$\begin{aligned} \mu_{AM} &= \mu_{AM}^0 + RT \ln(c_{AM}) \implies \\ &= \tilde{\mu}_{AM}^0 + RT \ln(x_{AM}) \end{aligned} \quad (2.1.1)$$

The subscript *AM* refers to Anesthetic in the Membrane. Where  $\mu$  is the chemical potential,  $\mu^0$  is the zero point chemical potential,  $RT$  is the gas constant and temperature,  $c$  is the concentration,  $x$  is the fraction of the substance in the state given by the subscript. And  $\tilde{\mu}^0$  is a renormalized zero point chemical potential, that includes the volume from the logarithmic term, so amount can be expressed in fraction.

For the lipid membrane, there is exactly two phases, and it is only the fluid

phase that interact with the anesthetic:

$$\mu_M^f = \tilde{\mu}_M^{0,f} + RT \ln(x_M^f) \quad \text{fluid state} \quad (2.1.2)$$

$$\mu_M^g = \tilde{\mu}_M^{0,g} \quad \text{gel state} \quad (2.1.3)$$

The superscripts  $f$  and  $g$  refers to the fluid and gel state, and the subscript  $M$  reveals that the properties are of the membrane.

The chemical potentials has the boundary condition, which also states that the anesthetic only is miscible in the fluid phase:

$$x_{AM} + x_M^f = 1 \quad (2.1.4)$$

In the equilibrium state, when there is no net change of the number of lipids in the fluid or gel state, the chemical potential of the fluid and gel state of the lipid will be equal (Gibbs-Duhem). Equating (2.1.2) and (2.1.3) and using the boundary condition (2.1.4).

$$\begin{aligned} \tilde{\mu}_M^{0,g} &= \tilde{\mu}_M^{0,f} + RT \ln(x_M^f) \iff \\ \ln(1 - x_{AM}) &= -\frac{\Delta\mu}{RT}, \quad \Delta\mu = \tilde{\mu}_M^{0,f} - \tilde{\mu}_M^{0,g} \end{aligned} \quad (2.1.5)$$

Then assuming a low fraction of anesthetic in the membrane to approximate the logarithmic term<sup>2</sup>. And given that  $\Delta\mu = \Delta G = \Delta H - T\Delta S$ , where the change in Gibbs free energy,  $\Delta G$ , must be in units of [J/mol].  $\Delta H$  is the enthalpy change, and  $\Delta S$  the entropy change of the phase transition. Where it is used that for the melting point,  $T_m$ , of the membrane without anesthetics the fraction of lipids is  $x_M^f = 1$ , which gives  $\Delta\mu = 0$ , thus  $\Delta S = \Delta H/T_m$ :

$$\begin{aligned} x_{AM} &\approx -\frac{\Delta H - T\Delta S}{RT}, \quad \Delta S = \frac{\Delta H}{T_m} \\ &= -\frac{\Delta H}{R} \left( \frac{1}{T} - \frac{1}{T_m} \right) \\ &= -\frac{\Delta H}{R} \left( \frac{T_m - T}{T T_m} \right), \quad T T_m \approx T_m^2 \\ &\approx -\frac{\Delta H}{R} \left( \frac{T_m - T}{T_m^2} \right) \iff \\ \Delta T = T_m - T &= -\frac{RT_m^2}{\Delta H} x_{AM} \end{aligned} \quad (2.1.6)$$

From equation (2.1.6), it is seen that the melting point depression,  $\Delta T$ , is linearly dependent on the amount of anesthetic in the lipid membrane.

## 2.1.2 Partition coefficient

*How well does it penetrate?*

---

<sup>2</sup>for  $x \ll 1$  holds  $\ln(1 - x) \approx x$

If the melting point depression is indeed the mechanism for anesthesia, it is important to determine this amount of anesthetic in the membrane. The experimental setup in this thesis utilizes membranes dissolved in a buffer. It must then be established how much of the anesthetic is in the aquatic buffer, and how much in the fatty membrane - this is defined by the partition coefficient,  $P$ :

$$P \equiv \frac{c_{AM}}{c_{AS}} \quad (2.1.7)$$

Where  $c_{AM}$  is the concentration of anesthetic in the membrane and  $c_{AS}$  is the concentration of anesthetic in the solution/buffer. What needs to be known is the molar fraction of anesthetics in the membrane  $x_{AM} = n_{AM}/n_M$ , obtained in known quantities. From the definition, it is easily seen that:

$$P = \frac{n_{AM}}{n_{AS}} \frac{V_S}{V_M} = \frac{n_{AM}}{n_{AS}} \frac{\rho_M m_S}{\rho_S m_M} \quad (2.1.8)$$

Where  $n$ ,  $V$ ,  $\rho$ ,  $m$  defines moles, volume, density, and mass with the subscripts  $M$ ,  $S$  to indicate whether it is membrane or solution properties. It is then used, that the total molar amount of anesthetics is given by the combined amount in membrane and solution  $n_A = n_{AM} + n_{AS}$ :

$$\begin{aligned} P &= \frac{n_{AM}}{n_A - n_{AM}} \frac{\rho_M m_S}{\rho_S m_M} \iff \\ n_{AM} &= n_A \left( 1 + \frac{\rho_M m_S}{\rho_S m_M} \frac{1}{P} \right)^{-1} \implies \\ x_{AM} &= \frac{n_A}{n_M} \left( 1 + \frac{\rho_M m_S}{\rho_S m_M} \frac{1}{P} \right)^{-1} \end{aligned} \quad (2.1.9)$$

Most of these quantities are known from the experimental setup, i.e. it is known how much anesthetics, membrane and buffer is used. The only exception is  $P$ . This parameter proved somewhat difficult to establish since it very dependent on the type of lipids used, the type of buffer, and also for many anesthetics  $P$  has a strong pH dependency.

The intention for this project was to combine equations (2.1.6) and (2.1.9), and to experimentally verify that anesthetics change the melting point of the membrane as a linear function of their added concentration,  $c_A$ , - and thereby render plausible the eutectic assumption. This was reasonable well achieved (Sec. 4.1.2). The Meyer-Overton relation then implies that changes of the melting point must be given by the amount of anesthetic in the membrane - no matter the anesthetic used. So from equation (2.1.6) it is seen, that plotting  $\Delta T$  as a function of  $x_{AM}$  should fall on the same line, regardless of anesthetic. This collapse of data could not be achieved.

There is no reason to assume that the extensive collection of data by Overton is not valid. Therefore there must be a culprit responsible for the missing collapse in data. This culprit must be the partition coefficient,  $P$ , since it is the only variable not given from the experimental setup. Only one of the anesthetics

used had any partition coefficient given specific for DPPC. Therefore  $P_s$ , for all other anesthetics, were taken from the available system most like DPPC. However, determining  $P$  from literature proved difficult, as it vary with more than an order of magnitude between references (See table 5.1, page 84).

To try to determine the partition coefficient for the individual anesthetics, photo-spectroscopy experiments were conducted (Sec. 3.2), though without conclusion.

If the eutectic assumption is good, and Overton's data applies to the anesthetics in this thesis, partition coefficients can be calculated from data obtained in these experiments. So in order to determine  $P$ , equations (2.1.6) and (2.1.9) were combined while noticing  $n_A/n_M = x_A$

$$\begin{aligned} -\frac{\Delta H}{RT^2}\Delta T &= x_A \left(1 + \frac{\rho_M m_S}{\rho_S m_M} \frac{1}{P}\right)^{-1} \iff \\ 1 + \frac{\rho_M m_S}{\rho_S m_M} \frac{1}{P} &= -\frac{RT^2}{\Delta H} \left(\frac{\Delta T}{\Delta x_A}\right)^{-1} \iff \\ P &= -\frac{\rho_M m_S}{\rho_S m_M} \left(\frac{RT^2}{\Delta H} \left(\frac{\Delta T}{\Delta x_A}\right)^{-1} + 1\right)^{-1} \end{aligned} \quad (2.1.10)$$

deduces  $P$ , when noticing that  $\Delta T/\Delta x_A$  is the slope of the line fitted from plotting the melting temperature as a function of the fraction of anesthetics,  $x_A$ .

### 2.1.3 Pressure reversal

*Push it.*

Interestingly pressure shifts the melting temperature in the opposite direction of anesthetic:

$$\Delta T = \gamma_V \Delta p T_m \quad (2.1.11)$$

With the pressure dependence  $\gamma_V T_m \simeq 0.025$  [K/bar]. This result is valid for most lipid, lipid mixtures, and biological membranes [22]. In section (4.1.3) it will be experimentally shown, how pressure can also shift the phase transition in lipids with anesthetics.

So anesthetic action can be reversed by adding pressure. The amount can be determined using (2.1.11) with (2.1.6):

$$\begin{aligned} \Delta T_{pressure} &= -\Delta T_{anesthetic} \\ \gamma_V \Delta p T_m &= \frac{RT_m^2}{\Delta H} x_{AM} \iff \\ \Delta p &= \frac{RT_m}{\gamma_V \Delta H} x_{AM} \end{aligned} \quad (2.1.12)$$

Where  $x_{AM}$  can be determined from (2.1.9), or for experiments with large bulks of water<sup>3</sup>, the partition coefficient,  $P$ , can be approximated as:

$$\begin{aligned} P &\equiv \frac{c_{AM}}{c_{AS}} \\ &\approx \frac{c_{AM}}{c_A} = \frac{n_{AM}}{n_A} \frac{V_W}{V_M} = x_{AM} \frac{n_M}{n_A} \frac{V_W}{V_M} = \frac{x_{AM}}{c_A} \frac{n_M}{V_M} \quad \Longleftrightarrow \\ x_{AM} &\approx P \frac{V_M}{n_M} c_A \end{aligned} \quad (2.1.13)$$

#### 2.1.4 The Meyer-Overton Relation

From equation (2.1.13) the theoretical slope of the straight line in the Overton data (Fig. 1.2) can be derived. Assuming again that it is a shift in melting point that causes anesthesia, we have from equation (2.1.6) that this shift is linearly proportional to  $x_{AM}$ . Therefore, the left side of equation (2.1.13) is a constant for the anesthetic condition and:

$$c_A \propto P^{-1} \quad (2.1.14)$$

Which gives that the slope of partition coefficient as a function of anesthetic concentration in a log-log-plot should be -1. This is indeed the slope found in Overton's data. And this relation is commonly known as the Meyer-Overton Relation. The same proportionality can also be derived from equation (2.1.9), only adding a very small constant.

There has now been presented a lot of theory that predicts and describes the behavior of the the lipid membrane. Experiments which support and/or is explained by the theory derived are presented in chapter 4.

Now it is time to present the Nerve models.

---

<sup>3</sup>From equation 2.1.9 it can be seen that the exact requirement is that  $m_S \gg m_M \cdot P$ .

## 2.2 The Hodgkin-Huxley model

It is a fact that the nerve signal is associated with an electrical pulse. Classical experiments such as the contraction of frog muscles by applying voltage, to modern measurements of electrical pulses in the brain (EEG) rely on this fact. The Hodgkin-Huxley model (HHM) is a mathematical model based on electrical assumptions [9]. The HHM was developed in the early 50s, and has since the 60s been regarded as *the* model by a majority of the science community, especially the medical.<sup>4</sup>

The basic concept of the HHM is that proteins embedded in the nerve membrane act as channels, which transport ions from one side of the membrane to the other, as seen on figure (2.4).

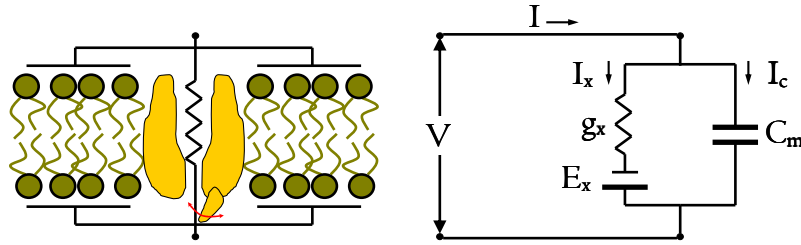


Figure 2.4: The equivalent circuit representation of the Hodgkin-Huxley Model: Gated protein channels in the biological membrane (picture left) represented as an electric circuit (picture right). Difference in ion concentration across the membrane generates a potential,  $E_X$ . Opening of channels allows for conductance,  $g_X$ , and flow of ions/current,  $I_X$ . Ions not allowed through the membrane act as capacitive current,  $I_C$ , as the membrane acts as a capacitor,  $C_M$ .

There are specific channels for specific ions, and it is the ion concentration on each side of the membrane that determines, if the transport flows from inside the cell to outside or visa versa. The flow of ions, which have electrical charges, is treated as an electric circuit. The electric pathways across the membrane are the potassium channel, the sodium channel, and a leak current, the latter being ions from other channels (e.g. calcium) or ions diffusing through the membrane. The membrane is otherwise regarded electrically impenetrable and as such functions as a capacitor. To generate the electric nerve signal, the ion channels open and close according to the voltage across the membrane and with respect to time.

The electric circuit (Fig. 2.5) is described by ten coupled differential equations, the primary one describing the circuit:

$$I = C_m \frac{dV}{dt} + g_K(t, V)(V - E_K) + g_{Na}(t, V)(V - E_{Na}) + g_L(V - E_L) \quad (2.2.1)$$

---

<sup>4</sup>All pictures of the HHM in this sections are adapted from the original article [9] by Hodgkin & Huxley.

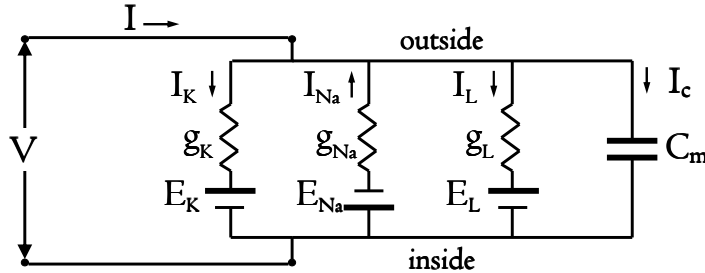


Figure 2.5: The combined electric circuit of the Hodgkin-Huxley Model is made from single circuits displayed in figure (2.4). Ions are sodium and potassium.  $L$  represents ions leaking through the membrane.

$I$  being the total current through and  $C_M$  the capacitance of the membrane,  $V$  the total voltage across the membrane, with  $E_X$  representing the equilibrium potential, generated by the difference in  $X$ -ion<sup>5</sup> concentration from the inner to the outer of the membrane, and  $g_X$  the conductance of the associated ion channel. The  $g_K$  and  $g_{Na}$  are functions of time and voltage in order to make equation (2.2.1) match a measured nerve pulse. The  $g_K$  and  $g_{Na}$  are governed by a total of nine differential equations that represent 'gating mechanics' in the proteins.

Evidently, for the nerve signal to be sent, billions of sodium and potassium channels along the nerve will have to open and close in a correlated fashion [20]. And afterwards, a similar amount of ion pumps will have to work to restore the ion concentrations on each side of the membrane in order for the nerve to be ready for the next signal. This entire process must happen at tremendous speed, since nerves can send signals up to around 120 m/s and up to hundreds of times per second.

In the HHM, anesthetics act by binding to ion channels, thereby blocking the channels and the nerve pulse [18]. The binding to the channels is suggested to be aided by proteins surrounding the channels, but nevertheless binding sites for *all* anesthetics are required to explain the sedative action! Even if binding sites existed for all anesthetics, it would still be necessary to explain how these can have binding affinities that are proportional to the solubility in oil, as the Overton data imply.

The difficulties in explaining the action of anesthetics in the HHM is not even the most serious problem for the model. Experiments conducted in the 80s suggest that many assumptions on which the model rely, are not very accurate. For one, Iwasa & Tasaki [19] measured that when a nerve signal pass a measuring point, it is not only electrical but also accompanied by a thickening of the mem-

<sup>5</sup>L being not an ion, but the leak current.

brane. This contradicts the assumption in the HHM that the membrane has a constant capacitance, since capacitance is reversely proportional to distance of capacitor plates – the membrane boundaries. Even worse, Ritchie & Keynes [20] measured that the nerve signal is accompanied by a heat release shortly followed by a heat uptake of roughly the same size, as seen in figure (2.6).

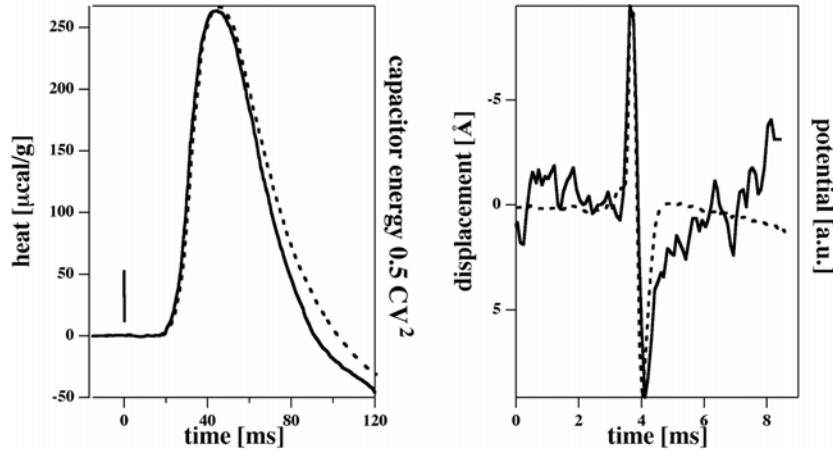


Figure 2.6: The action potential is associated with heat uptake and release (graph left, [19]) and thickness change of the nerve (graph right, [20]). Data adapted by Heimburg [1].

The rapid energy release and uptake is a clear indication that the nerve signal is a reversible process and therefore consumes (ideally) no energy. This is in conflict with HHM, which uses energy both to sustain the electric pulse, as electric conductors produce heat, and to 'reset' the system by re-establishing the ion concentration difference across the membrane.

To sum up – The Hodgkin-Huxley Model (HHM) is an intricate mathematical model which only depends on voltage and ion concentration difference across the membrane. It does not describe temperature, pressure, thickness changes, heat release and uptake, or anesthetic action in the membrane. Therefore it is time to introduce the Soliton Model.

## 2.3 The Soliton Model

*60 km of electrical wiring, or 60 km of soft fatty springs - what are 'the human nerves'?*

This section will present the Soliton model as proposed by Heimburg and Jackson (2005) [1].

Their motivation for proposing this new model stems from the evident inability of the Hodgkin-Huxley model to explain key features of the nerve pulse, as mentioned in Sec. (2.2)

The intention of the soliton model is to create an adiabatic wave theory, given that Ritchie and Keynes showed in 1985 [20] that the nerve pulse is isentropic, and Iwasa and Tasaki showed in 1980 that the nerve pulse is accompanied by a density pulse [19]. Taking this approach, the first obvious step is to consider a wave equation.

$$\frac{\partial^2 f}{\partial t^2} = \frac{\partial f}{\partial \mathbf{x}} \left( \frac{1}{c^2} \frac{\partial f}{\partial \mathbf{x}} \right) \quad (2.3.1)$$

The medium that carries this wave can only be the cellular membrane. The function,  $f$ , in (2.3.1) is then recognized as the area-density,  $\rho^A$ , of the membrane. The sound speed is related to the density and compressibility of a medium by  $c = (\kappa_S^A \rho^A)^{-\frac{1}{2}}$ :

$$\frac{\partial^2}{\partial t^2} \Delta \rho^A = \frac{\partial \Delta \rho^A}{\partial x} \left( \frac{1}{\kappa_S^A \rho^A} \frac{\partial \Delta \rho^A}{\partial x} \right) \quad (2.3.2)$$

The introduced  $\kappa_S^A$  is the area-compressibility of the membrane, which is also dependent on the density of the membrane. The  $S$  subscript on  $\kappa$  indicates that it is the adiabatic compressibility. How density and compressibility couples to each other and to the experiments conducted within this thesis, will be explained a little later. Firstly, it should be noted that the wave-equation is 1D, but is containing area-density and area-compressibility. This becomes valid if assuming that the soliton propagates uniformly along the nerve - like a ring along a cylinder. Secondly, the propagation velocity of waves is dependent of their frequencies, this will also be discussed more in-depth later, but a consequence is that a dispersion term must be added to the wave-equation [1]:

$$\frac{\partial^2}{\partial t^2} \Delta \rho^A = \frac{\partial \Delta \rho^A}{\partial x} \left( \frac{1}{\kappa_S^A \rho^A} \frac{\partial \Delta \rho^A}{\partial x} \right) - h \frac{\partial^4}{\partial x^4} \Delta \rho^A \quad (2.3.3)$$

It is then advantageous to change to a co-moving coordinate system by substituting  $z = x - vt$ , with  $v$  as the propagation velocity.

$$v^2 \frac{\partial^2}{\partial z^2} \Delta \rho^A = \frac{\partial \Delta \rho^A}{\partial z} \left( \frac{1}{\kappa_S^A \rho^A} \frac{\partial \Delta \rho^A}{\partial z} \right) - h \frac{\partial^4}{\partial z^4} \Delta \rho^A \quad (2.3.4)$$

This is the Soliton equation on which the Soliton Model is based.

As evident from equation (2.3.4), a soliton is dependent on the compressibility of the membrane, and it can be shown by means of thermodynamic equations and Maxwell's equations (Appendix A.1, [25]) that the isentropic compressibility of the lipid membrane is given by:

$$\kappa_S^A = \kappa_{T,0}^A + \frac{\gamma_A^2 T}{\langle A \rangle} \Delta c_P - \frac{T}{\langle A \rangle c_P(\omega)} \left( \frac{dA}{dT} \right)^2 \Big|_{P_A} \quad (2.3.5)$$

where  $\kappa_{T,0}^A$  are the isothermal compression not associated with the phase transition.  $\gamma_A$  is the proportionality factor between the change of area and the change of enthalpy,  $\Delta A(T) = \gamma_A \Delta H(T)$ .  $\langle A \rangle$  is the mean area.  $\Delta c_P$  is the excess heat capacity.  $c_P(\omega)$  is the frequency dependent heat capacity. And  $(dA/dT)_{P_A}^2$  is the derivative of area with respect to temperature, at constant lateral pressure.

The  $c_P(\omega)$  is the source of dispersion in the membrane, as it is dependent on frequency,  $\omega$ . However, measurements of  $c_P(\omega)$  has only been carried out in the megahertz regime, an order of magnitude higher than the frequencies of solitons. For very low frequencies, where timescales are on the order of the relaxation time of the membrane, the water surrounding the membrane will absorb heat. When the water acts as heat reservoir, the heat capacity becomes large and equation (2.3.5) can be approximated by:

$$\kappa_S^A \approx \kappa_{T,0}^A + \frac{\gamma_A^2 T}{\langle A \rangle} \Delta c_P \quad (2.3.6)$$

This approximation is used when calculating compressibility of the membrane, the frequency dependence is expressed in the dispersion term  $h \partial^4 \Delta \rho^A / \partial z^4$ .

It is seen from equation (2.3.6) that the nonlinearity of  $\kappa_S^A$  is only accessible in the phase transition. Curiously, a lot of biological membranes have melting points just around the 'body' temperature of the animal hosting them [15], as for example the bovine lung surfactant in figure (2.3).

This project has focused on numerical integration of equation (2.3.4), using data obtained from differential scanning calorimetry measurements (presented in section 3.1). From these calorimetry measurements  $\Delta c_P$  is obtained, and compressibility calculated from equation (2.3.6).  $\kappa_{T,0}^A$ ,  $\gamma_A$ , and  $\langle A \rangle$  are taken from literature. The *key feature* is that  $\kappa_S^A$  displays nonlinear properties around the *phase transition* of a bio-membrane, this enable solitons to propagate. (Figure 2.7)

### 2.3.1 The analytical solution

The SM-equation (2.3.4) can be solved analytically [1, 26] if the speed of sound in the membrane is approximated by:

$$c^2 = \frac{1}{\kappa_S^A \rho^A} = c_0^2 + p \Delta \rho^A + q (\Delta \rho^A)^2 + \dots \quad (2.3.7)$$

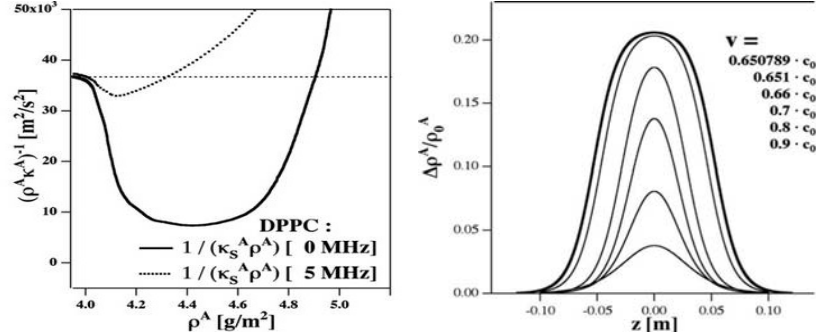


Figure 2.7: Sound speed,  $c^2 = (\rho^A \kappa^A)^{-1}$ , is dependent on density,  $\rho^A$ , area compressibility,  $\kappa^A$ , and frequency (picture left). In effect: Non-linear properties of the nerve membrane in phase transition regime sustain stable density waves –Solitons– (picture right) given by equation (2.3.4). From Heimburg, Jackson [1]

So substituting (2.3.7) to second order into (2.3.4) and integrating on both sides.

$$v^2 \frac{\partial}{\partial z} \Delta\rho^A = (c_0^2 + p \Delta\rho^A + q (\Delta\rho^A)^2) \frac{\partial \Delta\rho^A}{\partial z} - h \frac{\partial^3}{\partial z^3} \Delta\rho^A$$

Integrating once more:

$$v^2 \Delta\rho^A = c_0^2 \Delta\rho^A + \frac{1}{2} p (\Delta\rho^A)^2 + \frac{1}{3} q (\Delta\rho^A)^3 - h \frac{\partial^2}{\partial z^2} \Delta\rho^A \quad (2.3.8)$$

Multiplying each side with  $\partial(\Delta\rho^A)/\partial z$  and integrating:

$$h \left( \frac{\partial \Delta\rho^A}{\partial z} \right)^2 = (c_0^2 - v^2) (\Delta\rho^A)^2 + \frac{1}{3} p (\Delta\rho^A)^3 + \frac{1}{6} q (\Delta\rho^A)^4 \quad (2.3.9)$$

If  $\Delta\rho^A(z)$  is to have any localized solutions, it must display a maximum, which is equivalent to  $\partial(\Delta\rho^A)/\partial z = 0$ . Equation (2.3.9) gives some limits of the solutions. While there is a natural upper limit on the velocity of the solitons, given by the sound speed in the membrane  $c_0 \geq v$ . The lower limit of  $v$  is given when there is only one solution of quadratic equation from the right side of eq. (2.3.9)

$$v_{limit}^2 = c_0^2 - \frac{p^2}{6q} \quad (2.3.10)$$

which also yields a maximum amplitude of the soliton

$$\Delta\rho_{max,limit}^A = -\frac{p}{q} \quad (2.3.11)$$

An analytical solution for solitons was found by Lautrup [26]:

$$\frac{\Delta\rho^A(z)}{\rho_0^A} = \frac{2a_+a_-}{(a_+ + a_-) + (a_+ - a_-)\cosh\left(\frac{z}{h}\sqrt{c_0^2 - v^2}\right)} \quad (2.3.12)$$

$$a_{\pm} = -\frac{p}{q} \left( c_0^2 \pm \sqrt{\frac{v^2 - v_{limit}^2}{c_0^2 - v_{limit}^2}} \right)$$

The analytical solution and the polynomial approximation are compared to the numerical method used throughout this thesis in section (3.4).

Because the energy to change phase of the membrane is known, the energy of compression is handedly calculated. The soliton presses the membrane through the phase transition, the amount given by the change in area density. The total compression is the integral of  $\Delta\rho^A(z)/\Delta\rho_{PT}^A$  over  $dz$ . Where  $\Delta\rho_{PT}^A$  is the total change in area density of the membrane when going through phase transition, for DPPC  $\Delta\rho_{PT}^A/\rho_0$  is  $\approx 24\%$ . The integral is then multiplied with the total change in enthalpy,  $\Delta H$ , as measured by calorimetry. This gives the energy to compress the membrane into a soliton, but does not include the kinetic or capacitive energy.

Heimborg and Jackson calculated the mechanical energies by a Lagrangian formalism [1] and concluded that these are at least an order of magnitude larger than the capacitive energy, but two orders of magnitude less than the heat energy produced by compression.

The Soliton theory might at a first glance seem a bit exotic. But solitons are found in many physical systems, and have been of interest to many up through history. Therefore the next section is a short introduction to solitons in general.

### 2.3.2 A little soliton history

The term 'Soliton' was coined by Zabusky & Kruskal in 1965 [27] as a stable, localized wave with non-linear interactions in the Korteweg-de Vries equations, which originated in 1895 [28]. Korteweg and de Vries themselves, having derived the equation with the purpose of showing these solitary waves, had named them 'cnoidal' waves, but it was the soliton name that stuck. The soliton equation of Heimborg and Jackson is however of the Boussinesq type, which originated in 1871 [29]. And thus having name dropped back through history, we will start from the beginning...

On a beautiful August day in the year 1834, the 26 year old Professor of Natural Science at the Edinburgh University - Mr. John Scott Russell came riding along the English Canal in Edinburgh. That day he was riding along a towboat drawn by horses, when suddenly the cables between horses and boat snapped and the boat slowed quickly to a halt. Mr. Russell took notice of the bow wave of the boat, which seemed to release itself from the bow and continued on its

own down the canal. By his own accord, he followed this wave for nearly three kilometers down the canal, without it changing size or speed [30]. Russell was so fascinated by this event that he devised and carried out a number of experiments with regard to this wave before initially reporting on it in 1837, where he named it: "The Great Wave of Translation".

Professor Russell claimed that this "solitary shallow water wave" that he had observed and experimentally verified could not be explained by the ordinary wave equation

$$\frac{\partial^2 f}{\partial t^2} = \omega^2 \frac{\partial^2 f}{\partial x^2} \quad (2.3.13)$$

where the speed of a stable wave is only determined by the width of the wave, as opposed to Russell's experiments that required dependence on the amplitude as well.

It should be more than 30 years before Russell's wave would get a mathematical description.

$$\frac{\partial^2 h}{\partial t^2} = gH \frac{\partial^2 h}{\partial x^2} + gH \frac{\partial^2}{\partial x^2} \left[ \frac{3h^2}{2H} + \frac{H^2}{3} \frac{\partial^2 h}{\partial x^2} \right] \quad (2.3.14)$$

is the Boussinesq equation [29] from 1871, which describes how the displacement of the watersurface,  $h(x, t)$ , in a shallow canal of constant depth,  $H$ , under the influence of earth gravitational field,  $g$ , behaves. This equation has solutions of type that describes solitary waves.

In 1895 Diederek Korteweg and Gustav de Vries derived an equation (KdV) [28] for shallow water waves which included viscosity and surface tension. This equation showed solutions of the same form as the Boussinesq equation. It was in the normalized KdV equation

$$\frac{\partial \phi}{\partial t} + \frac{\partial^3 \phi}{\partial x^3} + \phi \frac{\partial \phi}{\partial x} = 0 \quad (2.3.15)$$

that Zabusky & Kruskal in 1965 discovered stable solitary solutions for collisionless plasma and named them "Solitons" [27].

This also marks the starting point of a verbal conflict, since nowadays the term 'soliton' is used by many as a reference only to a stable localized wave, like in the original paper on the Soliton model [1]. However, already in the 1965 paper Zabusky & Kruskal imposed some extra conditions which have been further expanded by other modern mathematical physicists.

The mathematical definitions are without specific importance for this thesis; nevertheless, it should be noted that the stable and localized properties of the SM-equation has been shown by B. Lautrup [26] and some additional solitonic behaviors by A. Ludu [31]. Therefore the 'solitons' of the SM are very plausible to be solitons - also according to the strict mathematical definition.

It was earlier loosely stated that the SM-equation is of the Boussinesq type.

That statement is precisely valid for the parabolic approximation of the compressibility. Which was expressed in a normalized form

$$\frac{\partial^2 \psi}{\partial t^2} = \frac{\partial}{\partial t} \left( (1 + \alpha\psi + \beta\psi^2) \frac{\partial \psi}{\partial x} \right) - \frac{\partial^4 \psi}{\partial x^4} \quad (2.3.16)$$

that lead to the analytic solutions, as solved by Benny Lautrup [26]. Equation (2.3.16) can then be compared to the normalized Boussinesq equation:

$$\frac{\partial^2 \psi}{\partial t^2} = \frac{\partial}{\partial t} \left( (1 + \alpha\psi) \frac{\partial \psi}{\partial x} \right) - \frac{\partial^4 \psi}{\partial x^4} \quad (2.3.17)$$

The addition of a higher order term in the SM is the only difference. There exist more than 30 recognized equations of Boussinesq-type, characterized by additions or small modifications of the original one. To add a higher order term could be termed 'close' family between Boussinesq and SM. Especially since the Boussinesq were derived using low order terms of Taylor-expansions<sup>6</sup>.

Soliton equations in general are wave equations with nonlinear terms. These nonlinearities might be entirely mathematical but some can be constructed in physical systems. In 1973 it was discovered that these nonlinearities could be incorporated in optic fibers [32]. To send stable localized light waves over long distances was very helpful to the information industry - sometimes referred to as the 'World Wide Web'.

Soliton has also been proposed to exist in tidal waves, tsunamis, vortices in water as well as in the fabric of space, cloud formation, quantum physics and many more systems.

---

<sup>6</sup>in the velocity field and stream function - the full derivation is rather lengthy and beyond the scope of this thesis.

## 2.4 Computer Simulations

*Where I'm the God of little colored balls!*

Computer simulations have for a long time been important for practically all branches of science. Membrane physics is certainly no exception. A wide variety of techniques are implemented to simulate every thinkable property of membranes and proteins integrated in or adhered to membranes.

This section will shortly review a few methods of simulation both to emphasize the power of computer simulation, but even more to give an idea of why I chose to create a bastard model.

The ultimate way of simulating is to mimic reality. This is done by many groups in various ways. They deploy a multitude of algorithms commonly referred to as Molecular Dynamics Simulations (MDS). MDS includes every atom and every bond in the lipids of the membrane, and it also includes water surrounding the membrane. When having these basic things in place, they can then add ions to the water phase or proteins to the membrane or put an electrical field across the membrane. These simulations are a rich source of information, as well as extremely beautiful (Fig. 2.8). The drawback is that it takes months on supercomputers to calculate nanoseconds of time with only a few hundred lipids. That this method is unfeasible for exploring the phase transition is shown by the research of Seeger [33], who showed that relaxation times of the phase transition is of the order of milliseconds.

The other extreme, and the simplest way of simulating lipids, is the Ising two-state model. This is often used model, as it has a wide range of applicability, and can just as well represent spin states in metals as lipid states in membranes. The principle of such a model is to place 'lipids' in a triangular grid, allowing them only to be fluid or gel-state and only to interact with their nearest neighbors. This may sound incredibly simple and uninteresting, but there is lots of information retrievable from such systems, as will be demonstrated in the next section. The advantage of such simulation is that they are fast and can be carried out with a large numbers of lipids. In addition, it is very easy to switch between lipid types and to apply external fields.

In between MDS and the Ising-model there is a large variety of simulations of different complexity to be found. One example would be pressure simulations by Cantor [34], who simulates the pressure profile in the lipid membrane, to demonstrate how channels might open and close, according to how added anesthetics change the internal pressure.

Many questions about the membrane and the action of anesthetics therein are unanswered - Like how does size or chirality influence function of anesthetics, where the anesthetics adhere, and do they induce holes in the membrane and so on. Therefore the intent of this author was to create a model somewhere in between MDS and the Ising model. To construct an environment where all these questions could be answered. And to take use of the simplicity of the Ising model, and then expand it with free movement, with variable size lipids, with

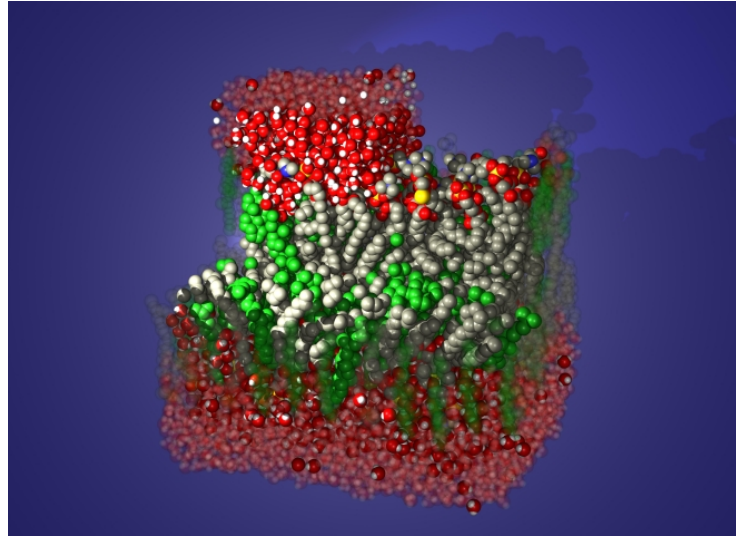


Figure 2.8: Molecular Dynamic Simulation of a DPPC (grey) and Cholesterol (green) bilayer in water. Parts of the membrane have been removed to improve visibility. By Helmut Heller, LRZ Munich.

anesthetics of different sizes and chirality.

The resulting Bastard model is conceptually based on the "Random-lattice model for phase equilibria in two-dimensional condensed systems of particles with coupled internal and translational degrees of freedom" by Nielsen [35] which is based on the theory of Doniach [36]. Nielsen *et al* have successfully simulated nearly free-moving lipids and thereby been able to show and conceptualize the pre-phase transition in simulated systems. The Nielsen-model, however, did not present parameters that would make possible comparison of their model to real lipid systems. The model was not based on true free motion, and the lipid interaction was basically still a discrete interaction. The intention of the bastard approach was to create a model with completely free-moving lipids, with continuously change of size, that would replicate the characteristics of experiments. Then one can target the questions mentioned above and maybe also show some results on how anesthetics influence the pre-transition, as this is also an area in which many theories have their say [25, 37]. In hindsight this task was probably to big for a master thesis, but some goals were nevertheless achieved, and the future prospect of this approach should not be neglected.

#### 2.4.1 Monte Carlo Simulations

When simulating membranes it is important to notice that the size of the membrane system is so small that brownian motion is a noticeable effect. So when simulating, the endstate is not *one* static solution, but a dynamic equilibrium where everything fluctuates around the most likely state. In fact many of the

results of the simulations are extracted from these fluctuations. To ensure that fluctuations are present in the simulations, it is necessary to use a technique that does not rigorously lead the system towards an energy minimum or entropy maximum. Such a technique is a Monte Carlo Simulation (MCS) with a Metropolis Algorithm (MA) [38] or Glauber Algorithm (GA) [39].

A Monte Carlo Simulation is carried out by starting with a random selection of a chosen specimen. In the simple 2-state case this is equivalent to starting with placing a number of lipids on a 2D triangular lattice. These lipids are randomly assigned to be either in a gel or a fluid state. This is then portraying a monolayer membrane.

Next a series of Monte Carlo steps are taken. A Monte Carlo step is to randomly select objects and evaluate if they can change according to internal and external parameters. Within the framework of lipid membranes this corresponds to: Randomly selecting a lipid. Then, given parameters such as temperature, pressure, and neighbors state, is the lipid then likely to change from gel to fluid or visa versa - this is the 'melting step'. The likelihood of a change to happen is decided by the Metropolis or Glauber Algorithm.

Most MCSs of lipids also include a 'switch step'. This step is to randomly select two lipids and evaluate if switching position of these two lipids is favorable.

The Bastard model also includes an 'area step', which tests if a random change of the area available to the lipids is desirable. And a 'move step' that moves lipids relative to each other.

The length of a Monte Carlo Simulation is in this thesis referred to as Monte Carlo Cycles per Temperature step (MCCT), as depicted in Fig (2.9). In a system of  $N$  lipids, 1 Monte Carlo Cycle (MCC) is equal to  $N$  melt steps,  $N$  move steps<sup>7</sup>, and in case of the Bastard model also 10 area steps.

MCS is the basis of all the simulation methods mentioned in Sec. (2.4), only the number of accessible states and according steps vary. For instance the Molecular Dynamics Simulations would include state/steps to describe e.g. the interaction of atoms in the molecules<sup>8</sup>.

There are two formal requirements on MCS being:

*Ergodicity:* Every configuration of the system must be accessible. In the 2-state lipid membrane model this determines that any ratio of gel to fluid lipids must be able to be produced by the simulation. This requirement says nothing about the probability. That the membrane might be fully made up of gel far above the melting temperature must be possible, albeit unlikely.

*Detailed balance:* The likelihood,  $L_A$ , of being in a given state  $A$ , times the probability of switching to a different given state,  $P_{A \rightarrow B}$ , must be equal to the

---

<sup>7</sup>The 'move' step does in some of the simulations also include a 'switch' step.

<sup>8</sup>Not fully expressed by quantum mechanics, but approximated by Hookian springs.

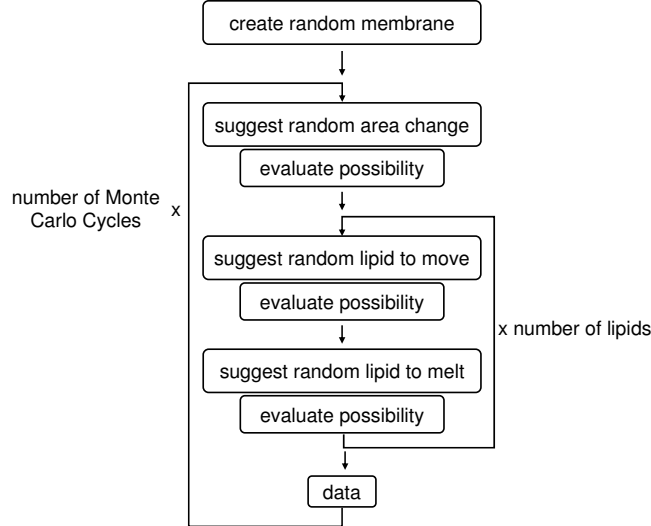


Figure 2.9: Monte Carlo Simulation flowchart for one temperature step of the continuous attached model.

likelihood of being in state  $B$  times the probability of switching back,  $P_{B \rightarrow A}$ :

$$L_A P_{A \rightarrow B} = L_B P_{B \rightarrow A} \quad (2.4.1)$$

If this requirement is not fulfilled, the system will 'drift' towards a non-equilibrium state.

Just having a system of hundreds of lipids moving around changing phases and so on, is slightly less than required to mimic the membrane [40]. In order to get some information from the system, it is imposed on the system to be a Boltzmann distribution as a function of Gibbs free energy. Such that the obtained results are among the likely that would occur, if this was a real system. This is obtained when:

$$\frac{L_A}{L_B} = e^{-(G_A - G_B)/RT} \quad (2.4.2)$$

Hence, the probability of changing state must be a function of the Boltzmann factor  $P_{A \rightarrow B} = f(e^{-\Delta G/RT})$  and while fulfilling detailed balance:

$$\frac{L_A}{L_B} = \frac{P_{B \rightarrow A}}{P_{A \rightarrow B}} = e^{-(G_A - G_B)/RT} \quad (2.4.3)$$

which yields for  $f(x)$  where  $x = e^{-\Delta G/RT}$ :

$$\frac{f(x)}{f(x^{-1})} = x \quad (2.4.4)$$

The method,  $f$ , which decides the probability to change state is optional as long as it fulfils the requirements above. The most widely used are the Metropolis Algorithm [38] and the Glauber Algorithm [39].

**Metropolis**  $f(x) = \min\{1, x\}$ ,  $f$  chooses whatever is the lowest value: 1 or  $x$ .

This algorithm sets the probability of going from higher to lower Gibbs free energy equal to one, which drive the system fast towards equilibrium, but increases the risk of 'trapping' the system in a false energy minimum.

**Glauber**  $f(x) = \frac{x}{1+x}$ . This algorithm determines that the system to go from high to low energy or visa versa with equal possibility.

for this project the Metropolis Algorithm was the most used, since simulations were on the timescale of days, a high drive towards equilibrium was favorable.

Collecting data from the simulations is primarily to record the fluctuations around equilibrium. The heat capacity profile is obtained by recording the enthalpy,  $H$ , after each MCC, and then use:

$$c_P = \left. \frac{d\langle H \rangle}{dT} \right|_P = \frac{\langle H^2 \rangle - \langle H \rangle^2}{RT^2} \quad (2.4.5)$$

when all MCCT is done to determine the  $c_P$  of the given temperature step (2.4.5 derived in Appendix A.1). The enthalpy,  $H$ , used to calculate the heat capacity includes all non-entropic terms of the Gibbs free energy equations describing the systems.

To obtain good statistics, simulations always run approximately 10% extra MCCT in the beginning, to let systems equilibrate, before recording data. Snapshots of the lipids are easily produced as the simulation knows the place of every lipid at all times - in principle films could be made of the building up and fluctuations of domains.

### 2.4.2 Static grid Ising model

The traditional way of simulating lipid membranes invokes placing the lipids on a static 2D triangular lattice.

Lipids are only found in their gel or fluid state, this is an interpretation of the spin-Ising model, with an energy function given by Sugar [40]:

$$\Delta G = \Delta H - T\Delta S + \Delta N\omega \quad (2.4.6)$$

Where  $\Delta G$  is the change in Gibbs free energy,  $\Delta H$  and  $\Delta S$  are respectively the change of enthalpy and entropy of the phase transition,  $T$  is the temperature, and  $\Delta N$  are the change in the number of interactions between gel and fluid lipids where  $\omega$  is the interaction energy (Fig. 2.11). Gibbs free energy is chosen since it is by definition is at minimum when temperature and pressure are constant.

The thermodynamic variables,  $\Delta H$  and  $\Delta S$ , can be derived from calorimetric measurements.  $H$  is measured directly by the calorimeter as the added thermal

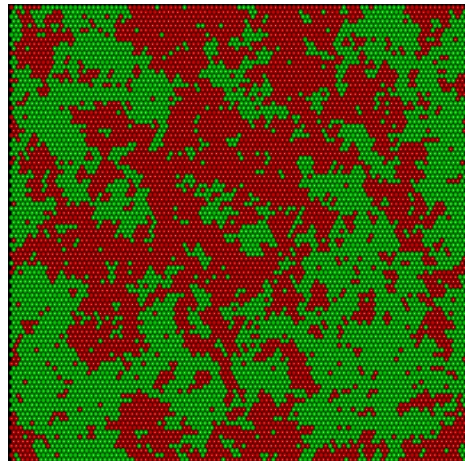


Figure 2.10: 2-state Ising static grid simulation at melting point,  $T_m = 41^\circ\text{C}$ . Red balls represent gels, green balls represent fluids.

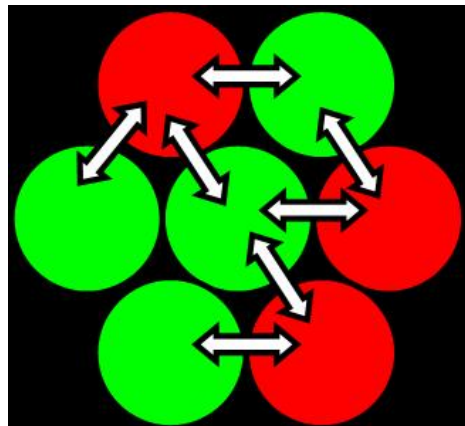


Figure 2.11: Arrows indicate interactions between lipids of different state. Here the number of interactions are  $N = 7$ . If the red gel in the lower right corner is changed to a green fluid, then  $\Delta N = 1$  given that two interactions are removed and one is created.

enthalpy, and  $\Delta H$  is determined as the enthalpy difference between the gel and fluid state of the system, equivalent to the total excess heat capacity of the phase transition.<sup>9</sup> In order to determine  $\Delta S$ , the following will have to be established for the energy equation, when at a specific temperature,  $T_m$ :

$$\Delta G = \Delta H - T_m \Delta S \equiv 0 \implies \quad (2.4.7)$$

$$\Delta S = \frac{\Delta H}{T_m} \quad (2.4.8)$$

The  $T_m$  is specified to be the temperature where it is equally possible to be in the gel as the fluid state.  $\Delta G$ , when given in units of [J/mol], is equal to  $\Delta\mu$ , the chemical potential.  $\Delta\mu$  is per definition equal to zero at  $T_m$ . Therefore  $\Delta G \equiv 0$  in equation (2.4.7). At melting temperature,  $T_m$ ,  $\Delta N$  must also be zero. Since it is equally possible to change lipids from fluid to gel, it is also equally possible to change from more to less gel-fluid interactions, and on average the change will be zero. To put it in mathematical terms: It can be noticed that in both a total fluid and a total gel state of the system has  $N(T_g, T_f) = 0$ , there are no interactions between gel and fluids. And  $N(T_m) = \max$ , the maximum numbers of interactions, must be where there is a maximum of different lipids. Hence  $N(T)$  is a function with an extremum at  $T_m$  and  $\lim_{T \rightarrow T_m} \frac{\Delta N}{\Delta T} = 0$ . Thus  $\Delta S$  can be expressed by  $\Delta H$  and  $T_m$  as given by (2.4.8).

The size of  $\omega$  determines the cooperativity of the membrane. That is, the higher  $\omega$  the more favorable it is for lipids of same phase to be next to each other. The result is a narrowing of the temperature range wherein the change from gel to fluid state takes place, which ensures a narrower heat capacity profile. Thus,  $\omega$  is adjusted so the simulated heat capacity mimics experiments. The cooperativity parameter for the static grid was adjusted to 1326 J/mol.

A high cooperativity of the membrane also induces formation of gel and fluid domains as seen on figure (2.10).

That the lipids are confined to a static grid does not mean that they cannot move. The move step of the Monte Carlo Cycle is in the static grid model equivalent to switching position of two random lipids. This might seem obsolete, since it is either the same as two phase changes - if the two selected lipids are of different phases. Or status quo - if the lipids are of the same phase. However, this move step decreases the simulation time needed to reach equilibrium, with nearly a factor of 10.

When visualizing the simulation 'lipids', what is shown is a square box of lipids like in figure (2.10). The lipids do not 'feel' this box as the program emulates periodicity – that is, lipids on the right edge of the 'box', have the lipids of the left side of the 'box' as neighbors. The same happens at the top and bottom of the 'box'. Implementing periodicity is to avoid 'edge effects' – if  $4\sqrt{n}$  of  $n$  lipids in a simulation have a different amount of neighbors than the

---

<sup>9</sup>excess meaning that it exceeds the enthalpy of simply heating, and only being the heat capacity of the actual phase transition.

rest, it would have a profound influence on the outcome.

Adding anesthetics to the simulation is done with the assumptions of the eutectic model, see Sec. (2.1.1), which is assuming that anesthetics are miscible only in the fluid phase of the lipids. The simplest way to achieve this is to let lipids act as anesthetics by only allowing them to be in their fluid phase. This method is very easy to implement and the results follow nicely the predicted melting point depression given by Eq. (2.1.6). Anesthetics can be added as a separate species in the simulations, but this will not change the phase transition noticeably, only induce domain formations of anesthetics.

In Static grid Ising models introducing an external pressure is done by adding a pressure term  $\gamma_V p T_{m,\Delta p=0} \Delta S$  to the energy equation (2.4.6). Where  $\gamma_V$  is a experimentally derived constant, and  $T_{m,\Delta p=0}$  is the melting temperature with zero added pressure.

$$\begin{aligned}\Delta G &= \Delta H - T\Delta S + \Delta N\omega + \gamma_V p T_{m,\Delta p=0} \Delta S \\ &= \Delta H + (\gamma_V p T_{m,\Delta p=0} - T) \Delta S + \Delta N\omega\end{aligned}\quad (2.4.9)$$

Wherefrom it can be seen, that the pressure term is mathematically equivalent to nothing else than a shift in  $T$ . This means that all results obtained with pressure are identical to those obtained without pressure, except for the shift in temperature.

### 2.4.3 The Bastard model

*I did it my way. (- And I really tried coming up with a better name.)*

In creating a new simulation model there was an idea of wanting to address some questions regarding the membrane and the role of anesthetics in the membrane, like: Can the change of permeability during phase transition be seen in simulation? Can diffusion times be replicated? What is the influence of the size of anesthetics? How to explain the different potencies of chiral anesthetics? Does anesthetics have preferred sites of attachment? How do anesthetics affect permeability and compressibility? These are just a few question that would be very interesting to answer.

To answer these questions, a long programming period was spent on establishing the basic concepts of what was needed in this expanded Nielsen-model. And even more time on fitting the new parameters introduced. Firstly, the lipids needed to be able to move around freely and to change size according to their phase. This prompted an interaction formula for the lipids and that the size of the system needed to be able to change. Inspiration was taken from the Nielsen-model [35]. The resulting Gibbs free energy equation consists of contributions from the lipids melting,  $\Delta G_{melting}$ , interaction between neighboring

lipids,  $\Delta G_{interaction}$ , and energy of area change,  $\Delta G_{area}$ :

$$\begin{aligned}\Delta G_{total} &= \Delta G_{melting} + \Delta G_{interaction} + \Delta G_{area} \quad (2.4.10) \\ \Delta G_{melting} &= \Delta H_{melting} - T\Delta S_{melting} \\ \Delta G_{interaction} &= \Delta N\omega + \Delta \sum \gamma f_{LJ}(a, r) \\ \Delta G_{area} &= p_A \Delta A - RT\Delta \ln(A)\end{aligned}$$

$\Delta H_{melting}$  and  $\Delta S_{melting}$  describes the melting enthalpy and entropy *not* associated with movement and area change - that is primarily the melting of the lipid chains.  $N$  is the numbers of interactions between neighboring gel and fluids, where  $\omega$  denotes the interaction of neighbors not associated with moving and melting.  $\gamma f_{LJ}(a, r)$  represent the in plane interaction between lipids, to be described in detail later,  $p_A$  is the lateral hydrophobic pressure in the membrane and  $\Delta A$  is the change of area of the system.

The Bastard model can be thought of as little cylinders representing the lipids, as it is depicted in figure (2.12).

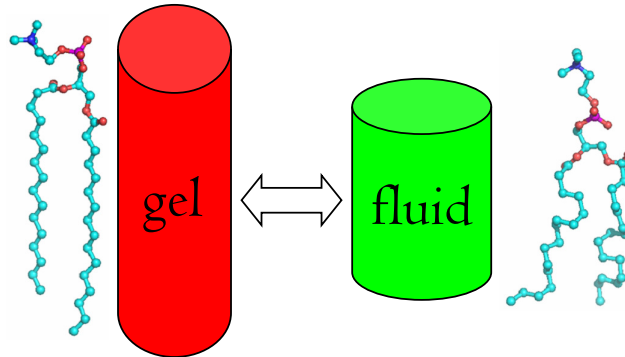


Figure 2.12: In the Bastard model lipids are represented in the simulation by little cylinders. These 'artificial lipids' change their area during phase transition to mimic real lipids.

When 'melting' the cylinders change area with the same ratio as DPPC. These 'artificial lipids' are then let loose to move around and interact with each other according to the Gibbs free energy equation (2.4.10).

The  $\Delta G_{melting}$  is in the cylinder picture equivalent to the free energy needed to change from a tall thin cylinder to a small wide, if it had no neighbors. The  $\Delta G_{interaction}$  are divided into two interactions:  $\Delta \sum \gamma f_{LJ}(a, r)$  is the way the cylinders 'feel' the distance between them. And  $\Delta N\omega$  is how they 'see' the height difference.  $\Delta G_{area}$  regulates the size of 'the playground' for the cylinders.

The Bastard model is as before mentioned loosely based on the Nielsen-model, which represents the interaction of nearly free moving lipids with a two-step model that approximates a Lennard-Jones potential. The Bastard model uses a full Lennard-Jones potential to evaluate interaction of freely moving lipids.

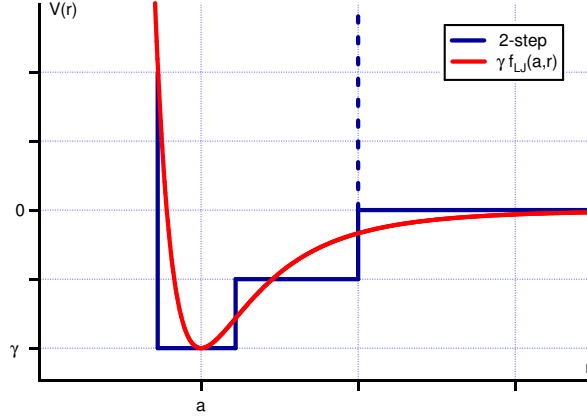


Figure 2.13: Lennard-Jones potential and 2-step approximation of same. These potentials ensure that the favorable position of 'lipids' in the simulation, is right next to their neighbors – thus mimicking the lipophilic behavior of lipids. When a lipid move, this interaction potential will be evaluated for each of its neighbors.  $\gamma$  is the strength of the potential.  $r$  is the distance between the centers of lipids. And  $a$  is the combined radius of the two neighboring lipids,  $a = r_1 + r_2$ . Fractured line represent cut-off in the Nielsen-model.

The reason for choosing the Lennard-Jones potential is its simplicity:

$$f_{LJ}(a, r) = \left( \left( \frac{a}{r} \right)^{12} - 2 \left( \frac{a}{r} \right)^6 \right) \quad (2.4.11)$$

where  $r$  is the variable and  $a$  is a parameter that gives the location of the minimum. The lipids interact by means of this potential, i.e. two lipids approaching each other will have their distance between centers,  $r$ , and their combined radius,  $r_1 + r_2 = a$ , evaluated. With this approach the favored position of two lipids will be exactly next to each other. The proximity of the lipids mimics their natural lipophilic behavior; however, if the strength of  $f_{LJ}$  given by the parameter  $\gamma$  is too strong, the membrane will attain crystalline structure above, as well as below the melting temperature. A crystalline structure above the melting point is not desirable, since it is well known that the diffusion constant in gel compared to fluid state vary by orders of magnitude [57].

The introduction of moving lipids leads to some grave considerations on their interactions. In the simple statical grid simulation the interaction energy,  $\omega$ , is the only unknown variable. This interaction energy is equivalent to the hydrophobic pressure felt by lipids, which have not fully screened their hydrophobic parts.

The free movement in the Bastard model introduces two new parameters namely the strength of the Lennard-Jones-potential and a lateral pressure in the system -  $\gamma$  and  $p_A$ . These two unknown and presumably not theoretically deductible variables make up for the total lateral hydrophobic pressure. Whereas  $\omega$  represent the remaining interactions with neighboring lipids, primarily consisting of the vertical hydrophobic pressure, see figure (2.14).

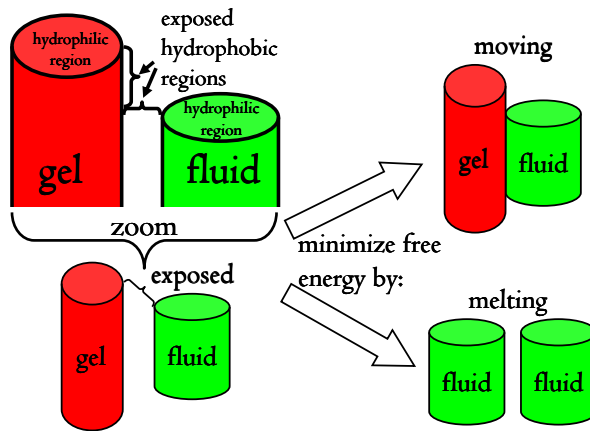


Figure 2.14: When neighboring lipids are of different state, or not situated next to each other, they expose hydrophobic regions to the water surrounding the membrane. The lipids can reduce this exposure by moving closer to each other and/or changing state. Reducing exposed regions in the simulations is to minimize Gibbs free energy, represented by  $\Delta G_{interaction}$  in equation (2.4.10). The horizontal interaction is represented by a Leonard-Jones potential depicted in figure (2.13). The remaining interactions are represented by the interaction energy  $\omega$ , these are primarily the vertical exposed regions.

The lateral pressure,  $p_A$ , serves an extra purpose, namely to prevent the system from exploding. That the membrane tends to expand if no pressure is present is an entropic effect, represented by the term  $RT\Delta \ln(A)$ . A larger system makes more space/states available for the lipids thus increasing entropy. *In vivo* the membrane does not explode, again because of the lipophilic nature of the lipids. In the Gibbs free energy equation the lipophilic behavior is given by the hydrophobic pressure term,  $p_A\Delta A$ , which prevents the system from uncontrollable expansion. And  $\gamma$  which keeps lipid neighbors close.

In effect:  $\gamma$  together with  $p_A$  are parameters to adjust the 'tightness' of the membrane - the larger  $p_A$  and  $\gamma$  the less movement of the lipids.

In equation (2.4.10),  $\Delta G_{melting}$  resembles the first two terms of the static grid model (Eq. 2.4.6), but since the translational energy and the energy of area change have been expressed explicitly, the relations of these parameters at  $T_m$

are

$$\Delta H = \Delta H_{melting} + \Delta \sum \gamma f_{LJ}(a, r) + p_A \Delta A \quad (2.4.12)$$

$$\Delta S = \frac{\Delta H}{T_m} = \Delta S_{melting} + R \Delta \ln(A) \quad (2.4.13)$$

with  $\Delta H$ , and  $\Delta A$  being experimentally determined,  $\Delta S_{melting}$  can be derived from (2.4.13), and (2.4.12) sets boundary conditions for the unknown parameters  $\Delta H_{melting}$ ,  $p_A$  and  $\gamma$ . That  $\Delta N\omega$  is omitted from eq. (2.4.12) is given the same arguments for omitting it in eq. (2.4.7).

When lipids melt, they change their size, as mentioned in Sec. (1.2). The influence on this size-change on the simulated system was of great concern. Therefore, as the program developed, two different approaches emerged which combinatorial gave rise to four different program behaviors. The first was whether to use a 2-state or a continuous melting behavior of the lipids. The second was whether size should influence melting or not - a decoupling of the parameters.

The reason for creating these different variants was to explore how the interaction parameters influence especially the melting point and the equilibration time. Decoupling parameters in practice is to evaluate parts of the energy equation in separate turns.

The first behavioral type is the most similar to the regular 2-state static grid Ising model, in the sense that it is 2-state and that melting is only dependent on neighboring lipids state. Movement of the lipids is evaluated only on basis of the distance to neighboring lipids.

The second behavioral type is 2-state with coupled area and melting, that is the full free energy equation (2.4.10) is evaluated for every state change.

The third and fourth behavioral types are similar to the first two except that the lipids may change state in a continuous manner, which is done by multiplying the  $\Delta G_{melting}$  term with a fluidization parameter,  $f$ , ranging from 0, gel state, to 1, fluid state. And also letting the radius a lipid being proportional with this parameter,  $r_{lipid} = r_{gel}(1 + f\Delta r_{gel \rightarrow fluid})$ , as seen in figure (2.15).

It seems obvious that a 2-state system should equilibrate faster due to the fewer possible states. However, this advantage might be offset if lipids of gel state have no space to expand into fluids. If membrane surrounding a lipid is in relative equilibrium – fitting tightly around the lipid – then expanding fully at once becomes less plausible. In this case it might reduce simulation time to decouple the phase change from the spatial interactions.

When lipids can change continuously to any size, it might however speed up the simulation to couple size and melting. When the overall area changed by small amounts, the system will be driven towards equilibrium much faster by added incitement from the coupled interactions.

In the data section (4.2) results will be presented for the 2-state with detached energy of movement and the continuous melting with attached energy of movement model.

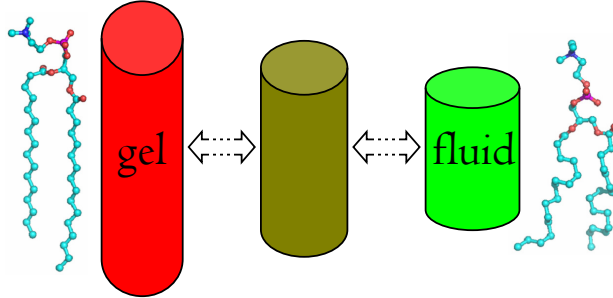


Figure 2.15: In the bastard model lipids are represented in the simulation by little cylinders. These 'artificial lipids' change their area during phase transition to mimic real lipids. This can be done as a 2-state model depicted in figure (2.12), or continuously as in this figure.

If diffusion of single lipids is not desired to track, introducing a switch move similar to the one used in static grid simulation drastically lower simulation times. If fluctuations have been measured in previous simulations, information on fluctuations may be used to introduce a multiple switch mode to further decrease simulation time.

A multiple switch mode could be defined as follows: For a given temperature,  $T_1$ , the fluctuations in the number of particles in a given state is known from previous simulations,  $NF(T_1)$ . When running a similar simulation let the program find a random number,  $1 \leq x \leq \frac{1}{2}NF(T_1)$ , of lipids to switch. The upper limit of  $\frac{1}{2}NF(T_1)$  is an estimation, and should be optimized by experiment.

The ideal use for a multiple switch algorithm is to run an initial simulation with few temperature steps and then interpolate a fluctuation function,  $NF(T)$ . Then the simulation can be repeated in greater detail and fast by implementing the algorithm. Another use may be when observing a shift in the phase transition, either by anesthetics or pressure. After one simulation, a predicted shift can be calculated, which may be more rapidly verified by using the multiple shift algorithm.

Since the multiple shift algorithm is only proposed and was never implemented, the effectiveness can only be estimated. Based on the experience that the single switch mode speed up simulation by an approximate factor 10, a cautious estimation is that the multiple switch algorithm may reduce simulation time by a factor of 2-10.

The program is structured to easily implement rotational freedom and thus explore effects of chirality, in particular domain formation of lipids and potency of stereo-isomer drugs. This extra degree of freedom was never activated due to time issues. Also one extra degree of freedom would further slow the program, which was already no less than a factor of ten slower than the traditional 2-state static grid.

Experiments have shown [12] that the membrane becomes more permeable to ions during the phase transition. It is speculated that this is due to structural defects (holes) that arise around domain boundaries, because of the different sizes of the gel and fluid lipids. This should be readily observed from the fully developed bastard model, but no area analysis was done on the preliminary results of this thesis.

Implementing anesthetics of different size and tracking them in the membrane is also a build-in feature of the program that was never activated. It was speculated that anesthetics would adhere in the region around domain boundaries due to the structural defects.

Upon a fine tuning of the parameters there is possible even more information retrievable by this bastard model. This is to be seen in future experiments.

# Interlude

In summary, this master thesis intends to contribute to the literature by showing a possible new path of nerve research. So far, theoretical and experimental arguments for dismissing the old theory of Hodgkin and Huxley have been presented, along with reasons to adapt a membrane and thermodynamical model of nerves. Since much data has already been shown against the Hodgkin-Huxley Model, no more will be produced within this master project. The goal is to show how anesthetics will be fitted into a membrane model, and therefore data has been produced to investigate this claim.

The experimental setup will be thoroughly explained in the next chapter, but in short experiments are conducted on artificial nerve membranes and the bastard simulation model is set loose.

(During this thesis an idea of testing anesthetics on flowers came up. Anesthetics should by principle affect all kind of movement, and flowers also moves. It was intended to anesthetize tulips, since they open as a response to heat. However, no previous experiments has been done on this, so the anesthetic dose needed was not known. The experiments on flowers resulted either in dead flowers or a happy girl friend. So if anyone tries to replicate these experiment: Placing tulips in 2mM concentration of Octanol in tab water – does not influence the life of tulips, and they can afterward be happily handed over to acquaintance of appropriate sex. Injecting more than .01 cc Propofol into the neck of tulips - results in dead of the tulips, seemingly by dehydration.

During the writing of this thesis an idea of putting pretty flowers in an Interlude came up...)

# Chapter 3

# Methods and Materials

All experiments were carried out at the membrane laboratory rooms Kk4 and PK5-6 at NBI. All equipment were carefully cleaned no less than one time before and after experiment with milliQ water ( $>18\text{ M}\Omega$ ) and 99% ethanol, then dried with gaseous nitrogen.

*...let us remember that chloroform does not act solely on the nerve tissues. Far from that, it has an action on all the tissues and attacks each one at a time which is a function of its susceptibility... An anesthetic is not a special poison for the nervous system. It anesthetizes all the cells, numbing all the tissues, and stopping temporarily their irritability... We can study elsewhere than in the central nerve cells the phenomenon which causes this stoppage of action and... It is permissible to assume that something similar happens in the nerve cell.*

Claude Bernard  
Leçons sur les anesthésiques et sur l'asphyxie, 1875 [16]

### 3.1 Differential Scanning Calorimetry

*Turn up the heat.*

The thermodynamical properties of DPPC vesicles was investigated on a differential scanning calorimeter (DSC).

The DSC used was a MicroCal Inc. VP-DSC. The differential scanning calorimeter function by controlling and thereby measuring thermal energy. As seen on figure (3.1), the DSC consist of two chambers, which holds a sample and a reference liquid solution. When the sample is DPPC in buffer, the reference will be the buffer.

The two chambers are individually heated and connected by a thermocouple. When heating the thermocouple controls the effect of the heaters,  $P_{1,2}$ , so that the temperatures of the two chambers are the same. The difference in added heat,  $\Delta Q$ , can then be determined:

$$\Delta Q = \Delta P \Delta t \quad , \quad \Delta P = P_1 - P_2$$

Where  $\Delta t$  is the time of the heating. The chambers are kept under constant pressure,  $\Delta p = 0$ . So from the differential form of enthalpy,  $\Delta H$ :

$$\begin{aligned} \Delta H &= \Delta Q - V\Delta p \\ &= \Delta Q \end{aligned}$$

And since  $\Delta Q$  is known from measurements, the heat capacity,  $c_P$ , can be derived from its definition:

$$c_P \equiv \frac{\Delta H}{\Delta T} = \frac{\Delta Q}{\Delta T} \quad (3.1.1)$$

Where  $T$  is the temperature.

The samples for the DSC is prepared as explained in the following paragraphs.

#### 3.1.1 DPPC vesicles

The primary target of investigation is DPPC vesicles. These are produced from pure DPPC lipids (Avanti Lipids, [avantilipids.com](http://avantilipids.com)) according to the following recipe.

1. DPPC is thawed in unopened container, to room temperature.
2. Thawed DPPC is dissolved in buffer (10 mM Hepes, 1 mM EDTA buffer with pH = 7.0) at app. 45°C, until no visible clumps.



VP-DSC

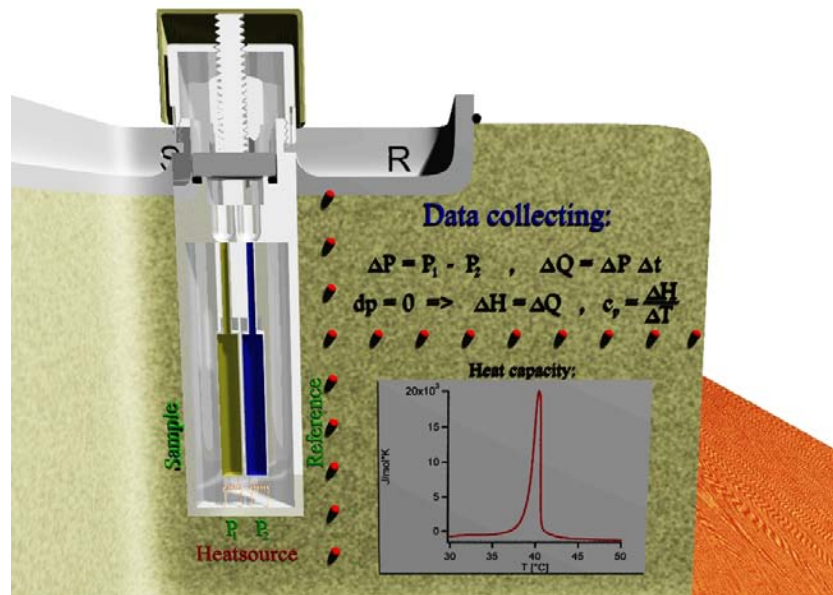


Figure 3.1: Interpretation of the inside of the Differential Scanning Calorimeter (DSC), with heat capacity profile obtained from DPPC. The DSC consist of a sample and a reference chamber, who are individually heated to the same temperature. Since experiments are conducted at constant pressure, difference in effect from heating,  $\Delta P$ , can be used to derive heat capacity.

3. The dissolved DPPC is extruded at 50°C at least 30 times.
4. Extruded DPPC is kept at 5°C when not used, and have a duration period of approximate two weeks.

Thawing DPPC before opening is to prevent it from absorbing water from the air, which would cause it to change molecular mass and clump.

The buffer contains Hepes, which act as a pH-buffer, and EDTA, which acts as a Ca<sup>2+</sup> buffer. The pH-value is adjusted in the buffer to 7.0, the buffer is important since melting points in charged lipids are heavily influenced by ions. The buffer can to great advantage be produced in bulk amounts since it is durable for at least one year.

Without extrusion the above recipe will produce multi-lamellar vesicles (MLV), where membrane layer upon membrane layer form onion like structures with total size of order 1-10 μm, they are characteristic by a large cooperativity in the melting region - and therefore have a very narrow heat capacity profile.

All of the experiments conducted during this project were done on large uni-lamellar vesicles (LUV), which are vesicles of one bilayer. Extruding is the means by which this cell-like structure is achieved. Extruding the DPPC-vesicles are basically pressing them repeatedly through a filter with pores of 100 nm (purchased from Avestin Europe, Mannheim Germany), this is repeated at least 30 times by a homebuild machine in our lab, as seen on figure (3.2).

The duration period of the DPPC-LUV lipids is given by an aggregation time, the small vesicles will fuse back together to MLV and thereby losing the special characteristics of a single bilayer which are of concern in this thesis.

### 3.1.2 Anesthetics

The anesthetics were added to DPPC in two distinct ways. One was simply dissolving the anesthetic in the buffer and then follow the recipe given above. This method has the advantage that the small concentrations needed could be easily obtained by dissolving in large amounts of buffer and then further dilute by addition of pure buffer. The anesthetics who were prepared with this method was: Octanol, Bupivacaine, and Pentobarbital. (All anesthetics supplied by Sigma-Aldrich, sigma-aldrich.com) The disadvantage of this method is that many of the anesthetics are so hydrophobic that even small amounts are impossible to dissolve.

The second method of adding anesthetic to the DPPC is a little more intricate, and the procedure is as following:

1. Make a 2:1 solution of methanol:di-chloro-methane.
2. Add anesthetic and dilute to desired concentration.
3. Mix with thawed DPPC and carefully heat to evaporate liquids.
4. Desiccate over night to fully extract methanol and di-chloro-methane.
5. Rehydrate with buffer.

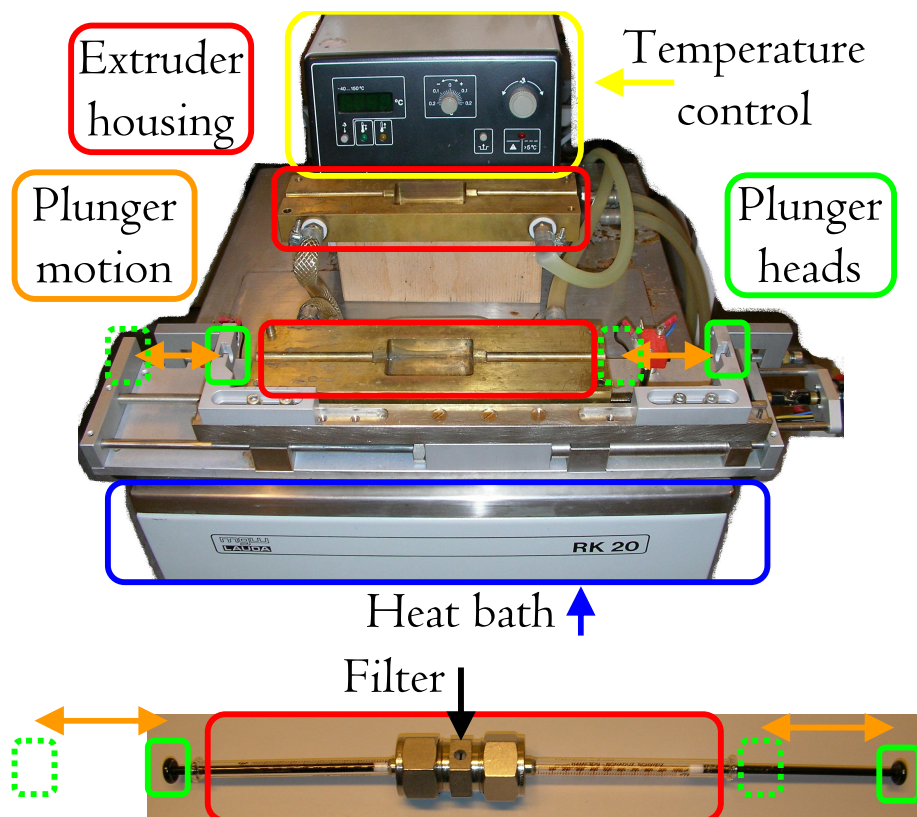


Figure 3.2: DPPC mixed in buffer self organize into multi lamellar vesicles. To obtain uni lamellar structure of the vesicles, they are extruded. This process is to repeatedly pressing the sample through a filter (bottom picture). The extrusion process is best done around phase transition temperature, therefore the sample and filter is placed within a brass housing connected to a heat bath (top picture). Plunger heads are placed in holders which are electronically controlled, they move with a frequency of 1 cycle per minute.

### 6. Extrude

This method was used only with anesthetics with low evaporation pressures, as to avoid evaporation during exsiccation. The anesthetics who were prepared with this method were: Lidocaine and Propofol.

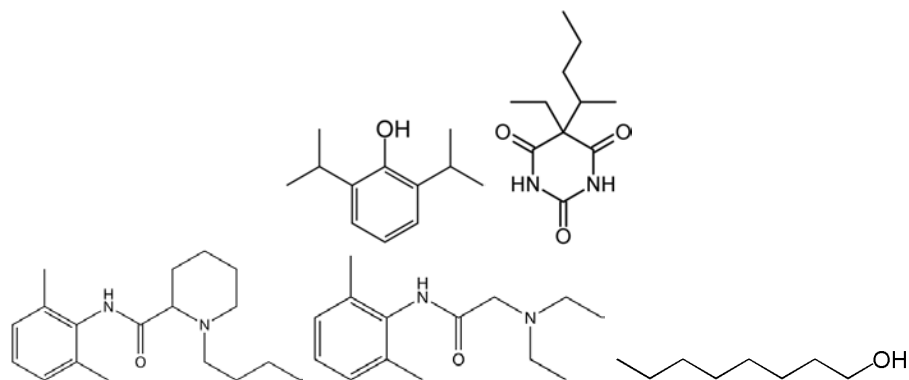


Figure 3.3: Molecular structure of the anesthetics. (From top left) Propofol, pentobarbital, bupivacaine, lidocaine, 1-octanol. Diagrams from Wikimedia used under GNU License.

Anesthetics were chosen with following argumentations:

**Octanol** is used in many experiments with regard to anesthetics and partition coefficients. The isomer used throughout the thesis is 1-octanol, as it is both the most common and most used in literature.

**Propofol** is a general anesthetic in daily use at most hospitals. Was introduced in the late 1970s.

**Pentobarbital** is part of the barbiturate group, which is a large group of widely used anesthetics. Pentobarbital is also an often used drug for euthanasia.

**Lidocaine** is a local anesthetic the active ingredient in a multiple of medical creams, and used in combination with general anesthetics in full body narcose, as many general anesthetics induce local pain. First synthesized in 1943.

**Bupivacaine** A stereo-isomer, originally it was intended to examine chirality importance of anesthetics. Bupivacaine has been replaced in human medicine, but is still widely used by veterinarians, it was used widely as spinal block at labors.

### 3.1.3 Pressure cell

The pressure cell is an addition to the MicroCalorimeter. It is a single capillary which is inserted into the sample cell of the calorimeter. The sample cell is previously filled with water to improve thermal contact with the pressure cell. The pressure is achieved with pure gaseous nitrogen. When using this setup



Figure 3.4: The pressure cell used in pressure experiments. To the right is the capillary which holds the sample. To the left is the head which is attached to pressurized nitrogen.

the introduction of a 'large' metal container in the calorimeter naturally affects the measurements. The pressure cell having a heat capacity of its own, is as best as possible deducted from presented data, and should be just a part of the baseline, since no phase transition occurs in the metal. However data indicates a much lower  $\Delta H$  for these measurements, this is not of vital importance, since  $\Delta H$  was established by other measurements and the property of interest is the shift of melting point. The presumed reason for the 'missing' enthalpy is that on regular scans as much as 95% of the sample is in the sample cell chamber, whereas this number may be as low as 30% for the pressure setup. The leftover percentages are in the capillary leading down to the chamber. The pressure cell is one long capillary, and as such only exposes approximately 30% of its surface in the sample cell chamber - thus leading to the lower measured  $\Delta H$ .

## 3.2 Photo-spectrometry

*Shine a light on me.*

In order to determine the partition-coefficients of the selected anesthetics in DPPC a series of experiments were conducted on a Perkin-Elmer Lambda 5 UV/VIS Photospectrometer. The Photospectrometer functions by sending electromagnetic waves through solutions at varying or fixed wavelengths, the intensity of the light is measured after passing the solution, and is compared to a reference solution.

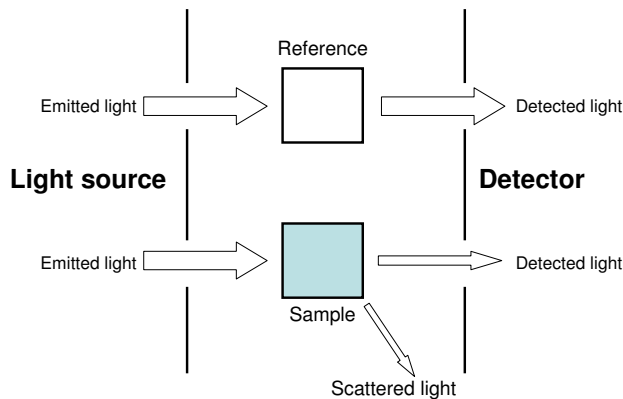


Figure 3.5: Schematic of Photospectrometer. Light is send through a reference and a sample solution. Concentration difference between solutions can then be determined by using Guilan-Berret law, as higher concentrations scatter more light.

The idea was to measure the light-absorbance of varying concentration of the anesthetics in the buffer. From this experiment it should be possible to determine the concentration of anesthetics as a function of absorbance.

Then various concentrations of DPPC-LUV would be added and absorb part of the anesthetic, whereafter the sample would be centrifuged and the solution decanted and thus re-separated from the lipids. The solution would again be measured in the photospectrometer, and the amount of absorbed anesthetics could be deduced.

Note: When using the term "absorbed light" it refers to all light not reaching the detector, regardless of whether this light is absorbed by the medium, and then remitted in random directions, or being scattered by the physical properties of the molecules in the samples.

Unfortunately no results came of these experiments. For one group of anesthetics this was due to the fact that they are not dissolvable in the buffer in quantities that could be detected.

The rest of the anesthetics were measured but gave no clear results. There seemed to be no change in absorbance, no matter the amount of lipid added to the system. The absence of any result may be due to the separation process, the lighter density anesthetics might have been pulled from the lipids and back into the solution during the centrifuging, this is especially a problem since centrifuging could not be done while heating, so lipids might have cooled to below melting point thereby releasing anesthetics back into the solution. A suggestion to improve this experiment might be trying different separation methods such as filtering, or use a heated centrifuge.

In the appendix A.2 can be found a more thorough experimental guide and a theoretically calculated example on how to determine the partition coefficient if having good results.

### 3.3 Simulations

All simulations where written in Fortran 90 code by the author of this thesis. Source code can be obtained by mail. Runtime were provided by the Niels Bohr Institute - Machines were IBM with Intel processors running Linux. The compiler used was 'ifort' with the '-arch SSE2' specification. Total simulation time was no less than 8000 CPU-hours.

### 3.4 Data processing

Data was handled in Igor Pro ver. 5.03 using modules written by T. Heimburg and the author of this thesis.

T. Heimburg had written modules to determine baseline of DSC data, and calculate elastic properties. I have expanded these modules to locate melting temperatures and calculate solitons and their properties as function of velocity.

Unless other is specified all graphs in this thesis are produced using Igor.

As previously mentioned this thesis uses a numerical method to solve for solitons directly from data.

To solve the Soliton equation (2.3.4), compressibility was derived from data using equation (2.3.5) in the module build by T. Heimburg. Then integration was performed twice by the Runge-Kutta 4th order method.

Previous results by Jackson [1] were solved numerically for a polynomial fit of  $c^2$ . And analytical solutions of a polynomial fit of the sound speed can be derived, as shown by Lautrup and Ludu [26, 31]. To test the numerical solution routine and compare it to the analytical solution, following test was carried out: A data set was chosen. Data were polynomially fitted as required in equation (2.3.7), and then solved both numerically and analytically. Then resulting solitons can be compared as in figure (3.6).

From figure (3.6) it is evident that the numerical routine is strong - since

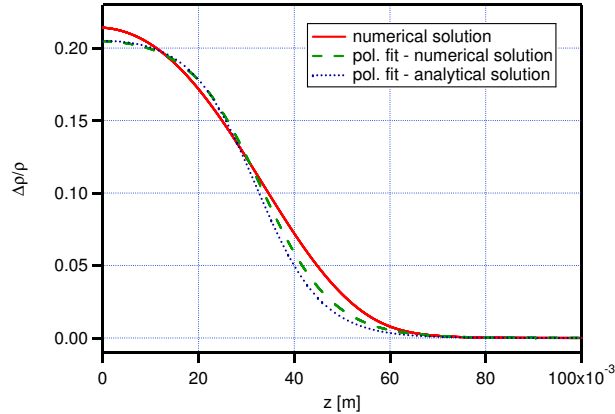


Figure 3.6: Comparison of half solitons calculated from same DPPC data by different methods. Sound speed is derived from heat capacity by equation (??), then numerically integrated directly from equation (2.3.4) (red solid line). Or derived sound speed is polynomially fitted, and then numerically integrated from equation (2.3.9) (dashed green line). Or analytically solved from the polynomial fit (dotted blue line) from equation (2.3.12). This comparison shows that solitons calculated by these three methods do not differ significantly. To obtain maximum amplitude the velocity used was  $v = 1.01 v_{limit}$ .

it reproduces the analytical solution from the polynomial fit. And that the polynomial approximation is acceptable - since the produced solitons do not differ from solitons generated directly from data.

### 3.5 Visualization

Many figures in this thesis have been produced by POV-ray. This is the 'Persistence of Vision Ray Tracer'™, which is a powerful visualization tool. That allows precise placement of objects. All snapshots of lipid simulations are made with POV-Ray. As figures can be generated from text files produced automatically by the Fortran program. Other figures made by POV-Ray are identified as such in their captions.

Figures not produced by Igor, POV-Ray or taken from others are made in Microsoft Office PowerPoint.

## Chapter 4

# Results

*Presenting data is the most important part of any experimental thesis. However the most valuable data is often not presented... Choosing data is like only picking your prettiest children to participate on Sunday dinner - even though bad data are the offspring of your shortcomings, and the driving force to do better, make you learn more and be a greater scientist.*

## 4.1 Calorimetry Data

This section will present the data obtained by differential scanning calorimetry.

All mentioning of DPPC refers to 10 mM extruded DPPC - large unilamellar vesicles in buffer prepared as described in Sec. (3.1).

The presented heat capacity profiles are not raw data, they represent the *excess* heat capacity of the phase transition - They show only the heat associated with the changing of phase in the lipids. The heat of 'heating' the lipids from prior till after the phase transition has been subtracted from the portrayed data. All theoretical considerations are done on the basis of excess heat capacity, therefore all data are presented as such, and all referring to heat capacity is implicitly to excess heat capacity.

The making of one heat capacity profile is referred to as a 'scan', since the calorimeter scans a given temperature range. The DSC can either start from a low temperature and scan up to a high temperature, this is called an 'up-scan', or start at a high temperature slowly cooling the sample - a 'down-scan'.

The reason to differ up- and down-scans is that a certain amount of hysteresis occurs in the measurements - the melting temperature is not the same for the two different scans. This is a time problem. Hysteresis can be avoided if scans are done slow enough, however since the DSC is valuable equipment, slow scans were not an attainable luxury. Scans were done at 5 K/h, to avoid hysteresis they need to be done at less than 1 K/h.

- *Scan time is money!*

Calorimetry scans and results are presented without error bars. In pure DPPC measurements the mayor systematic error is the extrusion process, in which the filter most likely retains some lipid, the amount in no way consistent, but data indicate that as much as 5% may have been lost in the filtering process. However a near similar percentage of anesthetics were most likely lost. Due to the small amounts being weighed off 3-5% is estimated to have retained on the weighing boat.

In effect the systematic errors are larger than any other errors. Results are given with only two deciding digits, since this was the precision of the weighing of primarily the small amounts of anesthetics. Systemic and other errors are mostly contained within the deciding digits.

### 4.1.1 DPPC

- *A first look*

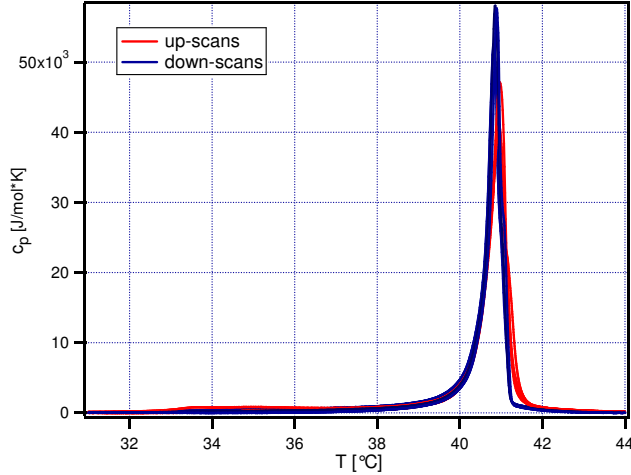


Figure 4.1: Excess specific heat capacity of the phase transition in DPPC-LUV. Heat capacity profiles varies, even for scans of the same sample, because of long relaxation times and hysteresis. Presented are eight scans of two samples.

As mentioned in section (2.1) the phase transition stretches over 10 K, this is not entirely evident from Fig. (4.1), so next figures zooms in on the features of the transition:

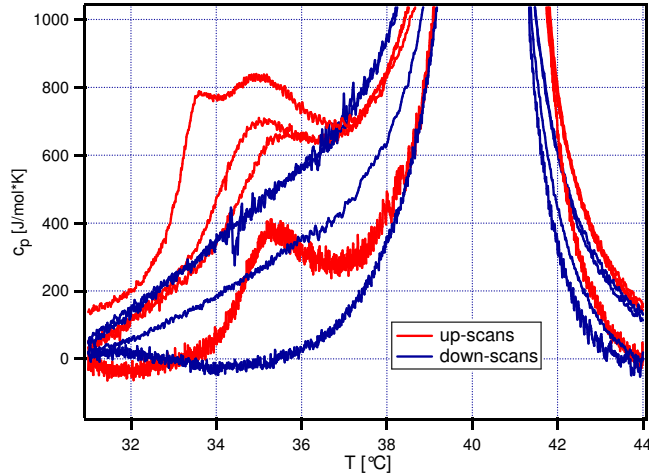


Figure 4.2: Zoom of fig. (4.1). Around 32–36°C a small bump is seen on the up-scans, this is the pre-transition. This feature of the phase transition is caused by a structural reorganization of the membrane.

The pre-transition, zoomed into on figure (4.2), is caused by a so-called

'ripple-phase', where the membrane displays ripple formation. The specific arrangement of the lipids are not known, but there are at least three different theories to explain it. One speculates that the solid phase has two states, one of which the head groups displays a 'kink', which favors repeated tilts in the membrane. Another explains the ripples by assuming that domain formation happens in a cooperative way between the inner and outer layer of the lipid bilayer, which would give rise to ripples. And a third suggest that in the phase transition it might be favorable for the lipid chains of the inner and outer lipid layer to pack, effectively nearly reducing the thickness of some of the membrane to half, causing the ripple phase. What is also remarkable of the pre-transition, is that at this scan rate it is only visible on up-scans. Which indicates that the organization that goes on is very slow, as it cannot happen on down-scans even within the 12 minutes it takes to scan across it. Therefore it must be primarily connected with the gel state, as it is only appears when going from gel to fluid state.

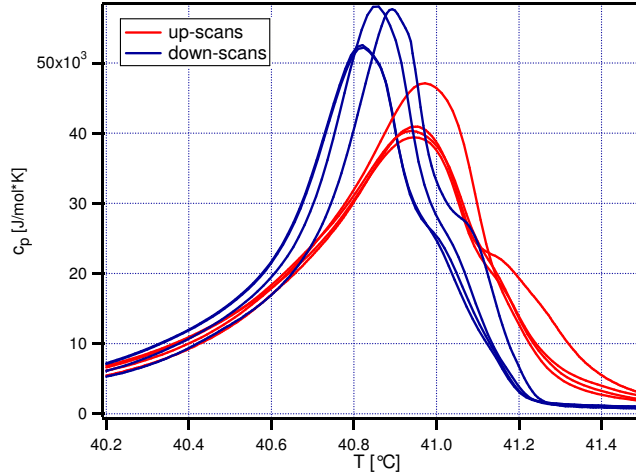


Figure 4.3: Zoom onto main-transition of fig. (4.1). The Upper Phase Boundary (UPB) is determined by extrapolating the slope of the heat capacity profile to intersect with 0. UPBs on this figure ranges between 41.25 and 41.50 degrees Celsius. From the displacement between up-scans and down-scans hysteresis is estimated to be 0.25K.

The large peak between 40 and 41°C is the main-transition, which marks the upper boundary of the phase transition and also makes up for more than 95% of the energy. It is therefore the prime investigated target in this thesis, and no further will be said of the pre-transition.

As derived in section (3.1) the total heat necessary to take the membrane through the phase transition can be expressed by the total change in enthalpy,  $\Delta H$ . The average value of  $\Delta H$  for the whole transition is determined to be 36 kJ/mol. This number is obtained by integrating heat capacity between 30 and 45°C.

From figure (4.3) hysteresis can be observed to be approximately 0.25K.

### 4.1.2 Anesthetics

Calorimetric scans of 10 mM DPPC with anesthetics. Anesthetic samples are referred only by their molar concentration the presence of DPPC is implied.

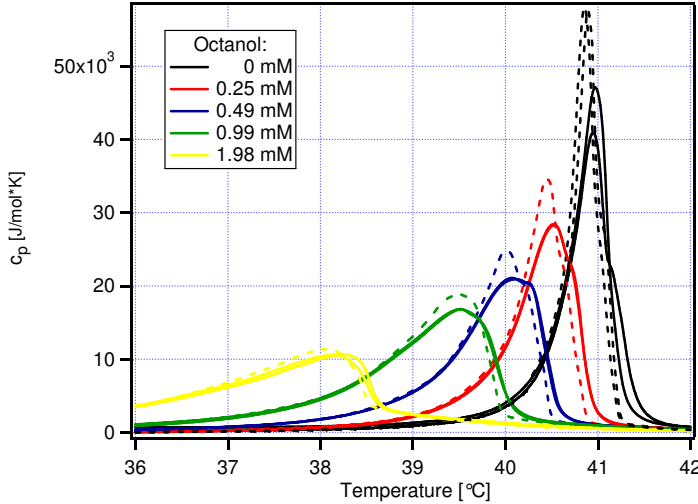


Figure 4.4: Heat capacity profiles of 10 mM DPPC with octanol. Solid lines are up-scans, dotted lines are down-scans. The anesthetic shifts the melting temperature and broadens the phase transition.

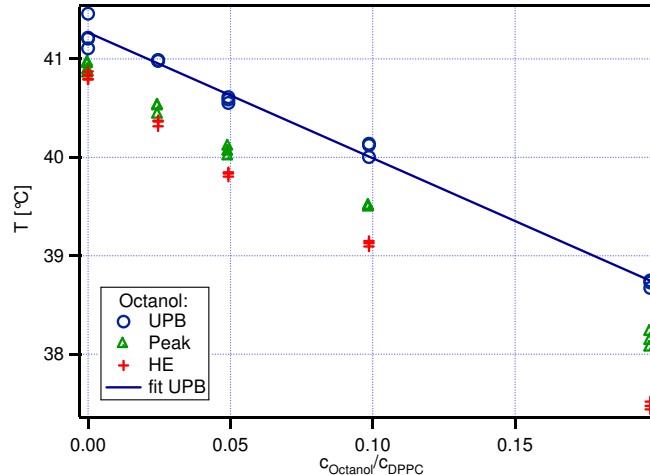


Figure 4.5: Melting temperatures of octanol from figure (4.4). The Upper Phase Boundary (UPB) is shifted linearly as derived in section (2.1.1). The broadening of the heat capacity profile is represented in the split of the different melting temperatures, as the Peak and the Half Enthalpy (HE) shift more than the UPB. Abbreviations are explained on page 58.

The legend in Fig. (4.5) and coming figures of melting temperatures refers to:

**UPB** Upper Phase Boundary: The temperature which is shifted according to regular solution theory, as derived in section (2.1.1).

**Peak** the temperature at maximum of the heat capacity profile.

**HE** Half Enthalpy: Halfway through the phase transition by measure of enthalpy, also the temperature were it for pure DPPC is equally likely for a lipid to be in gel or fluid state.

**fit UPB** Linear fit of Upper Phase Boundary.

As mentioned in Sec. (2.1.2) the fitted slope determines the partition coefficient of the anesthetic by equation (2.1.10). The results are displayed in Table (4.1).

	-[K]	$R^2$	$P$
Octanol	12	.991	150
Bupivacaine	5.1	.956	39
Lidocaine	0.79-3.1	.155-.978	4.9-21
Pentobarbital	5.4	.970	42
Propofol	3.0-6.7	.680-.888	20-49

Table 4.1: The first data column contains the fitted slopes of upper phase boundary from data presented in this section. With  $R^2$  being the square of the correlation coefficient,  $R^2 = 1$  denotes perfect linear behavior. Partition coefficients,  $P$ , are calculated from equation (2.1.10), where  $c_{\text{Anesthetic}}/c_{\text{DPPC}} = x_A$ . For calculating  $P$  the found  $\Delta H$  of 36 kJ/mol was used.

In table (4.1) the calculated partition coefficients as derived from data,  $P$ , are displayed. Some anesthetics have more than one, this is due to different fits of the data, which will be commented over the next pages, as data is presented.

From data on the following pages it can be noted that the anesthetic fraction  $x_A = c_{\text{Anesthetic}} / c_{\text{DPPC}}$  is as high as 1. In the section on melting point depression (Sec. 2.1.1), a low fraction of anesthetic in the membrane was used to approximate the logarithmic term. However, the approximation done in eq. (2.1.6) is on the mol% of anesthetics in the membrane,  $x_{AM}$ . Assuming 10 mol% anesthetic in the membrane, which gives an error of 5%<sup>1</sup>, results in  $\Delta T = 2.3\text{K}$ . None of the anesthetics have data fitted for more than a 3K shift in melting temperature.<sup>2</sup>

---

<sup>1</sup> $\ln(1 - 0.100) = -0.105$

<sup>2</sup>which gives a 7% error in the approximation.

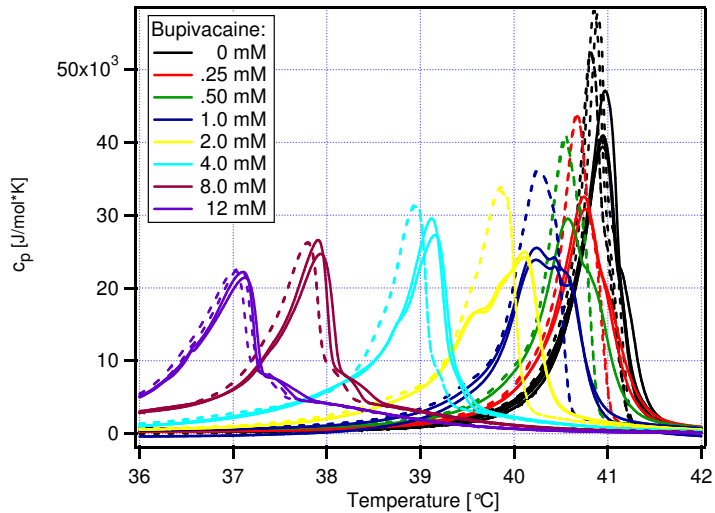


Figure 4.6: Heat capacity profiles of DDPC with bupivacaine. Solid lines are up-scans, dotted lines are down-scans. The anesthetic shifts the melting temperature and broadens the phase transition.

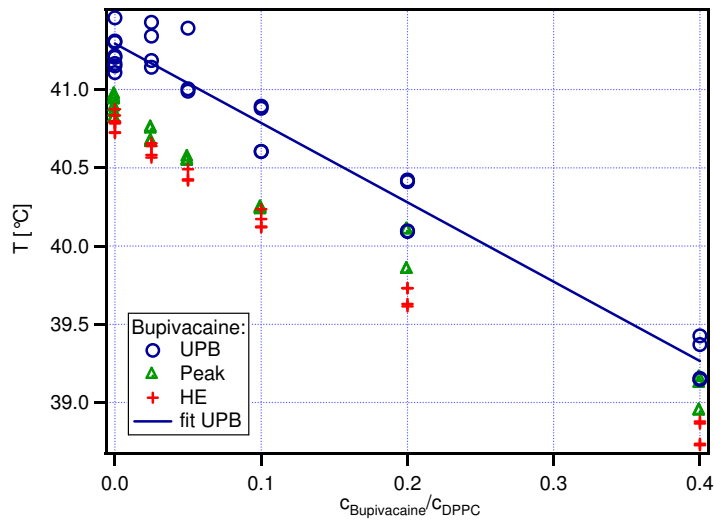


Figure 4.7: Melting temperatures of bupivacaine from figure (4.6). Anesthetic fractions of 0.8 and 1.2 are omitted from this graph and not fitted, because they exceed a shift in melting temperature of 3 Kelvin, thereby nearing the limit of the approximation made to make a linear prediction. (And indeed they do not fall on the fitted line.) Abbreviations are explained on page 58.

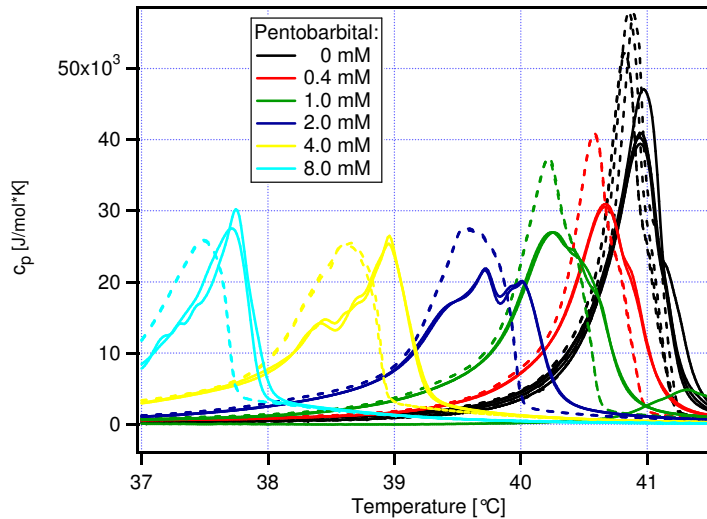


Figure 4.8: Heat capacity profiles of DDPC with pentobarbital. Solid lines are up-scans, dotted lines are down-scans. The anesthetic shifts the melting temperature. Pentobarbital also broadens the phase transition but not as much as octanol (Fig. 4.4 ).

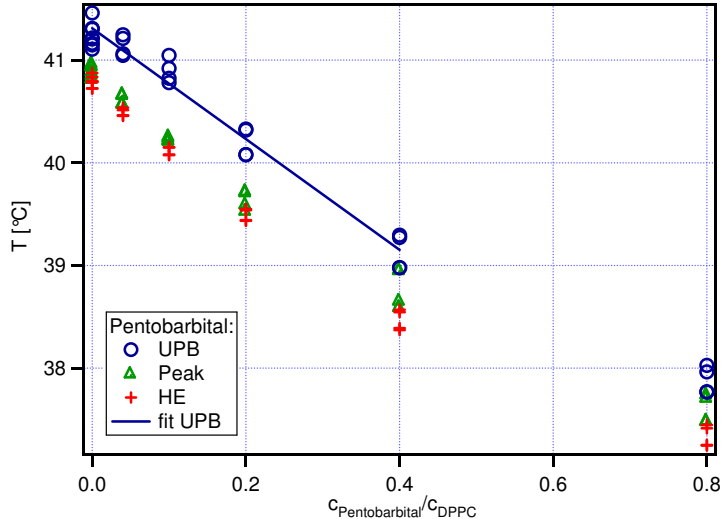


Figure 4.9: Melting temperatures of pentobarbital from figure (4.8). Only data within a shift of 3 Kelvin is fitted, because of approximations to derive equation (2.1.6). Abbreviations are explained on page 58.

Previous data sets of octanol, bupivacaine and pentobarbital were produced by making the highest concentration of anesthetic in buffer and then thinning before mixing with pure DPPC (See Sec 3.1.2). This ensures that even if some of the anesthetic is lost during weighing and mixing a linear dependence of concentration will still be revealed. The samples for propofol and lidocaine were made individually for each concentration, this gives less linear correlation. For this reason a minimum and a maximum slope were fitted on the data from propofol and lidocaine.

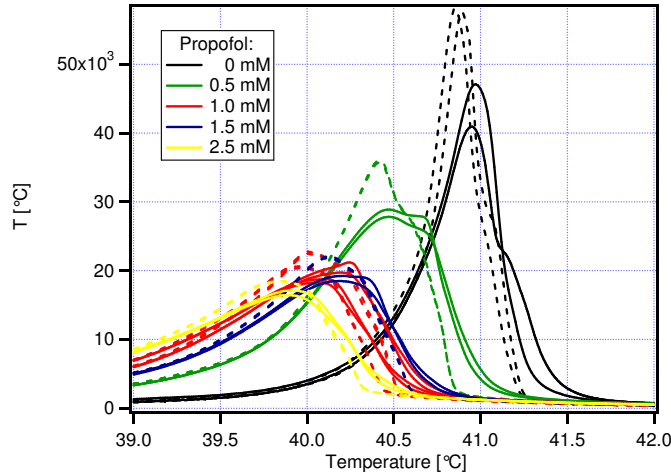


Figure 4.10: Heat capacity profiles of DDPC with propofol. Solid lines are up-scans, dotted lines are down-scans. The anesthetic shifts the melting temperature and broadens the phase transition, but seemingly only until a certain concentration is reached.

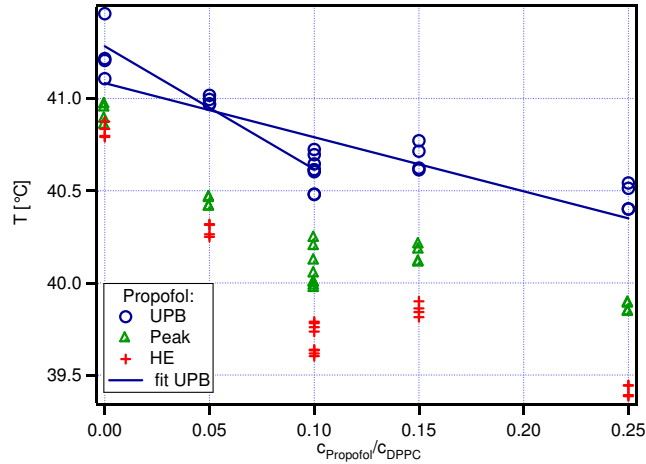


Figure 4.11: Melting points of propofol from figure (4.10). This data does not display a clear linear behavior, so multiple fits are made of the upper phase boundary (UPB). Abbreviations are explained on page 58.

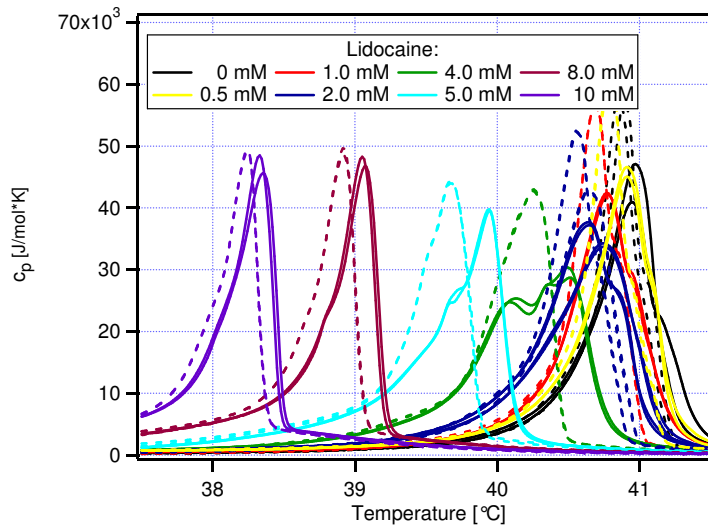


Figure 4.12: Heat capacity profiles of DDPC with lidocaine. Solid lines are up-scans, dotted lines are down-scans. Lidocaine shifts the melting temperature of the phase transition. But does not broaden the heat capacity profile significantly.

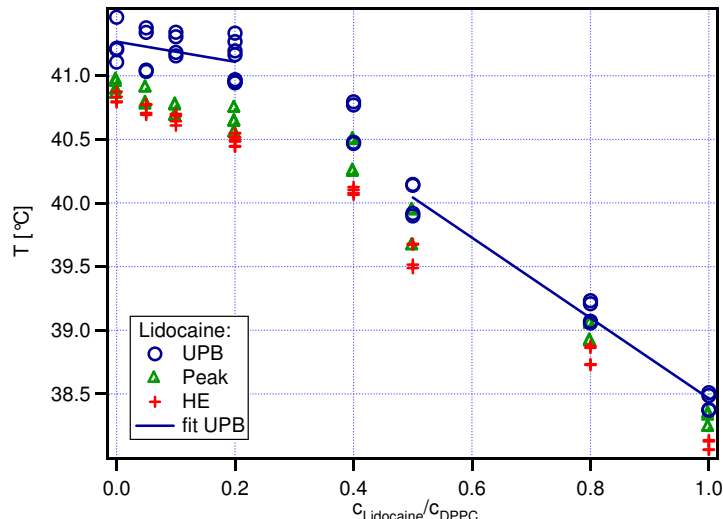


Figure 4.13: Melting temperatures of lidocaine from figure (4.12). The maximum and minimum slope linear fits are depicted. Abbreviations are explained on page 58.

### 4.1.3 Pressure

*Oh, the pressure.*

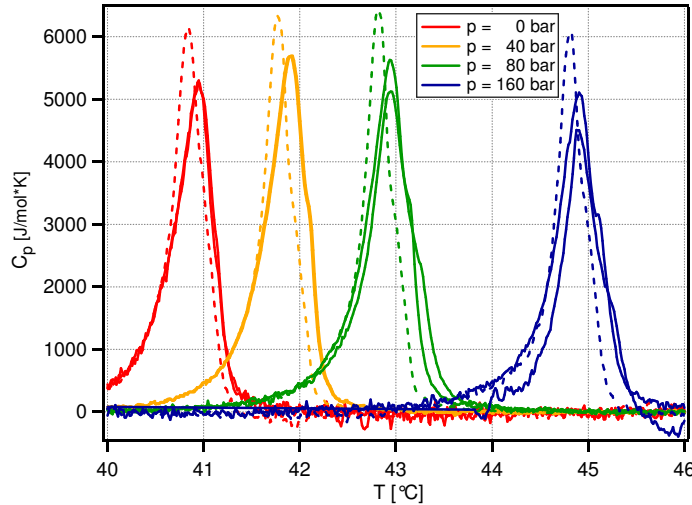


Figure 4.14: Heat capacity for DPPC as a function of pressure. Solid lines are up-scans, dotted lines are down-scans. Pressure shifts the melting temperature upwards without changing the shape of the profile.

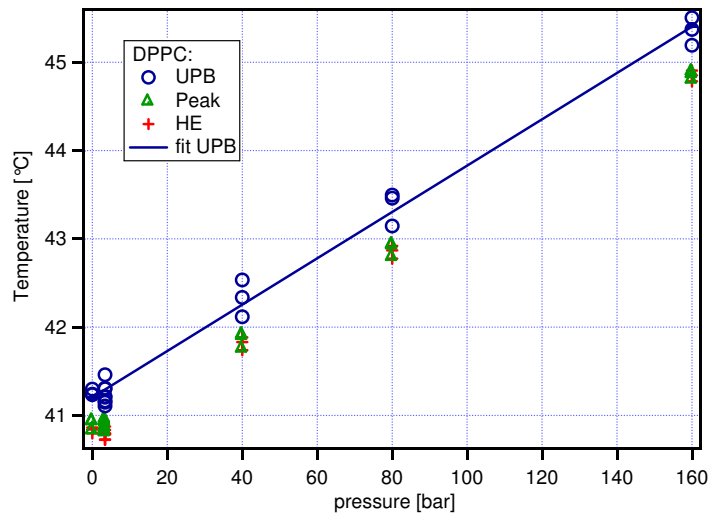


Figure 4.15: Melting points for DPPC as a function of pressure. Abbreviations are explained on page 58.

As mentioned in section (2.1.3) pressure moves the melting point of the phase transition in the opposite direction of anesthetics. Experiments were done for both pure DPPC and DPPC with added anesthetics, and in all cases the the result gave perfect linear behavior as seen in table (4.2).

The slope of the fitted data is given inversely, as this is gives the 'natural' way of thinking - becoming the 'amount of pressure [bar] to move the phase transition 1K'.

	mM	$[K/\text{bar}]^{-1}$	$R^2$
DPPC	10	39	.989
+ Bupivacaine	12	39	.985
+ Lidocaine	8.0	43	.998
+ Pentobarbital	8.0	40	.997
+ Propofol	2.5	42	.986

Table 4.2: DPPC and DPPC + the referred anesthetic were subjected to added pressures of 0-40-80-160 bar. This results in a shift in upper phase boundary of the phase transition. Column three shows that the pressure influence is independent of added anesthetics. And column four displays  $R^2$  which is the square of the correlation coefficient. As  $R^2 = 1$  denotes perfect linear behavior, these results are very close to being perfectly linear.

That the peak value and total size of the heat capacity profiles obtained with pressure differ from those without, is due to the experimental setup as described in section (3.1.3).

For Propofol:

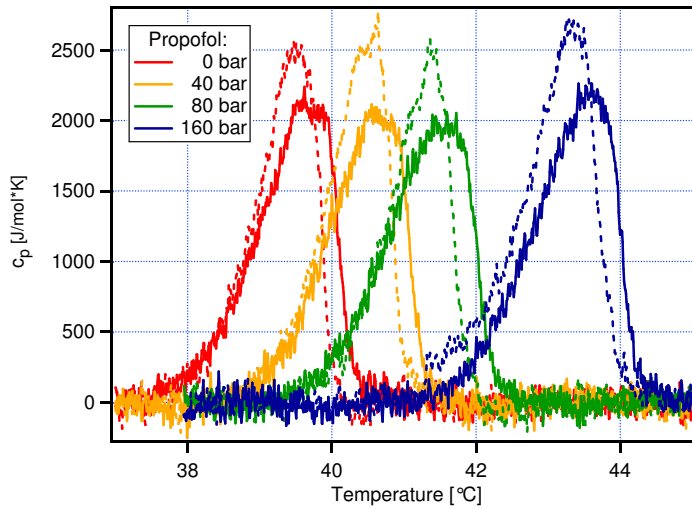


Figure 4.16: Heat capacity of 10 mM DPPC + 2.5 mM propofol with added pressure. Solid lines are up-scans, dotted lines are down-scans. Pressure shifts the melting temperature upwards without changing the shape of the profile.

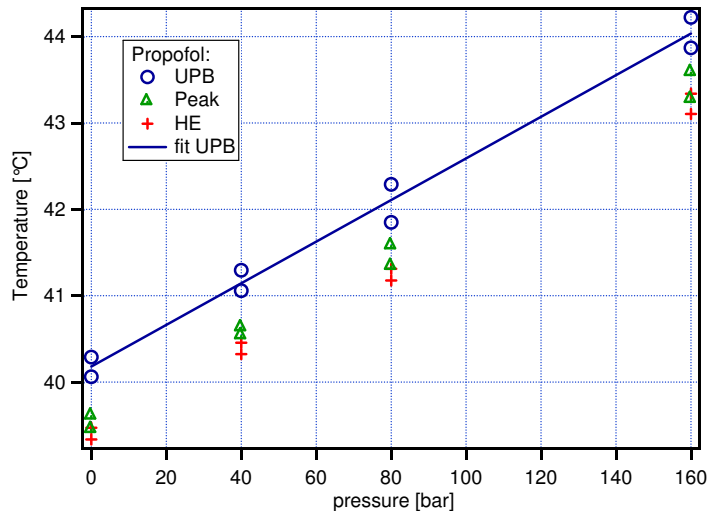


Figure 4.17: Melting points of DPPC and propofol as function of pressure from figure (4.16). Abbreviations are explained on page 58.

As evident from table 4.2 all pressure reversal behaves beautifully and therefore is a little repetitive, so the rest of the anesthetics can be found in appendix A.3.

## 4.2 Simulation Data

To compare the information retrieved from simulations, ordinary 2-state static grid simulation results will be presented before results from the Bastard model.

### 4.2.1 Static grid Ising-model

Since many of the membrane's most significant features is proportional to the heat capacity, see Sec. (2.3), The foremost result of the simulations is the heat capacity profile:

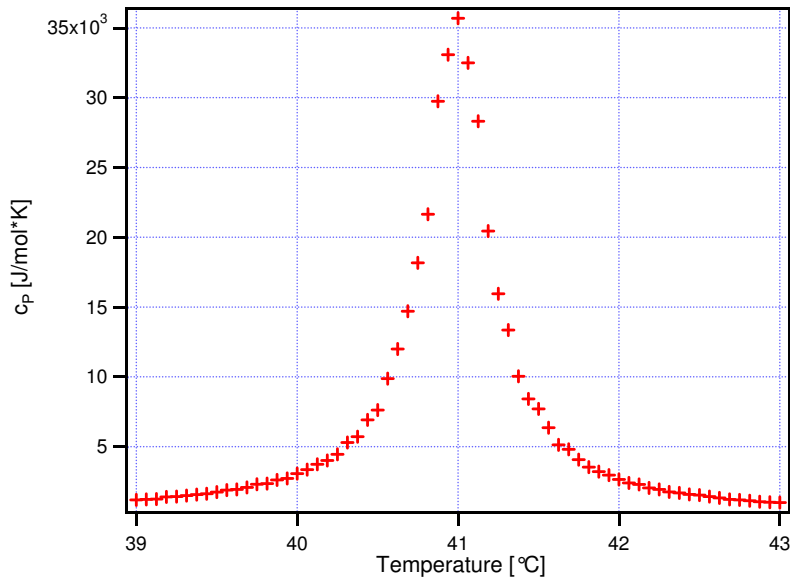


Figure 4.18: Heat capacity profile obtained with static grid model. 10,000 lipids 100,000 MCCT.

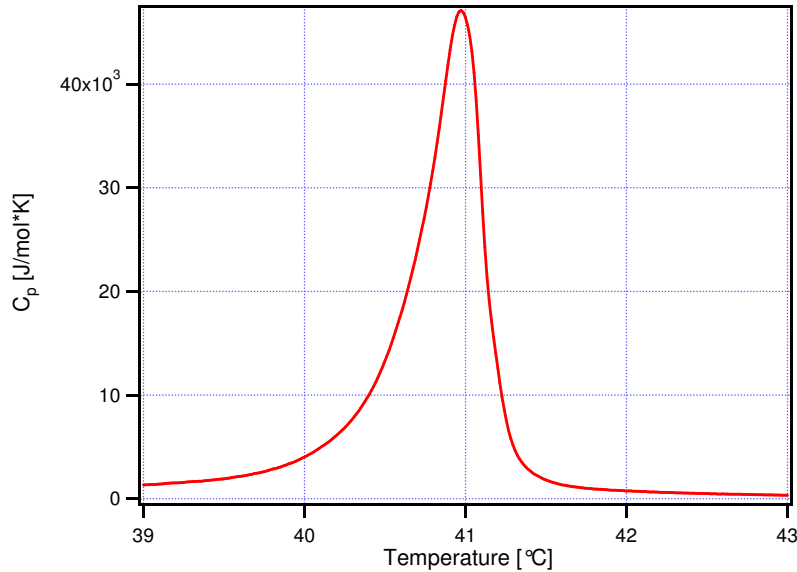


Figure 4.19: Heat capacity profile of DPPC obtained by calorimetric measurement (main transition).

Simulations have been adjusted so that the half width at half height and the integrated value of the heat capacity profile of the simulation is the same as the measurement. As seen from Fig. (4.18) and (4.19) this gives a slightly smaller max value, and a slightly larger base width of the simulated result, this discrepancy is caused by the simulation being inherently symmetric (See Appendix A.4).

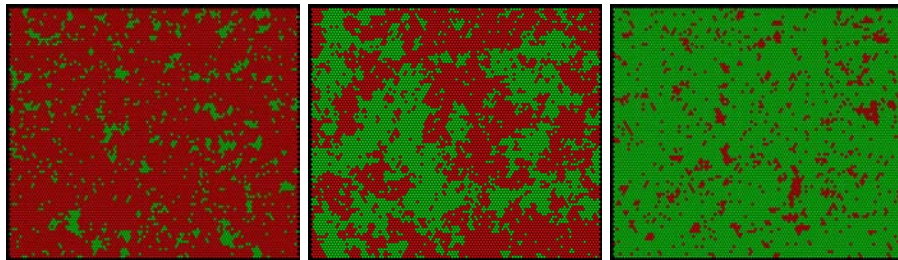


Figure 4.20: Snapshots of static grid simulation from figure (4.18) at 39, 41, and 43°C. Red circles represent gels, green fluids.

Very apparent from Figure (4.20) is also formation of domains in the phase transition. These domains are observed *in vivo* (Fig. 4.21) and if the simulations did not produce domains, they would be in fact worthless.

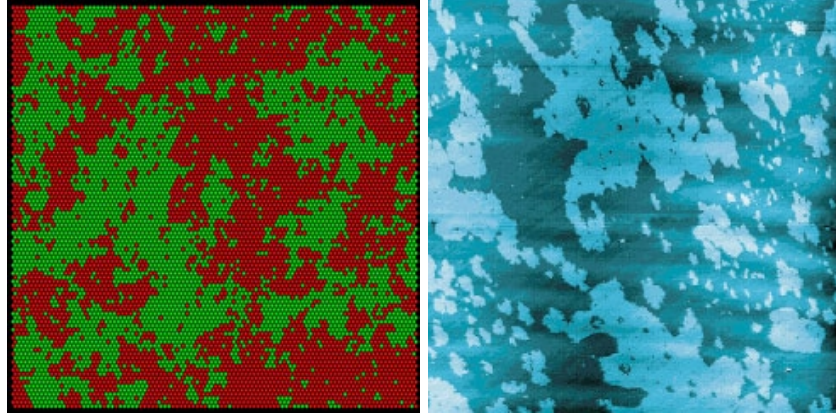


Figure 4.21: (left) Simulated lipids in the phase transition. (right) Atomic force microscopy of domains in DMPC membrane during phase transition by Nielsen [49]

Simulations were also done with anesthetics:

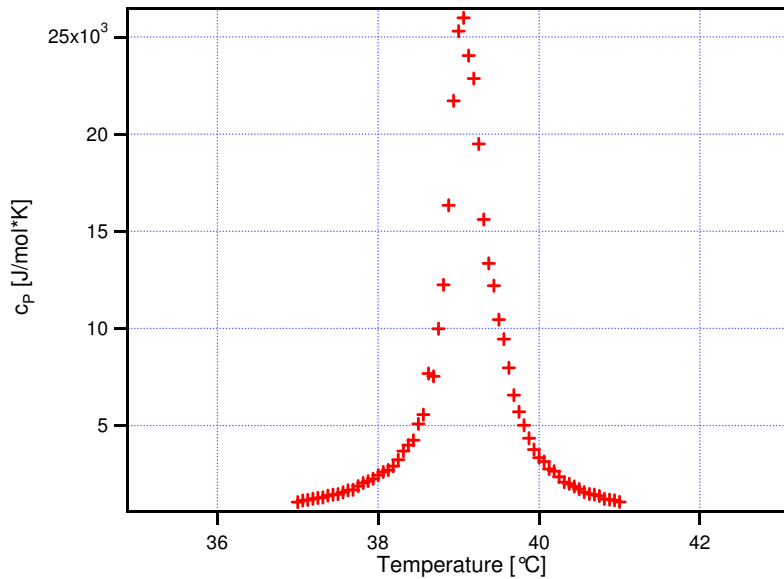


Figure 4.22: Heat capacity profile with 10 mol% anesthetic. 10,000 lipids 10,000 MCCT. Notice the shift in melting temperature from figure (4.18).

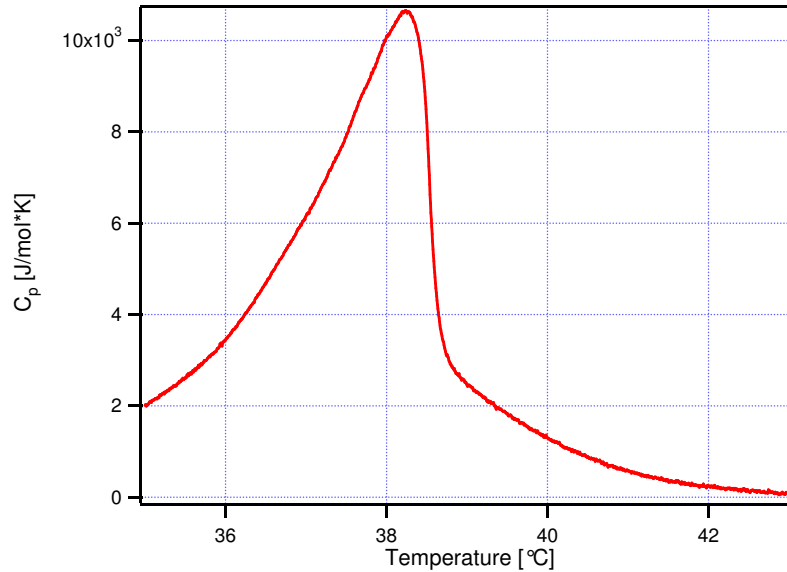


Figure 4.23: Heat capacity profile of DPPC obtained by calorimetric measurement with 1.98 mM octanol correspondent to  $\approx 12$  mol%. The difference between simulation (figure 4.22) and measurement is particularly the asymmetry and width of the heat capacity profile.

Notice the increased widening of the profile in calorimetric measurement, Fig. (4.23), is not fully replicated by simulation Fig. (4.22), also the asymmetry is more pronounced in calorimetric measurements. The theoretic shift in melting point as calculated by regular solution theory, Sec. (2.1.6), is for 10% anesthetic  $\Delta T = 2.3\text{K}$ .

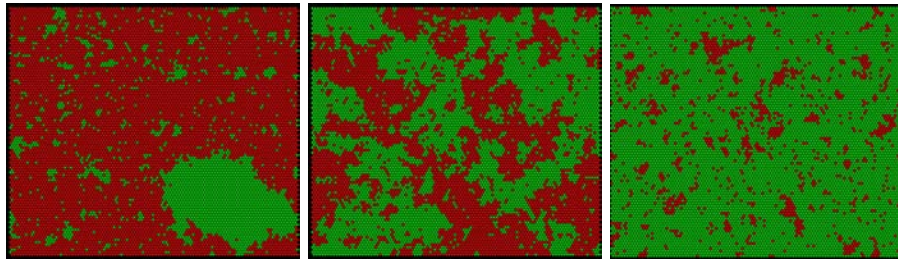


Figure 4.24: Snapshots of simulation with 10 mol% anesthetics at 37, 39, and 41 degrees Celsius. Red circles represent gels, green fluids. The picture to the left displays an artefact, where anesthetics help induce a fluid domain. A domain of this size is not stable for very long below the melting point.

These are the fundamental results gained from traditional Monte Carlo simulations of lipid membrane. From these it was learned that the cooperativity of the membrane can be attributed to the interaction of the single lipid with its

neighbors. And that this cooperativity is also the source of large scale domain formation. Furthermore, when assuming the eutectic model of phase behavior, the shift in melting temperature when adding anesthetics could be replicated, which indicates the validity of these model assumptions. For more in depth analysis of similar results see e.g. Blicher 2007 [47].

And so it is time for the results of the new model...

#### 4.2.2 Bastard results

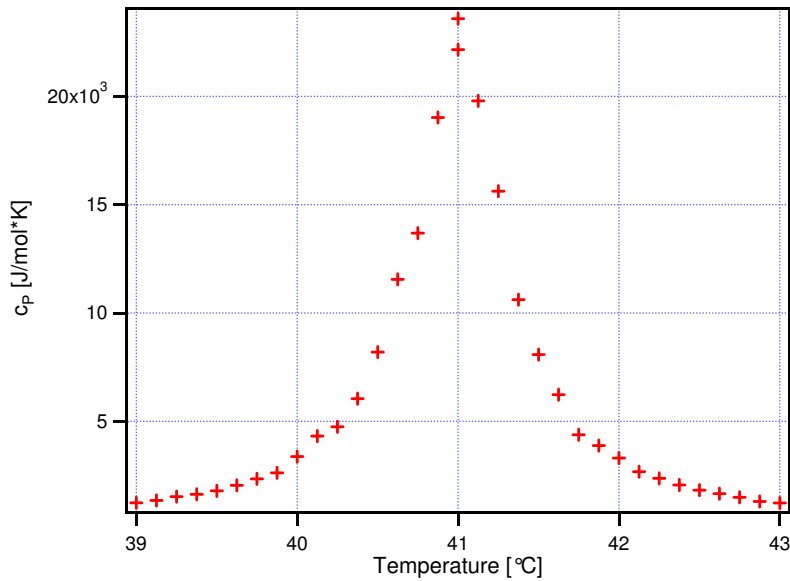


Figure 4.25: Heat capacity profile for 2-state with detached melting. 2340 lipids 150,000 MCCT.  $p_A = 0.16 \text{ N/m}$ ,  $\gamma = 6.5 \text{ kJ/mol}$ ,  $\omega = 1.3 \text{ kJ/mol}$

From figures (4.25) and (4.26) it is seen that the 2-state detached sub-model reproduces something very similar to the results of the static grid simulation. The heat capacity profile is roughly the same width, it is symmetric and within a factor 2 of  $\Delta H$ . There is domain formation of the expected scale. Furthermore an amount of holes and cracks can be identified.

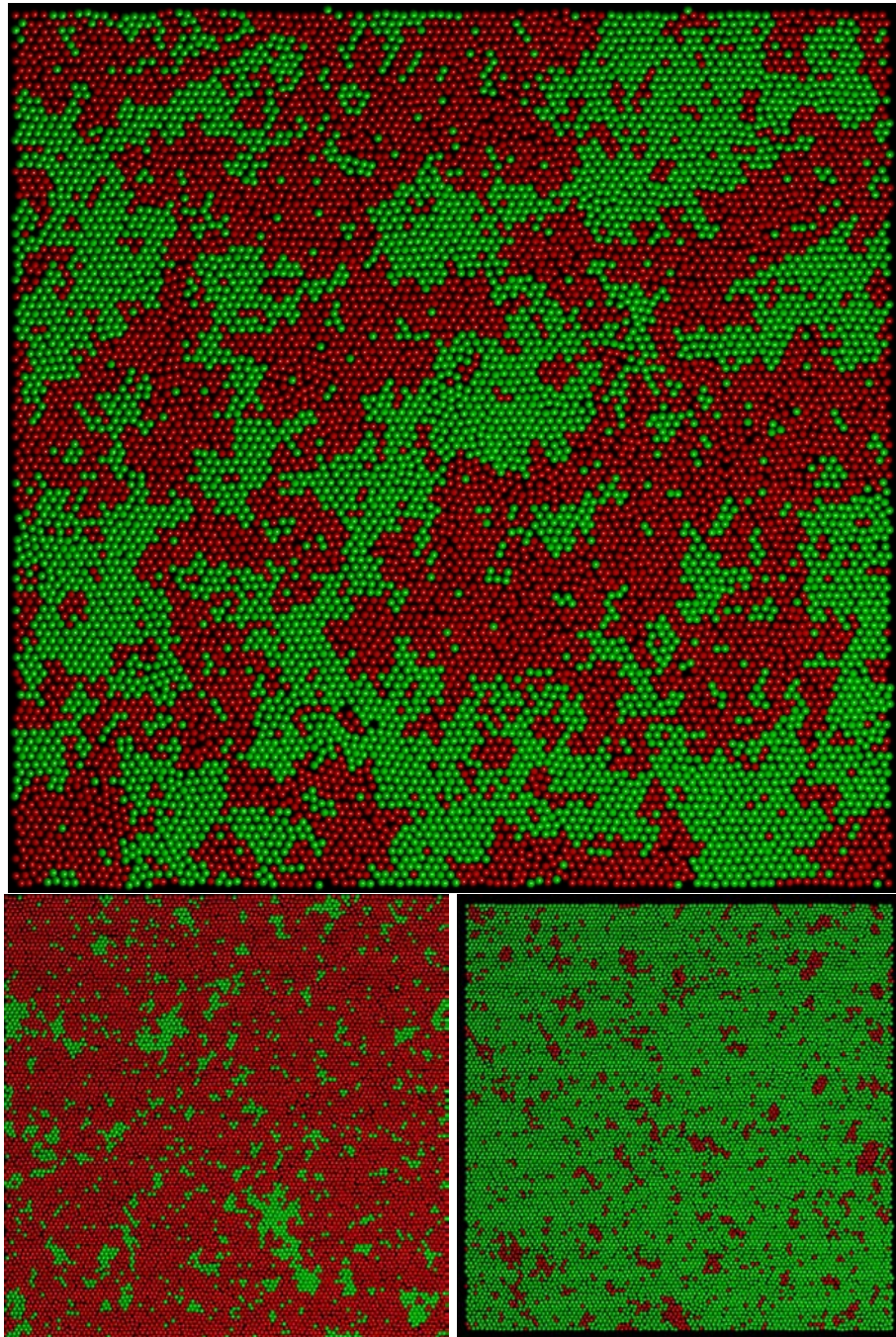


Figure 4.26: Snapshot from simulation on figure (4.25). (Bottom left) at 39°C. (Bottom right) at 43°C. (top) at 41°C. Notice domain and hole formation in the phase transition.

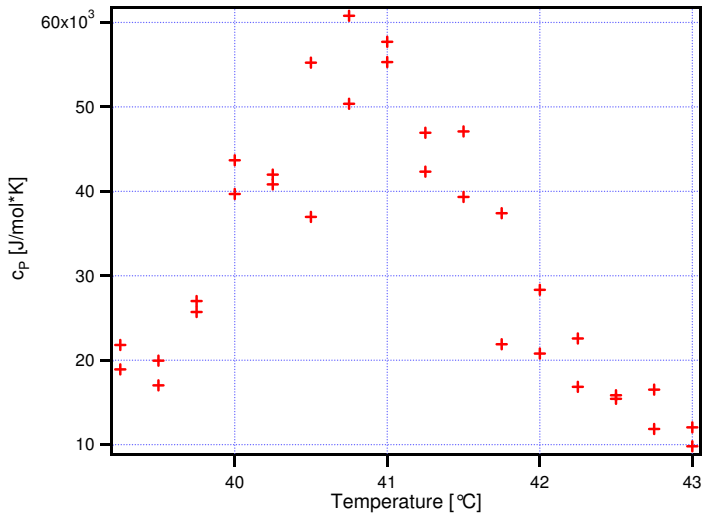


Figure 4.27: Heat capacity profile for continuous attached melting. 418 lipids 3,000,000 MCCT.  $p_A = 0.061$  N/m,  $\gamma = 14.2$  kJ/mol,  $\omega = 78$  kJ/mol

The results of the continuous attached model (figures 4.27 and 4.28) are somewhat similar to those of the 2-state detached model. The heat capacity profile are though not as smooth due to the extreme long relaxation times - the CA model required 20 times the MCCT to present this much more ragged heat capacity profile than the 2S model. It should be noted how  $p$ ,  $\gamma$ , and  $\omega$  differs between models. A deviation of approximative 10% or more on any of these parameters will cause simulations not to produce gel/fluid domains or heat capacity profiles similar in width, size, or melting temperature to those of experiments.

The interaction energy  $\omega$  is the same for static grid and for the 2-state detached model. This is because the melting and moving have been detached from each other in this model, and the melting and domain formation of lipids are governed by a part of the energy equation similar to that of static grid. The  $\omega$  of the continuous attached model is nearly two orders of magnitude larger than in the other simulations. If the interaction energy is not set that high the simulation will not produce domains. And in the phase transition lipids will not fluctuate all the way from gel to fluid and back, rather a little around halfway between and snapshots of the simulation will show nearly all lipids in shades of brown.

Compare the pressure,  $p_A$ , and the the strength of Lennard-Jones interaction potential,  $\gamma$ , in the two Bastard sub-models. It is observed that  $p_A$  is twice as high in the 2-state detached model as the continuous attached model. But  $\gamma$  half the size. This reverse proportionality between  $p_A$  and  $\gamma$  is given by the boundary condition of equation (2.4.12). There are, however, in the two models different limits of this relation. But for both goes that if  $p_A$  is to low the area of 'the membrane' will expand until it ruptures and lipids will clump in little patches. If pressure is to high movement of lipids will cease.

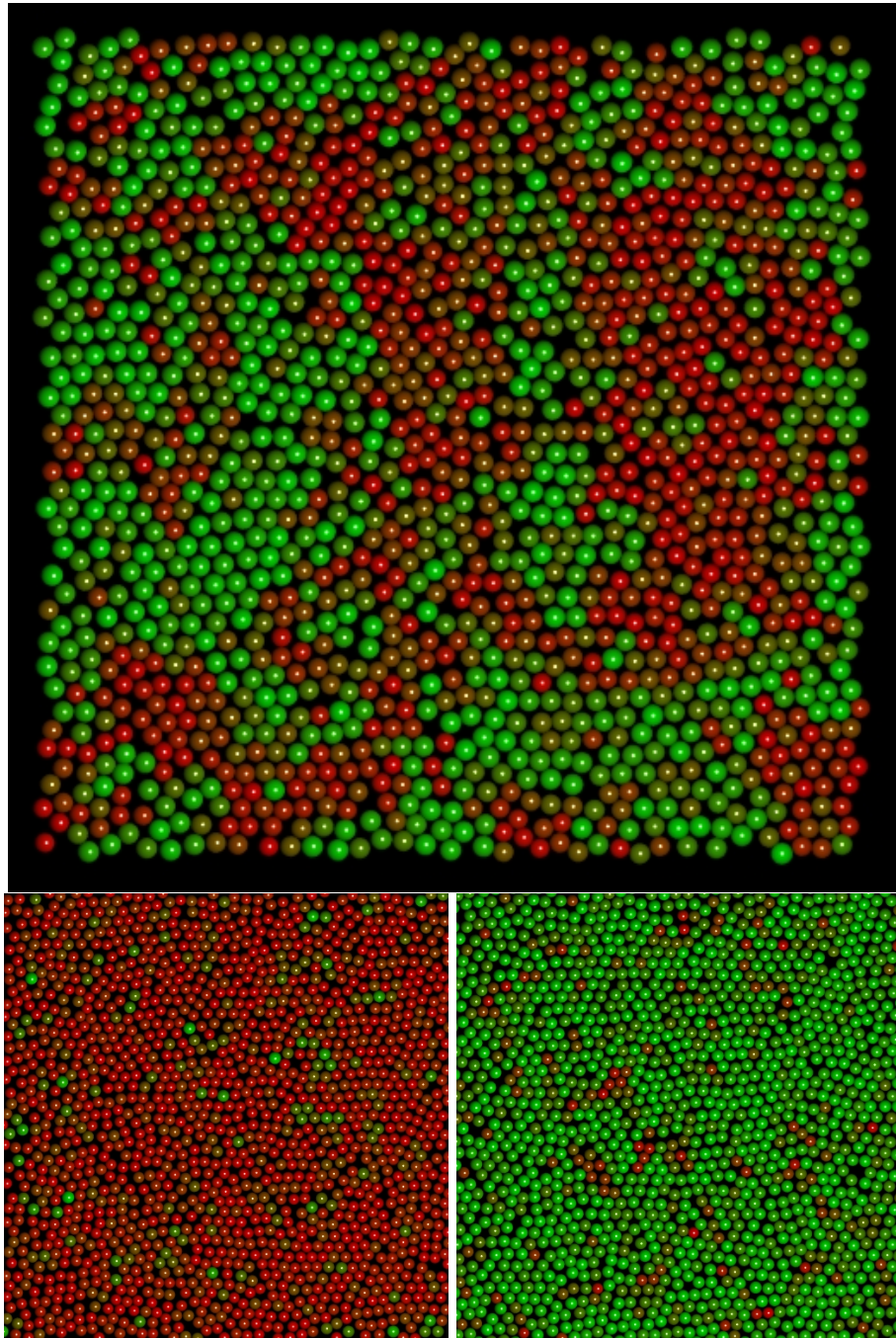


Figure 4.28: Snapshot from simulation on figure (4.27). (Bottom left) at 39°C. (Bottom right) at 43°C. (top) at 41°C. Notice domain and hole formation in the phase transition.

Simulations of the bastard model with anesthetics were also carried out, figures (4.29) and (4.30). These figures reveals that the parameters two sub-models are not properly normalized, in that the melting points are moved to much by the addition of anesthetics.

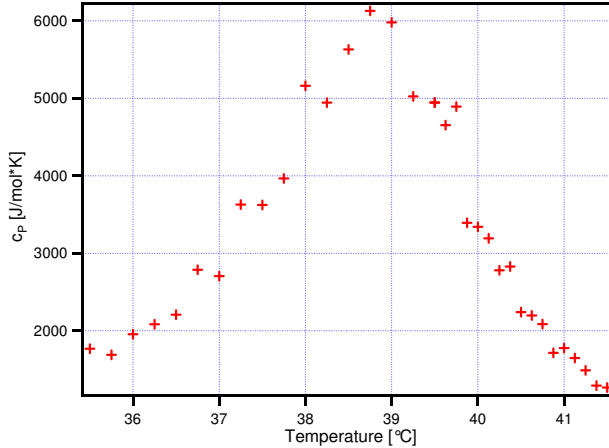


Figure 4.29: Heat capacity for 2-state, detached melting with 5 mol% anesthetics. 2340 lipids 60,000 MCCT.  $p_A = 0.16$  N/m,  $\gamma = 6.5$  kJ/mol,  $\omega = 1.3$  kJ/mol. Notice the shift in melting temperature of  $\approx 2$ K.

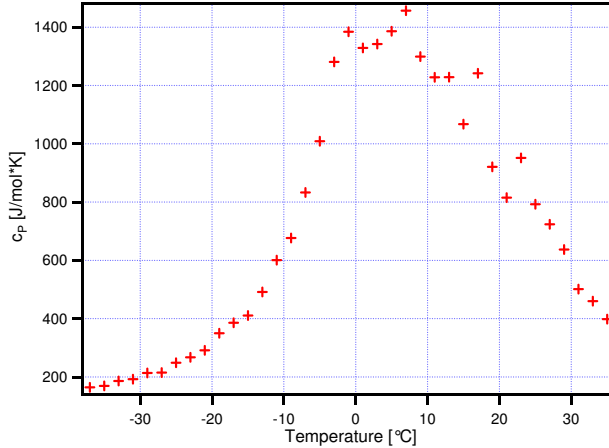


Figure 4.30: Heat capacity for continuous, attached melting with 1 mol% anesthetics. 418 lipids 200,000 MCCT.  $p_A = 0.061$  N/m,  $\gamma = 14.2$  kJ/mol,  $\omega = 78$  kJ/mol. Notice the extreme shift in peak melting temperature of  $\approx 30$ K.

The profiles display asymmetries which was desired, however it seems that only the 2S model is asymmetric in a way comparable to DPPC. Further investigation should be done of this. It is to be noted that the anesthetic simulations were done with a switch move (Sec. 2.4.3), which has brought down simulation times with at least a factor 10.

Simulations of added lateral pressure were conducted in the continuous attached model. These initial results shows perfect linearity, and bodes well for the model as such. If the parameters can be properly normalized, such pressure scans could tell a lot about lateral pressure in the membrane. If pressure in the simulation is lowered by approximately 5%, the area will increase towards infinity – The membrane explodes.

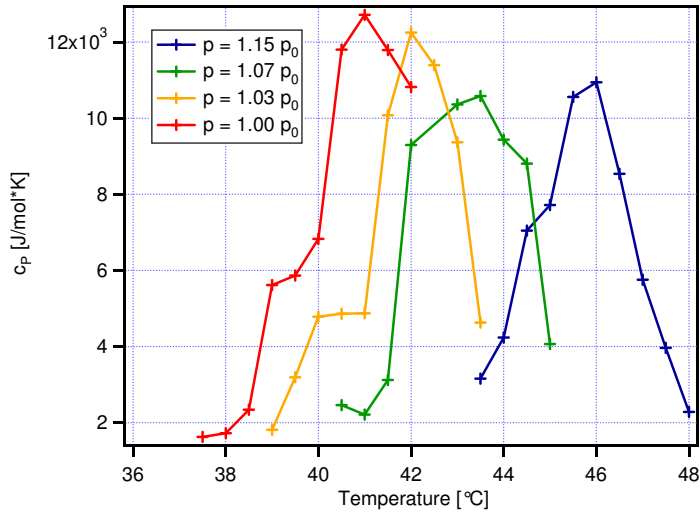


Figure 4.31: Heat capacity profile for continuous, attached melting. 418 lipids 300,000 MCCT.  $p_0 = 0.061 \text{ N/m}$ ,  $\gamma = 14.2 \text{ kJ/mol}$ ,  $\omega = 78 \text{ kJ/mol}$ .

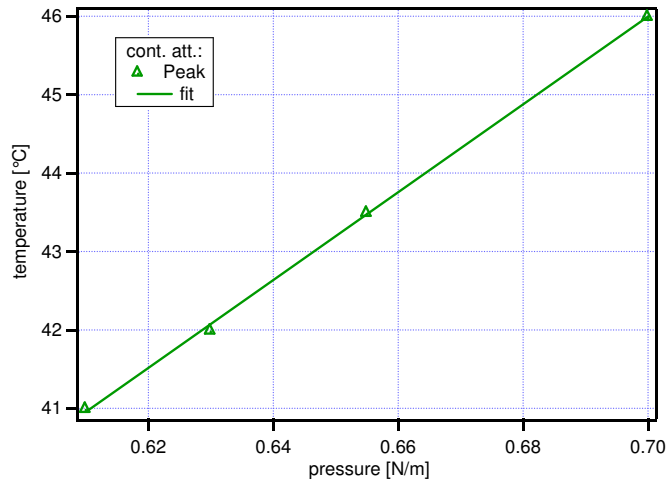


Figure 4.32: Peak melting points for Fig. (4.31). Fitted slope: 56 [K m/N].  $R^2$ : .999.

### 4.3 Solitons

As mentioned in Sec. (2.3) solitons are very stable, but their shape is very sensitive and differs clearly with changes in initial conditions - which are the shape of the heat capacity profile, choice of initial density,  $\rho_0^A$ , and velocity,  $v$ . For all solitons the initial density was  $\rho_0^A = 40.35 \text{ g/m}^2$  of fluid DPPC, and velocity 1% over the limit velocity for the given system,  $v = 1.01v_{limit}$ , to produce solitons of maximum amplitude

As evident from equation (2.3.9) solitons are symmetric around  $z = 0$ . This allows for depicting only half the soliton, as will be done throughout this section.

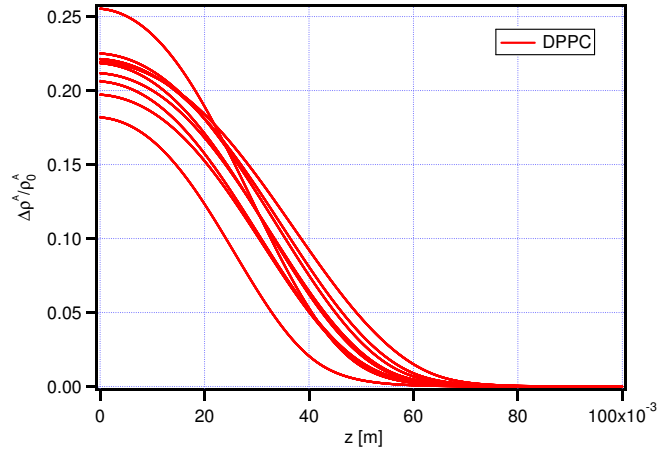


Figure 4.33: Solitons calculated from heat capacity profiles obtained by repeated calorimetric scans of DPPC. The difference in shape reflects the sensitivity of solitons on the shape of heat capacity profiles.

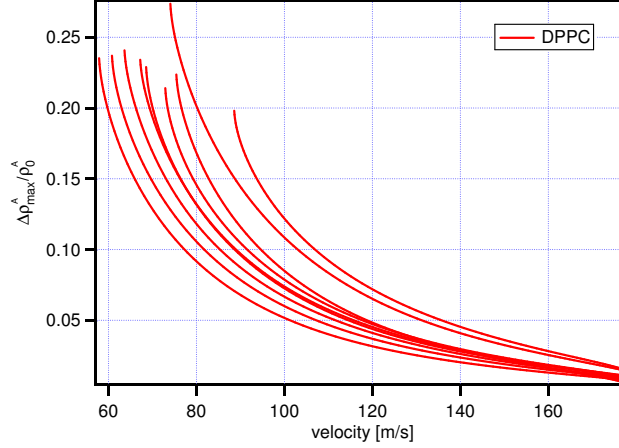


Figure 4.34: DPPC: Maximum compression of solitons as functions of soliton velocity. The upper limit is the sound velocity in DPPC. The lower limit is calculated from data. The spread in data reflects sensitivity to initial conditions of the equations.

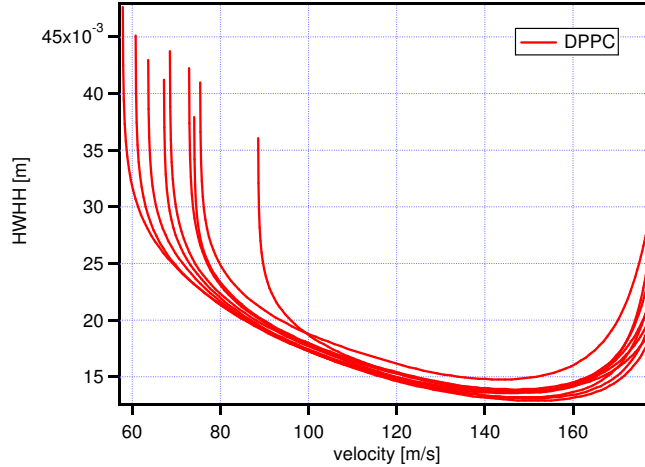


Figure 4.35: DPPC: Half Width at Half Height of solitons as functions of soliton velocity. The upper limit is the sound velocity in DPPC. The lower limit is calculated from data. The spread in data reflects sensitivity to initial conditions of the equations.

Figures (4.34) and (4.35) show compression and half width at half height (HWHH) of solitons as a function of velocity, here 'height' is equal to compression. Showing that solitons trend toward infinite width as they go towards limit velocity, which was predicted theoretically by A. Jackson [1].

Solitons for octanol of different concentrations:

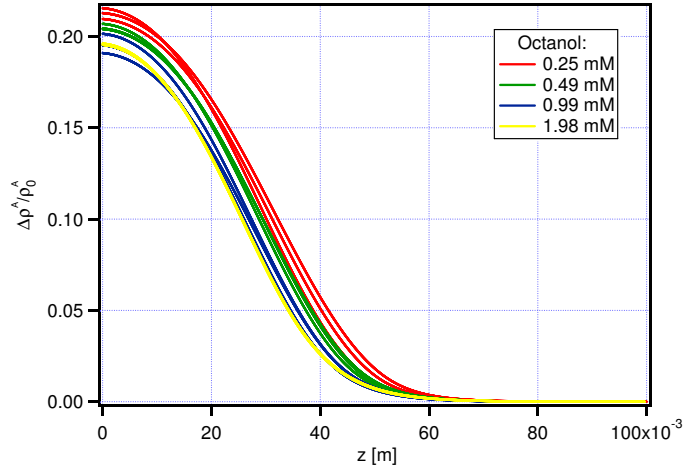


Figure 4.36: Solitons calculated from the heat capacity profiles of DPPC with octanol presented in figure (4.4).

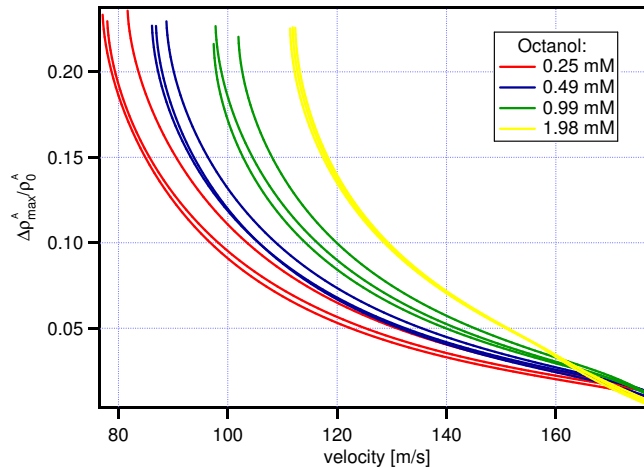


Figure 4.37: Octanol: Maximum compression of solitons as functions of soliton velocity.

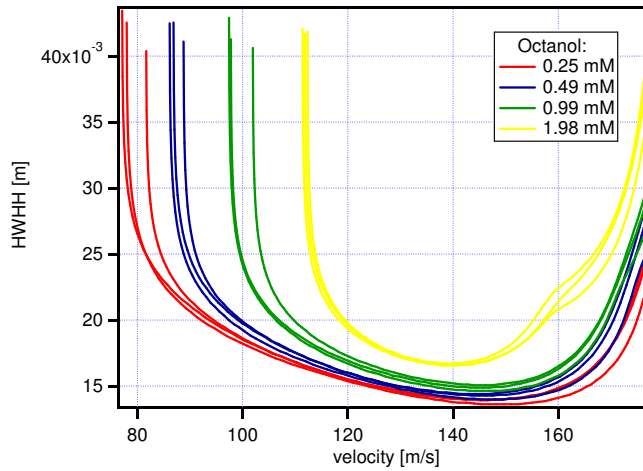


Figure 4.38: Octanol: Half Width at Half Height of solitons as function of soliton velocity.

From solitons calculated from DPPC with added octanol, it can be noticed how the addition of anesthetic does not change the shape of solitons. However, the broadening of the heat capacity profile, brings a shift in the limit velocity. The shift in melting temperature does not influence the shape of solitons, as they are only dependent on density and functions thereof.

These results are so typical that similar results for the other anesthetics have been located in Appendix A.5.

Solitons were also produced for the heat capacity profiles produced by simulations:

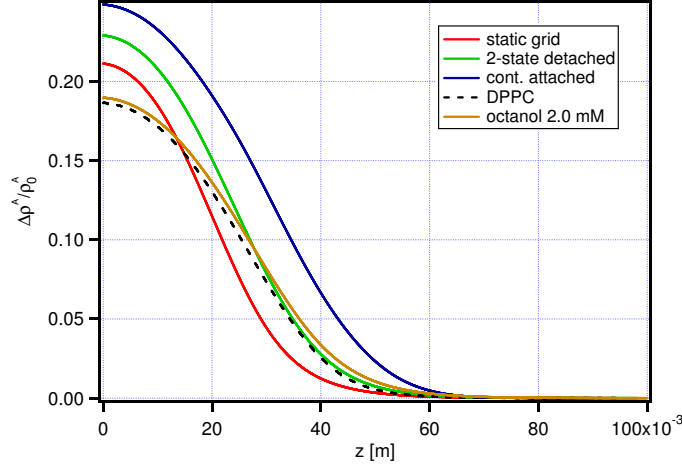


Figure 4.39: Solitons produced from heat capacity profiles obtained by experiments and simulations.

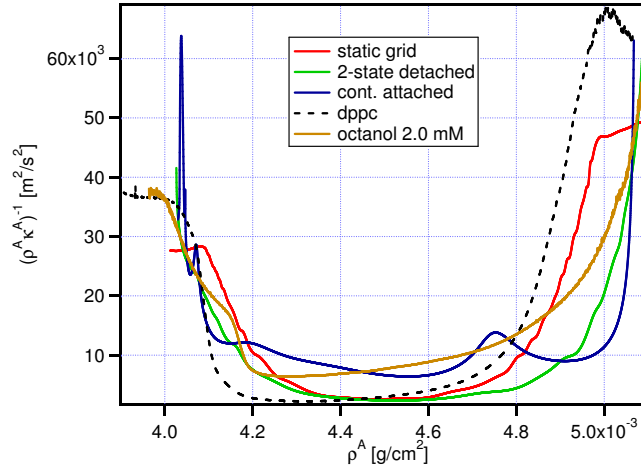


Figure 4.40: Sound velocity squared as a function of density from heat capacity profiles obtained by experiments and simulations.

Sound velocity squared in figure (4.40) is a function of compressibility and density,  $c^2 = (\rho^A \kappa^A)^{-1}$ . Where  $\kappa^A$  is given by equation (2.3.6). Data from simulations are obtained by first interpolating the heat capacity profiles in figures (4.25) and (4.27) using cubic splines. However, the smoothness of (4.27) was not enough to produce solitons in the high velocity limit, as seen on figure (4.42). Nevertheless, that solitons were produced for all types of data sets obtained experimental or simulated indicates that the solitons are generally achievable, not just a special mathematical occurrence in the equations.

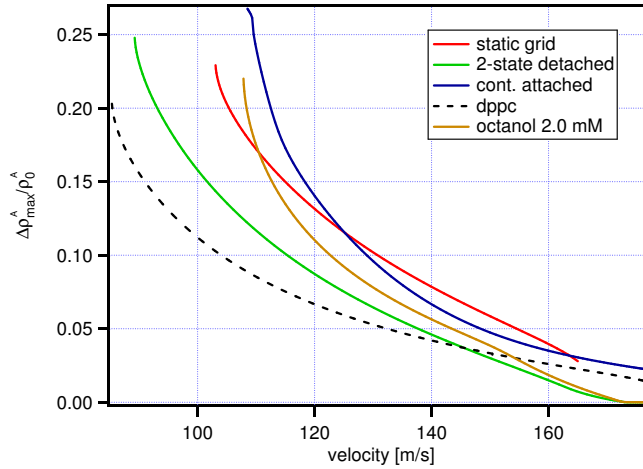


Figure 4.41: Maximum compression as a function of velocity from data and simulations.

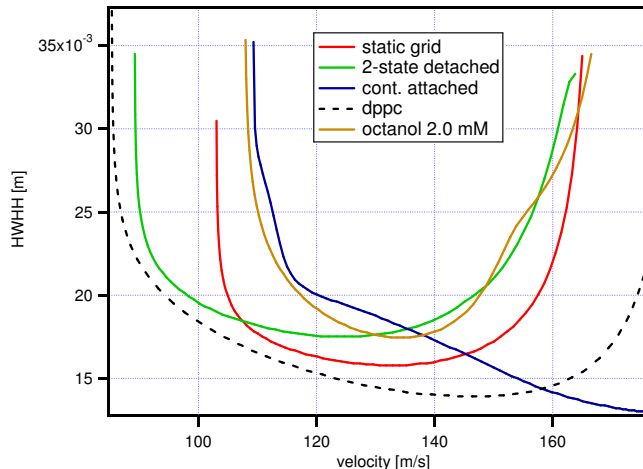


Figure 4.42: Half Width at Half Height as a function of velocity from data and simulations.

## Chapter 5

# Résumé, Discussion, and Conclusion

### 5.1 Résumé

It was the intention of this thesis to investigate how anesthetics influence the nerve membrane and the nerve pulse.

The nerves were represented by a pure lipid membrane of DPPC, and in computer simulations by small moving cylinders. The old model on the nerve signal – the Hodgkin-Huxley model – was discarded by its inability to explain physical features of the nerve pulse and anesthetic action. And Solitary waves – Solitons – in the wave equation for membranes at melting temperature, where identified as the nerve pulse.

Experiments and simulations showed that anesthetics shift the melting temperature of a lipid membrane towards lower temperature. And that pressure shifts it back towards higher temperatures. From these results partition coefficients of anesthetics into the lipid membrane were calculated. And it was shown that anesthetics do not change the influence of pressure on the melting temperature.

Finally, it was shown that solitons can be regularly produced from heat capacity profiles both with and without anesthetics.

### 5.2 Discussion

This thesis started out with presenting the Meyer-Overton relation. Which states that the potency of anesthetics is proportional to the solubility of anesthetics in oil. The Soliton model proposes that anesthesia is caused by change in melting temperature of the membrane. The experiments within this thesis verifies a change in melting temperature caused by anesthetics. In 2001 Kharakoz [23] showed that for alcohols of carbon-chain length 1-10, the anesthetic dose

for tadpoles equals a shift in melting point of  $\Delta T_{anesthesia} = -0.6 \pm 0.2K$ .

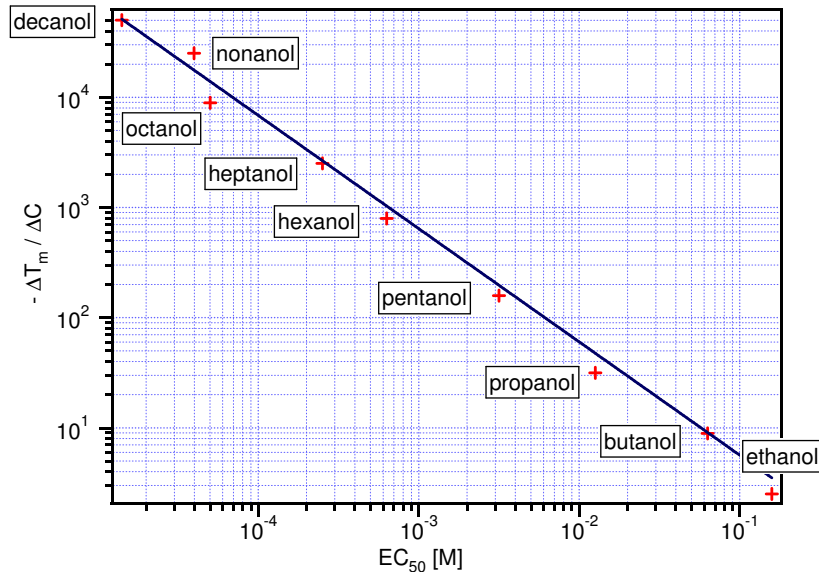


Figure 5.1: Correlation between the anesthetic concentration,  $EC_{50}$ , of alcohols in tadpoles, and potencies of the alcohols to change transition temperature in DPPC. The fitted line gives the shift in melting point caused by anesthetic dose,  $\Delta T_{anesthesia} = -0.6 \pm 0.2K = EC_{50} \cdot \Delta T_m / \Delta C$ .

The experiment of Kharakoz depicted in figure (5.1) is wonderfully simple. The anesthetics concentration,  $EC_{50}$ , is measured in tadpoles and displayed against  $\Delta T_m / \Delta C$ , the shift in melting temperature per shift in concentration in solution of DPPC membrane. The shift in melting point caused by anesthetic dose,  $\Delta T_{anesthesia} = -0.6 \pm 0.2K$ , is fitted from the data given  $\Delta T_{anesthesia} = EC_{50} \cdot \Delta T_m / \Delta C$ .

The connection between Kharakoz's and Overton's data is that the shift in melting temperature,  $\Delta T$ , is directly proportional to the amount of anesthetics in the membrane,  $x_{AM}$ , as derived in section (2.1.1) equation (2.1.6) on page 15. And for tadpole experiments with large bulk of water, the  $x_{AM}$  is directly proportional to the partition coefficient,  $P$ , as derived in section (2.1.3) equation (2.1.13) page 18. These proportionalities gives that Kharakoz's data is showing the same as Overton's, only with different units.

Experiments done for this thesis were not bulk water. Therefore the partition coefficient were calculated from the shift in melting temperature caused by anesthetics. The theory were derived in section (2.1.2) and results presented in table (4.1). In table (5.1) The partition coefficients obtained by experiments,  $P_{data}$ , are compared to partition coefficients found in literature,  $P_{literature}$ , in comparable systems.

What is immediately noticeable from table (5.1) is that the experimentally

	$P_{data}$	$P_{literature}$	'membrane' in literature	Ref.
Octanol	150	200-387	DPPC / Egg PC (PO/PLPC)	[58, 42]
Bupivacaine	39	69	Octanol/5	[43]
Lidocaine	4.9-21	27-50	synth. membrane / Octanol/5	[44, 45]
Pentobarbital	42	56-200	PC-chol. pH 7 / PC acid	[42]
Propofol	20-49	113-4700	Brain / Oil	[46]

Table 5.1: Partition coefficients from data,  $P_{data}$ , compared to partition coefficients from literature,  $P_{literature}$ . Column three displays the substance in which  $P_{literature}$  are measured. Except for propofol, all  $P_{data}$  are an approximate factor two lower than  $P_{literature}$ . Some of  $P_{literature}$  are given by 'Octanol/5', this is the partition coefficient of octanol divided by five, which is a standard way of estimating partition coefficient in lipids.

derived partition coefficients are, with the exception of propofol, approximately a factor of two lower than the partition coefficients from literature. This can be considered as a good result, as the spread in literature data is often more than a factor of two. Also, data from literature never refers to systems 100% comparable to those in this thesis, and often do not refer to pH or temperature, which are, for many of the anesthetics, very important for the partition coefficient. For octanol, bupivacaine, and pentobarbital, the  $P_{data}$  obtained in this thesis seems more valid for the anesthetic into DPPC in a Hepes/EDTA buffer with pH-value 7.0. Lidocaine and propofol were no good fits, lidocaine because of the bad fit to data. While propofol had a value way too low, probably because it was not mixed properly with the buffer. Propofol is a pale liquid at room temperature, and it can be difficult to determine if it has been well mixed into the buffer - the results indicates that it has not.

It was the proclaimed goal of this thesis to obtain data to be compared with the Overton data. Hence, it was intended to reproduce the partition coefficient versus anesthetic dose to match Overton. However, it became clear that compiling data for anesthetics strength was even more challenging than for partition coefficients. This because the simple experiments done by Overton on tadpoles, has nowadays been replaced by numerous different kind of experiments with each their different definition on anesthetic dose. An often done experiment is the dose to inject into mice or rats, to make them oblivious to heat changes - that they do not remove their tales from a heating plate. Another popular study is to remove nerves from rat/frog/cat/animal-of-choice and measure different responses to electric stimuli with and without anesthetics. This host of experiments has as mentioned given rise to numerous definitions on anesthesia.  $EC_{50}$  is the anesthetic concentration needed to anesthetize 50% of a sample population. This definition is used primarily when having bulk amount of water, like in tadpoles experiment or dissected nerves which can be soaked in anesthetics. However some papers refer to  $EC_{50}$  as  $ED_{50}$  which is short for anesthetic dose of 50% population.  $ED_{50}$  is mostly found in experiments where anesthetics are

injected into the lab-animal, and it can be given in units of concentration, or total moles, or most often as mg per kg bodyweight. Some papers uses  $EC_{50}$  to describe the concentration of the dose they have injected into lab-animals. For inhalation anesthetics the most common used measure of anesthetic strength is Minimal Alveolar Concentration (MAC) which is given in units of pressure, and used as a standard in medical procedures. Another definition with unit of pressure is  $EP_{50}$ , the anesthetic pressure, used for inhalation anesthetics. Then there is  $IC_{50}$  Inhibitory Concentration, that is the concentration of which 50% of nerve signals are inhibited. And the list goes on and on, making a comparison of data not strictly coherent.

The potencies of the anesthetics used in this thesis were not determined by explicitly comparable experiments, so a spread of these are presented in table (5.2).<sup>1</sup>

	$ED_{50}$		$EC_{50}$	
	[ $\mu M$ ]	experiment	[ $\mu M$ ]	experiment
Octanol	—	—	57-122	tadpole/DRG
Bupivacaine	6600	tail flick	—	—
Lidocaine	2,500-28,200	tail flicks	3,800	Frog sciatic nerve
Pentobarbital	—	—	50-334	NSC/DRG
Propofol	—	—	0.4-1.9-12.9	NSC/tadpole/DRG

Table 5.2: Anesthetic dose,  $ED_{50}$ , and anesthetic concentration,  $EC_{50}$ . NSC and DRG are both section of rat nerve respectively: Neocortical Slice Cultures and Dorsal Root Ganglion. References are for Octanol: [50, 51]. Bupivacaine: [52]. Lidocaine: [53, 52, 6]. Pentobarbital: [54, 51]. Propofol: [54, 55, 51].

Which can then be plotted versus the partition coefficients from table (5.1).

Figure (5.2) is this thesis' equivalent to Overton's (Fig. 1.2) and proportional to Kharakoz's (Fig. 5.1). The data does show the same tendencies as the literature, but no good fit could be made with so scarce and so imprecise data. It was derived in section (2.1.4) that the slope should be -1, while the fitted slopes of this data is  $\approx -0.5$ .

From figure (5.2), it can also be noted that the anesthetics usually known as local is found in the right end of the figure, that is, they are characterized by a low partition coefficient and a high anesthetic dose. If this is a general trend among local anesthetics, they may be local due to a need of high local concentration to penetrate into the membrane. They do not display a general anesthetic effect since the administered dose will be thinned as the anesthetic spread through the body, and then not be able to penetrate into the membrane.

To further validate this theory, a comprehensive list of *comparable* values for anesthetic strength and partition coefficient of both general and local anesthetics would have to be compiled. Much like the compilation of Overton done on tadpoles. But there needs to be established an experiment which can determine

<sup>1</sup>The Sakura paper [52] claims to have measured  $EC_{50}$  but since it is the dose injected into the lab-rat, as opposed to rat nerve in bath of anesthetic, it is here referenced as  $ED_{50}$

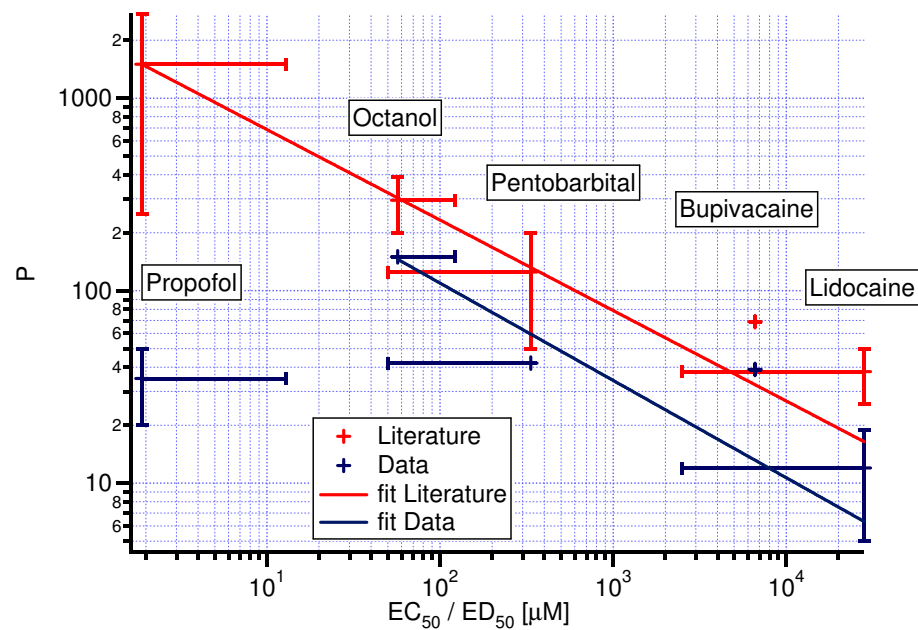


Figure 5.2: Partition coefficient (Table 5.1) versus anesthetic potency (Table 5.2).

the anesthetic concentration also for anesthetics that are not easily dissolvable in water. Or alternatively determining anesthetic dose for a multitude of anesthetics in comparable experiments.

The clearest results of this thesis, were those of pressure reversal (Sec. 4.1.3). For DPPC and all types of anesthetics, the shifting of melting temperature showed remarkable linearity. The experiments show that pressure shifts the melting temperature 1 degree upwards per 40 bars. This result allows for calculating the pressure needed to reverse anesthesia from Kharakoz's experiment. If anesthetic dose is equivalent to shifting the melting temperature -0.6 K, then the pressure to reverse it is 24 bar. In 1950 Johnson and Flagler demonstrated that for ethanol the pressure to reverse anesthesia in tadpoles was approximately 50 bars [21]. This result is as good an indication for the validity of the SM model as the Overton data, and it shows -again- how anesthesia is connected to melting point depression.

As a small side note, it can be mentioned that a lowering of *pH* also shifts the melting point in the opposite direction of anesthetics [25]. It is known that inflammation lowers *pH*, and it is common medical practice to heighten the anesthetic dose in inflammatory tissue. This is another indication, that anesthesia is related to a change in melting temperature.

This thesis also succeeded in producing solitons from real as well as simulated heat capacity profiles (Sec. 4.3). It was qualitatively demonstrated how stable the equations are, and how soliton shape depends of the shape of the heat capacity profile.

Solitons could also be produced from heat capacity profiles of DPPC with anesthetics. This might seem surprising, but in experiments by Büyükkılıç [24], it was observed that anesthetic dose in frog nerves only weakens the nerve pulse with approximately 20%. The soliton equation in itself contains no predictions on whether there is enough energy to obtain maximum solitons, but only if it is possible for solitons to exist. That soliton amplitude is lowered when adding anesthetics, can be seen by shifting the temperature in figure (5.3).

There are some features of the nerve signal that the Soliton Model has no *a priori* answers for. That does not mean that answers cannot be found, as the model is still young and many questions have not had the chance to be addressed. Following two examples are questions that supporters of Hodgkin and Huxley often present to our group. I will try to point at a direction in which the answer might lay.

The first example is: When nerves are triggered to fire, they cannot fire again before a given time has passed - the retention time - the mathematical soliton wave are theoretically ready to go at any moment. This might, however, be explained by relaxation times of the membrane. Pressure jump experiments where DPPC is pushed through the phase transition by pressure, which is subsequently removed, revealed that membranes need a certain relaxation time to

regain the original configuration [33]. Thus, a soliton density wave might need some retention time.

Also, not *yet* explained by the Soliton model is the 'all-or-none' principle - when nerves are artificially stimulated, one must pass a certain threshold for them to fire, and when this threshold is reached at approximately 15 mV, the nerve will release the action potential of  $\sim 100$  mV, as seen on figure (1.3). The SM can deliver solitons of continuous sizes - it has no threshold. The 'none' part of the 'all-or-none' principle is, however, not entirely correct. Nerves experience 'failed initiations' - equal to very weak signals - before reaching the threshold. The Soliton model can explain this easily, but not quite the discontinuous jump in excitation when reaching the threshold. However, as figure (5.3) shows, the soliton model produces solitons of continuous amplitude in area density, and the change from small to large amplitude may happen fast.

Simulation of membranes was an exciting experience (Sec. 4.2). The produced heat capacity profiles and pictures of domain formation were of similar quality as traditional solid grid simulations. Unfortunately the simulation times were much longer, and adding anesthetics revealed that the bastard models' parameters were not properly normalized. Nevertheless, the brighter prospects are that if parameters can be fine tuned; the simulation might be able to replicate permeability results, the asymmetric heat capacity profile, and exposure to pressure - which were all seen in the preliminary results. Furthermore, these simulations are prepared for tracking of molecules lipids or anesthetics, investigating site of anesthetics action, and possibly explain the pre-transition. All done within reasonable time scale on normal desktop computers.

### 5.3 Conclusion

Anesthetics influence the nerve membrane by changing properties of the gel-fluid phase transition. Thereby changing the conditions for the nerve pulse to be created, if it is assumed that the nerve pulse is described by a density pulse - as claimed by the Soliton model.

This thesis has presented a wide range of results, all in support of the Soliton model as *the* framework for the function of nerves.

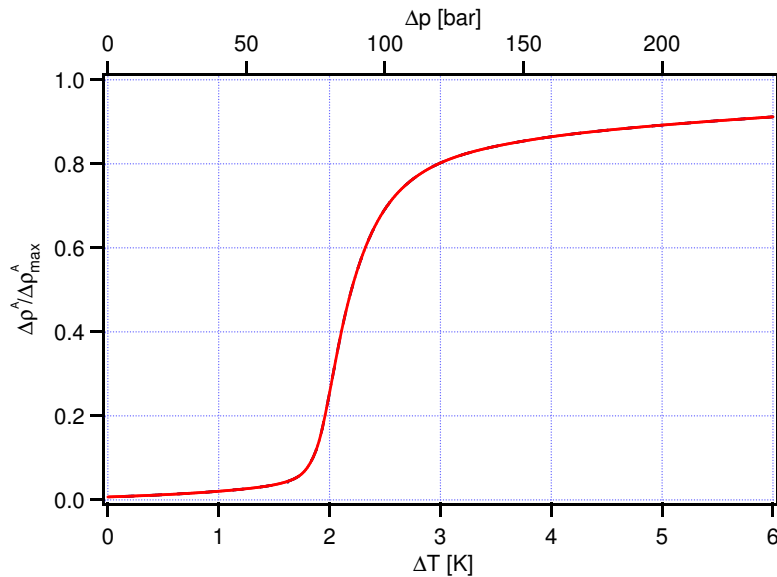


Figure 5.3: If a 'body temperature' of  $44^\circ\text{C}$  is assumed for a lab-animal with nerves of pure DPPC. The energy needed to initiate a nerve pulse of a certain size can be expressed by a change in temperature or pressure. For small stimulation only very small solitons are produced. Then, around  $\Delta T = 2\text{K}$  and  $\Delta p = 80$  bar solitons goes from an amplitude of less than 10% of maximum possible amplitude to  $\approx 80\%$  within a very small energy interval. Thus displaying a 'continuous' threshold. Adding anesthetics or additional pressure will shift the graph right or left respectively. If the energy available to create a density pulse is equivalent to  $\Delta T = 3\text{K}$ , then adding anesthetic in amounts to shift the temperature 1K, reduces soliton amplitude from 0.8 to  $0.2 \Delta p^A / \Delta p_{max}^A$ . This graph is produced by a integral  $-dT$  over the heat capacity of DPPC  $c_P(T)/\Delta H$ . Starting at  $44^\circ\text{C}$ . The threshold seen on this graph is therefore a result of the narrow heat capacity profile in DPPC. For real nerves with a broader phase transition this 'threshold' will not be as pronounced.

# Bibliography

- [1] T. Heimburg, A.D. Jackson:  
On soliton propagation in biomembranes and nerves.  
PNAS vol. 102 no. 28 pp. 9790–9795, 2005
- [2] B. Mengel, M. Christiansen:  
Influence of anaesthetics on the melting transition of lipid membranes.  
available from [www.membranes.nbi.dk](http://www.membranes.nbi.dk), Bachelorproject at NBI 2005
- [3] B.W. Urban:  
Die Meyer-Overton-Regel: Was ist geblieben?  
Anästhesie in Zürich: 100 Jahre Entwicklung 1901-2001.  
Inst. Anästhesiologie, Universitäts-Spital Zürich, pp. 15–23, 2002
- [4] C.E. Overton:  
Studien über die Narkose.  
Published by Gustav Fischer, Jena, 1901
- [5] C.E. Overton:  
Studies of Narcosis.  
Published by Chapman & Hall, 1991
- [6] P. Seeman:  
The Membrane Actions of Anesthetics and Tranquilizers. - Review article  
Pharm. Rev. vol. 24 no. 4, pp. 583–655, 1972
- [7] P.S. Sastry:  
Lipids of nervous tissue: Composition and metabolism.  
Prog. Lipid Res. Vol. 24, pp. 69–176, 1985
- [8] A.V. Hill:  
The heat production of muscle and nerve, 1848-1914.  
Annu. Rev. Physiol. 21, pp. 1–19, 1959
- [9] A.L. Hodgkin, A.F. Huxley:  
A quantitative description of membrane current and its application to conduction and excitation in nerve.  
J. Physiol. 117, 500–544, 1952

- [10] E. Neher, B. Sakmann:  
Single-channel currents recorded from membrane of denervated frog muscle fibres.  
Nature 260, pp. 799-802, 1976
- [11] D.J. Woodbury:  
Pure lipid vesicles can induce channel-like conductances in planar bilayers.  
Journal of Membrane Biology, vol. 109, pp. 145-150, 1989
- [12] K. Wodzinska:  
Pores in lipid membranes and the effect of anaesthetics.  
Master Thesis, available from [www.membranes.nbi.dk](http://www.membranes.nbi.dk), June 2008.
- [13] A.H. Lang, A. Puusa:  
Dual influence of temperature on compound nerve action potential.  
J. Neurol. Sci. 51(1), pp. 81-8, 1981
- [14] D.R. Haarder:  
Pressure-Induced Myogenic Activation of Cat Cerebral Arteries Is Dependent on Intact Endothelium.  
Circ. Res. 60, pp. 102-107, 1987
- [15] T. Heimburg:  
Thermal biophysics of membranes.  
Wiley-vch Verlag, 2007.
- [16] C.D. Leaks:  
Claude Bernard and anesthesia.  
Anesthesiology 35, pp. 112-113, 1971
- [17] J.M. Ritchie, R.B. Rogart:  
Density of sodium channels in mammalian myelinated nerve fibers and nature of the axonal membrane under the myelin sheath.  
Proc. Natl. Acad. Sci. USA Vol. 74, no. 1, pp. 211-215, 1977
- [18] N.P. Franks, W.R. Lieb:  
Molecular and cellular mechanisms of general anaesthesia. - Review article  
Nature vol. 367 no. 17, pp. 607-614, 1997
- [19] K. Iwasa, I. Tasaki, R.C. Gibbons:  
Mechanical changes in squid giant-axons associated with production of action potentials.  
Biochem. Biophys. Res. Commun: 95, pp. 1328-1331, 1980.
- [20] J.M. Ritchie, R.D. Keynes:  
The production and absorption of heat associated with electrical activity in nerve and electric organ.  
Quart. Rev. Biophys. 392, pp. 451-476, 1985

- [21] Johnson, F. H., and E. A. Flagler:  
Hydrostatic pressure reversal of narcosis in tadpoles.  
Science no. 112 pp. 91-92, 1950
- [22] T. Heimburg, A.W. Jackson:  
On the action potential as a propagating density pulse and the role of anesthetics.  
Biophys. Rev. vol. 2 no. 1, pp. 57–78, 2007
- [23] D.P. Kharakoz:  
Phase-transition-driven synaptic exocytosis: a hypothesis and its physiological and evolutionary implications.  
Biosci. Rep. 210 pp. 801-830, 2001
- [24] B. Büyükkılıç, Ü. Çömelekoğlu, O. Ögenler:  
Reversible Conduction Block in Frog Sciatic Nerve for Three Different Concentrations of Bupivacaine.  
Turk. J. Med. Sci. no. 33, pp. 357–361, 2003
- [25] T. Heimburg:  
Mechanical aspects of membrane thermodynamics. Estimation of the mechanical properties of lipid membranes close to the chain melting transition from calorimetry.  
Biochimica et Biophysica Acta vol. 1415, pp. 147–162, 1998
- [26] B. Lautrup, A.D. Jackson, T. Heimburg:  
The stability of solitons in biomembranes and nerves.  
unpublished manuscript, 2005
- [27] N.J. Zabusky, M.D. Kruskal:  
Interactions of "Solitons" in a collisionless plasma and the recurrence of initial states.  
Physical Rev. Let. vol. 15 no. 6 pp. 240–243, 1965
- [28] D.J. Korteweg, G. de Vries:  
On the Change of Form of Long Waves Advancing in a Rectangular Canal, and on a New Type of Long Stationary Waves.  
Phil. Mag., 39, pp. 422-443, 1895
- [29] J. Boussinesq:  
Théorie générale des mouvements, qui sont propagés dans un canal rectangulaire horizontal.  
C. R. Acad. Sci. Paris, 73, pp. 256-260, 1871
- [30] J.S. Russell:  
Report on Waves.  
Rept. Fourteenth Meeting of the British Association for the Advancement of Science; J. Murray, London, pp. 311-390, 1844.

- [31] A. Ludu:  
Unpublished manuscript, 2008
- [32] A. Hasegawa, F. Tappert:  
Transmission of stationary nonlinear optical pulses in dispersive dielectric fibers. I. Anomalous dispersion.  
Appl. Phys. Lett. vol. 23 no. 3, pp. 142–144, 1973
- [33] Heiko Seeger:  
Kinetics of domain formation processes in lipid membranes.  
available from [www.mwmembranes.nbi.dk](http://www.mwmembranes.nbi.dk), Ph.D. Thesis Georg-August-University Göttingen 2006
- [34] R.S. Cantor:  
The lateral pressure profile in membranes: A physical mechanism of general anesthesia.  
Biochemistry vol. 36 no. 9, pp. 2339–2344, 1997
- [35] M. Nielsen, L. Miao, J.H. Ipsen, O.G. Mouritsen, M.J Zuckermann:  
Random-lattice models and simulation algorithms for the phase equilibria in two-dimensional condensed systems of particles with coupled internal and translational degrees of freedom.  
Physical Review E vol. 54 no. 9 pp. 6889–6905, 1996
- [36] S. Doniach:  
Thermodynamic fluctuations in phospholipid bilayers.  
J. Chem. Phys. 68, pp. 4912–4916, 1978
- [37] T. Hata, T. Sakamoto, H. Matsuki, S. Kaneshina:  
Partition coefficients of charged and uncharged local anesthetics into di-palmitoylphosphatidylcholine bilayer membrane: estimation from pH dependence on the depression of phase transition temperatures.  
Colloids and Surfaces B: Biointerfaces 22 pp. 77-84, 2000
- [38] N. Metropolis, A.W. Rosenbluth, M.N. Rosenbluth, A.H. Teller:  
Equation of State Calculations by Fast Computing Machines.  
Jour. of Chem. Phys. vol. 21 no. 6, pp. 1087- 1092, 1953
- [39] R.J. Glauber:  
Time-Dependent Statistics of the Ising Model.  
Jour. Math. Phys. vol. 4 no. 2, pp. 294–307, 1963
- [40] I.P. Sugár, R.L. Biltonen, N. Mitchard:  
Monte Carlo simulations of membranes: phase transition of small unilamellar dipalmitoylphosphatidylcholine vesicles.  
Methods in Enzymology vol. 240, pp. 569–593, 1994
- [41] L. Onsager:  
Crystal Statistics. I. A Two-Dimensional Model with an Order-Disorder

- Transition.  
Phys. Rev. 65 no. 3-4, pp. 117-149, 1944
- [42] L.L. Firestone, J.C. Miller, K.W. Miller:  
Tables of physical and pharmacological properties of anesthetics.  
Molecular and cellular mechanisms of anesthetics, Plenum, 1986
- [43] J. Tomin, J. Živanov-Čurlis, D. Popović, S. Glogovac, D. Bašić:  
Differences in local anesthetic effects of optically active isomers of local  
anesthetic compounds.  
Biotechnol. and Biotechnol. Eq. 20 no. 3, pp. 9–14, 2006
- [44] S. Fiala, M.B. Brown, S. Jones:  
An investigation into the influence of binary drug solutions upon diffusion  
and partition processes in model membranes.  
Jour. Pharmacy and Pharmacology vol. 60 no. 12, pp. 1615–1623, 2008
- [45] A. Broughton, A.O. Grant, C.F. Starmer, J.K. Klinger, B.S. Stambler, H.C. Strauss:  
Lipid solubility modulates pH potentiation of local anesthetic block of  
Vmax reactivation in guinea pig myocardium.  
Circulation Research, vol. 55, pp. 513–523, 1984
- [46] L. Gaohua, H. Kimura:  
Simulation of propofol anaesthesia for intracranial decompression using  
brain hypothermia treatment.  
Theoretical Biology and Medical Modelling 4:46, 2007
- [47] A. Blicher:  
Permeability studies of lipid vesicles by Fluorescence Correlation Spec-  
troscopy and Monte Carlo simulations.  
Master Thesis, available from [www.membranes.nbi.dk](http://www.membranes.nbi.dk), August 2007.
- [48] A.H. Wilson:  
Thermodynamics and Statistical Mechanics.  
Cambridge University Press, Cambridge, 1957
- [49] L.K. Nielsen, T. Bjørnholm, O.G. Mouritsen:  
Critical phenomena: Fluctuations caught in the act.  
Nature 404:352, 2000
- [50] J.K. Alifimoff, L.L. Firestone, K.W. Miller:  
Anaesthetic potencies of primary alkanols: implications for the molecular  
dimensions of the anaesthetic site.  
Br. J. Pharmacol. 96, pp. 9-16, 1989
- [51] S.M. Todorovic, C.J. Lingle:  
Pharmacological Properties of T-Type  $\text{Ca}^{2+}$  Current in Adult Rat Sensory  
Neurons: Effects of Anticonvulsant and Anesthetic Agents.  
J Neurophysiol 79, pp. 240-252, 1998

- [52] S. Sakura, A.W. Bollen, R. Ciriales, K. Drasner:  
Local Anesthetic Neurotoxicity Does Not Result from Blockade of Voltage-Gated Sodium Channels.  
*Anesth. Analg.* 81, 338–346, 1995
- [53] Y.A. Kolesnikov, I. Chereshnev, G.W. Pasternak:  
Analgesic Synergy between Topical Lidocaine and Topical Opioids.  
*Jour. Pharmacology And Exp. Therapeutics*, Vol. 295, No. 2, pp. 546551, 2000
- [54] B. Antkowiak:  
Different Actions of General Anesthetics on the Firing Patterns of Neocortical Neurons Mediated by the GABA<sub>A</sub> Receptor.  
*Anesthesiology* 91, pp. 500–511, 1999
- [55] P.H. Tonner, J. Scholz, L. Lamberz, N. Schlamp, J. Schulte Esch:  
Inhibition of Nitric Oxide Synthase Decreases Anesthetic Requirements of Intravenous Anesthetics in Xenopus laevis.  
*Anesthesiology*, Vol. 87(6), pp. 1479-1485, 1997
- [56] R.A. Sjodin, L.J. Mullins:  
Oscillatory behavior of the squid axon membrane potential.  
*J. Gen. Physiol.* vol. 42 no. 1, pp. 39–47, 1958
- [57] Z. Derzko, K. Jacobsen:  
Comparative Lateral Diffusion of Fluorescent Lipid Analogues in Phospholipid Multibilayers.  
*Biochemistry* 19 (26),pp. 6050-6057, 1980
- [58] M.K. Jain, J.L.V. Wray:  
Partition coefficients of alkanols in lipid bilayer/water.  
*Biochem. Pharmacol.* 275, pp. 12941295, 1978

## **Appendix A**

## **Appendix**

## A.1 Compressibility

For the phase transition many properties like  $c_P$ ,  $V$ ,  $A$ , and  $\kappa$  can be divided into a part stemming from just the heating of the membrane and a part for the actual phase transition - that is going from the solid ordered to the fluid disordered state. The following derivation concerns only the second part of these properties - the excess stemming from the phase transition.

In order to calculate the compressibility three relations are stated:

For heat capacity:

$$c_P = \frac{d\langle H \rangle}{dT} \Big|_P = \frac{\langle H^2 \rangle - \langle H \rangle^2}{RT^2} \quad (\text{A.1.1})$$

The area compressibility:

$$\kappa_T^V = -\frac{1}{\langle V \rangle} \frac{d\langle V \rangle}{dp} \Big|_T = \frac{\langle V^2 \rangle - \langle V \rangle^2}{V RT^2} \quad (\text{A.1.2})$$

The area compressibility:

$$\kappa_T^A = -\frac{1}{\langle A \rangle} \frac{d\langle A \rangle}{dp_A} \Big|_T = \frac{\langle A^2 \rangle - \langle A \rangle^2}{A RT^2} \quad (\text{A.1.3})$$

These relations have all been calculated by substituting them for  $X$  in the following classic statistical equation:

$$\langle X \rangle = \frac{1}{Z} \sum_i X_i \Omega_i \exp\left(\frac{H_i}{RT}\right) \quad (\text{A.1.4})$$

With  $Z$  being the Guggenheim partition function:

$$Z = \sum_i \Omega_i \exp\left(\frac{X_i}{RT}\right) \quad (\text{A.1.5})$$

By using Maxwell's equations [48]. The isentropic volume compressibility can be expressed:

$$\kappa_S^V = \kappa_T^V - \frac{T}{\langle V \rangle c_P(\omega)} \left( \frac{dV}{dT} \right)^2 \Big|_P \quad (\text{A.1.6})$$

where  $c_P(\omega)$  is the frequency dependent heat capacity. It can then be deduced that the isentropic area compressibility are given as:

$$\kappa_S^A = \kappa_T^A - \frac{T}{\langle A \rangle c_P(\omega)} \left( \frac{dA}{dT} \right)^2 \Big|_{P_A} \quad (\text{A.1.7})$$

From experiments [25] it was determined that:

$$V = \gamma_V H \quad (\text{A.1.8})$$

and assuming this goes for any substate  $V_i = \gamma_V H_i$ , gives by again using equations (A.1.4) and (A.1.5):

$$\kappa_T^V = \frac{\gamma_V^2 T}{V} c_P \quad (\text{A.1.9})$$

Which is then assumed to be valid for area as well:

$$\kappa_T^A = \frac{\gamma_A^2 T}{A} c_P \quad (\text{A.1.10})$$

Hence the compressibility can be expressed by means of experimentally retrievable quantities - Eq. (2.3.5).

## A.2 Spectrophotometry

The procedure for achieving a correlation between absorbance and anesthetics concentration using the Perkin-Elmer Lambda 5 UV/VIS Photospectrometer:

1. Prepare a suitable amount of solutions of varying anesthetics concentrations in buffer.
2. Turn on the Spectrometer and follow calibration procedure from manual.
3. Use buffer as reference and insert the highest concentration anesthetic as sample. Then scan over all wavelengths.
4. From the full scan select the wavelength with the highest absorbance to ensure maximum signal.
5. At the selected wavelength measure the absorbance of anesthetics at different concentrations. Make sure to use the same crystal container and facing it the same way in the apparatus for every measurement.

The data from above mentioned procedure should give the concentration of anesthetics in the solution,  $c_{AS}$ , as a function<sup>1</sup> of absorbance,  $A$ .

$$c_{AS} = f(A) \quad (\text{A.2.1})$$

Then the partition coefficient,  $P$ , is derived given that it is defined by the concentration of anesthetics in the membrane,  $c_{AM}$ , and concentration of anesthetic in the solution,  $c_{AS}$ :

$$\begin{aligned} P &= \frac{c_{AM}}{c_{AS}} && \text{definition} \\ &= \frac{1}{f(A)} \frac{n_{AM}}{V_M} && \text{A.2.1} \\ &= \frac{1}{f(A)} \frac{\rho_M (n_A - n_{AS})}{m_M} && n_A = n_{AM} + n_{AS} \\ &= \frac{(c_A - f(A)) \rho_M V}{f(A) m_M} \end{aligned}$$

Where  $V$  is the total volume, and  $n_A$ ,  $c_A$  the initial molar amount and molar concentration of anesthetic in the sample, and with subscript  $AM$ ,  $AS$  it is referring to anesthetics in the membrane or the solution.  $\rho_M$ ,  $m_M$  is referring to the density and the mass of membrane i.e. the DPPC. In the calculation it is approximated that the volume of the entire sample is the same as the liquid solution, since the density of the membrane is near water this approximation gives an error of less than one percent with a solution of 10 mM DPPC.

---

<sup>1</sup>This function should theoretically be given by the Beer-Lambert Law, but it is not necessary to know  $f$  specifically. A fit of data points is sufficient.

### A.3 Pressurized anesthetics

Results summarized in Table (4.2)

#### A.3.1 Bupivacaine

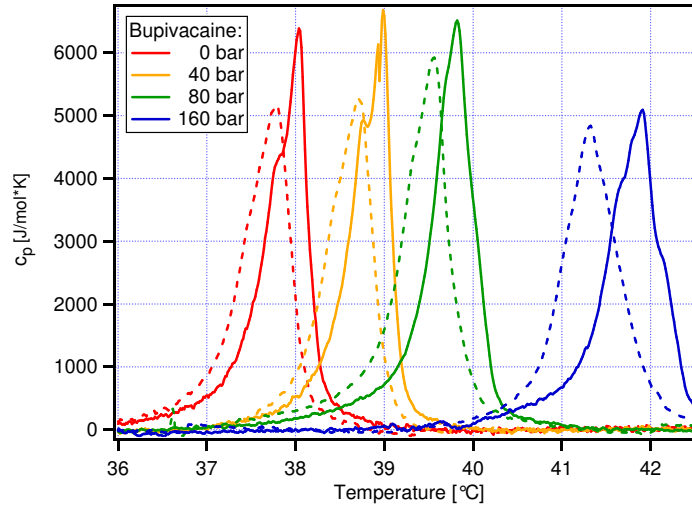


Figure A.1: Heat capacity profiles of Bupivacaine with added pressure. Solid lines are up-scans, dotted lines are down-scans.

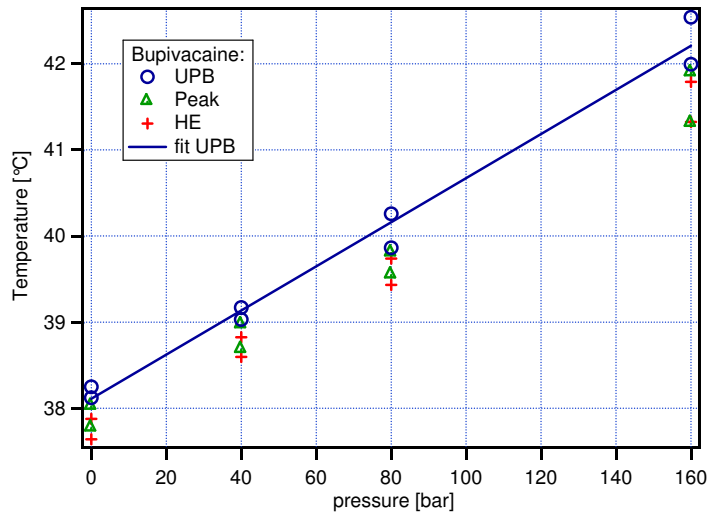


Figure A.2: Melting temperatures for Bupivacaine as function of pressure. Abbreviations are explained on page 58.

### A.3.2 Lidocaine

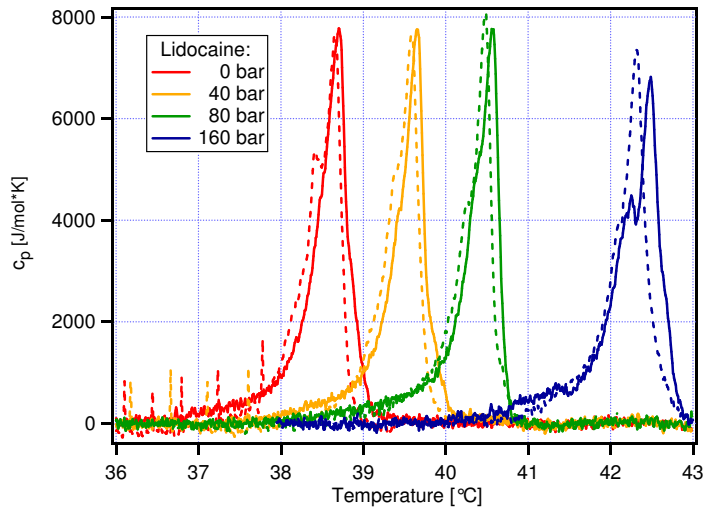


Figure A.3: Heat capacity profiles of Lidocaine with added pressure. Solid lines are up-scans, dotted lines are down-scans.

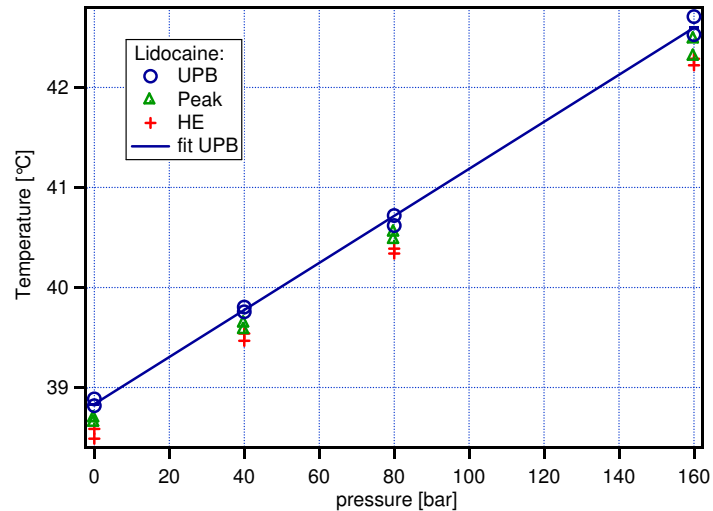


Figure A.4: Melting temperatures for Lidocaine as function of pressure. Abbreviations are explained on page 58.

### A.3.3 Pentobarbital

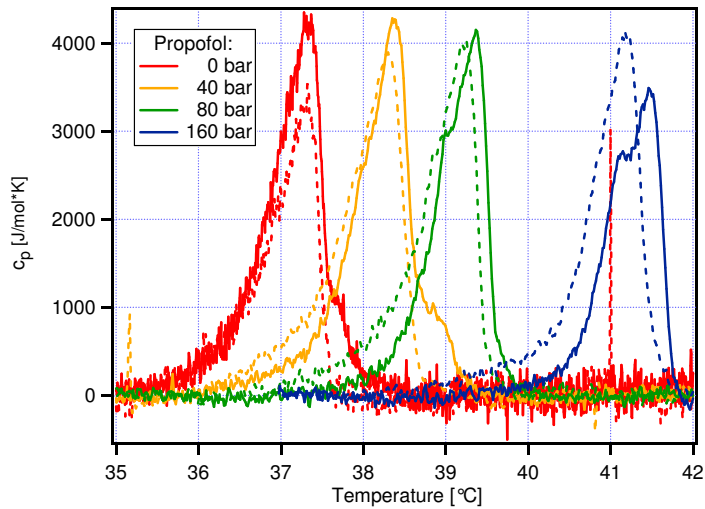


Figure A.5: Heat capacity profiles of Pentobarbital with added pressure. Solid lines are up-scans, dotted lines are down-scans.

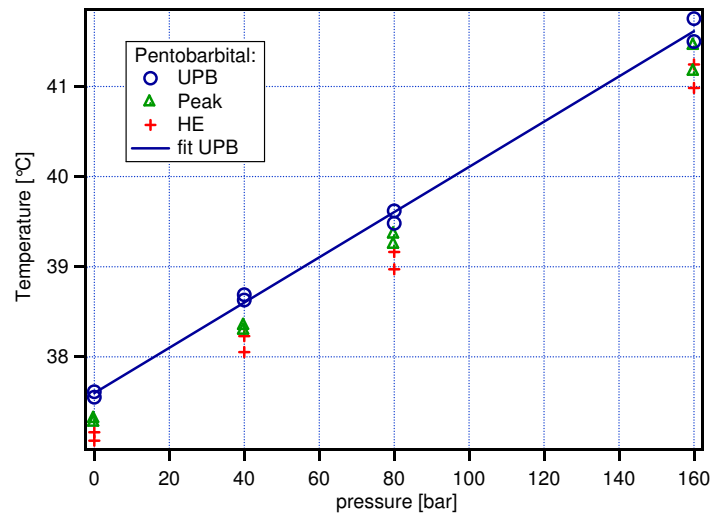


Figure A.6: Melting temperatures for Pentobarbital as function of pressure. Abbreviations are explained on page 58.

## A.4 Symmetry of simulated phase transitions

The symmetry of the solid grid deviates only slightly given that the relative probability of changing states around the melting point are:

$$\begin{aligned}
 \frac{P_{f \rightarrow g}(T_m + \Delta T)}{P_{g \rightarrow f}(T_m - \Delta T)} &= \frac{\exp\left(\frac{\Delta G(T_m + \Delta T)}{R(T_m + \Delta T)}\right)}{\exp\left(-\frac{\Delta G(T_m - \Delta T)}{R(T_m - \Delta T)}\right)} \\
 &\approx \frac{\exp\left(\frac{\Delta H - \Delta S(T_m + \Delta T)}{R(T_m + \Delta T)}\right)}{\exp\left(-\frac{\Delta H - \Delta S(T_m - \Delta T)}{R(T_m - \Delta T)}\right)} \\
 &= \exp\left(\frac{-\Delta S \Delta T}{R(T_m + \Delta T)} + \frac{\Delta S \Delta T}{R(T_m - \Delta T)}\right) \\
 &= \exp\left(\frac{2\Delta S(\Delta T)^2}{R(T_m^2 - (\Delta T)^2)}\right)
 \end{aligned}$$

This gives a deviation from symmetry of 0.03% for  $\Delta T = 1K$  and 3% for  $\Delta T = 10K$ . The approximation from step one to two is that  $\Delta N(T_m - \Delta T) \approx \Delta N(T_m + \Delta T)$  and that  $\Delta N \ll \Delta S T$ . The first approximation is selfevident in that the transition is nearly symmetric, the second approximation is true as long as  $T$  is close to or far from  $T_m$  where  $\Delta N = 0$  as argued in Sec. (2.4.2).

## A.5 Solitons of anesthetics

### A.5.1 Lidocaine

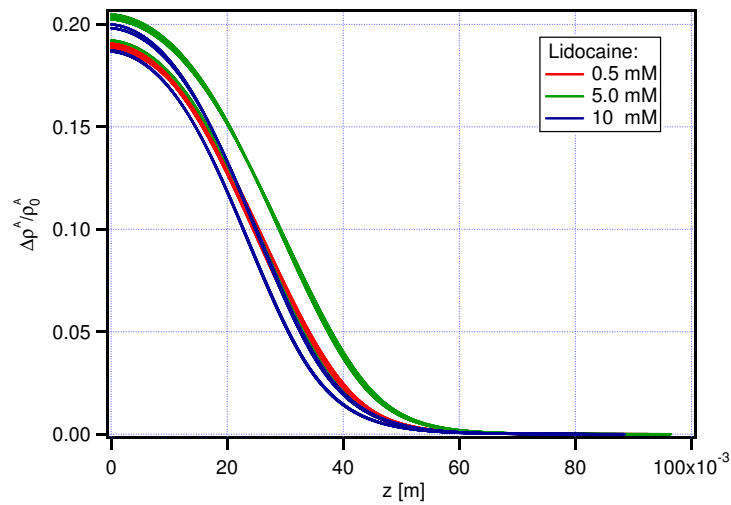


Figure A.7: Solitons from DPPC with Lidocaine.

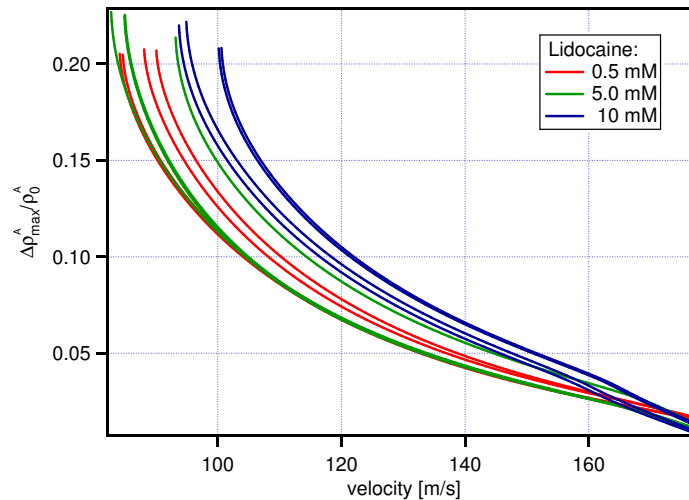


Figure A.8: Lidocaine: Compression of solitons as functions of soliton velocity.

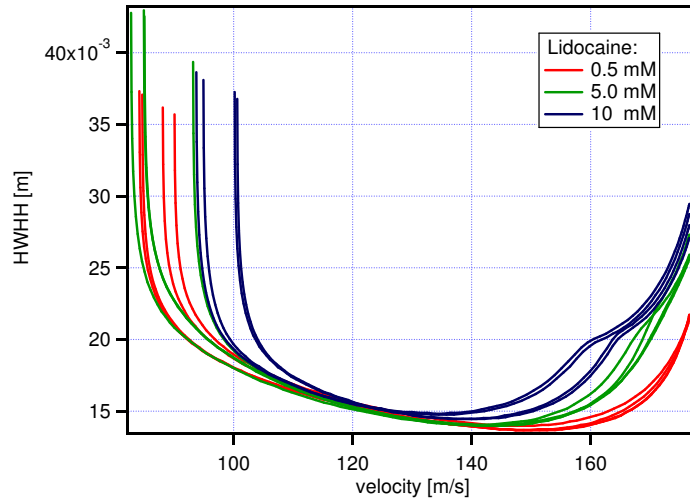


Figure A.9: Lidocaine: Half Width at Half Height of solitons as function of soliton velocity.

### A.5.2 Bupivacaine

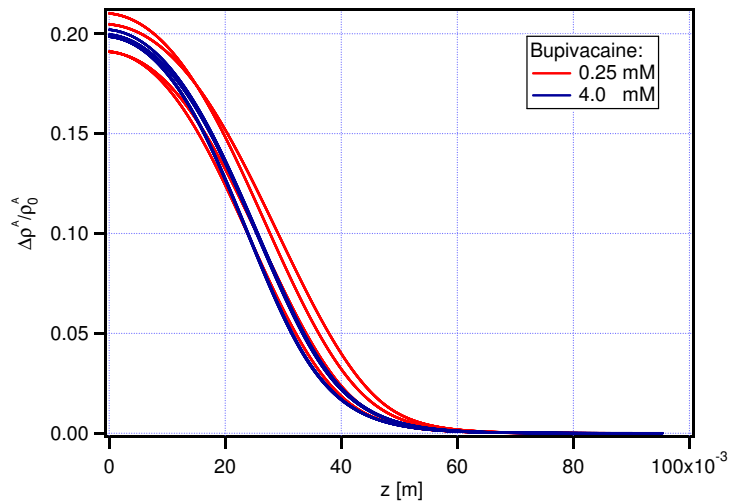


Figure A.10: Solitons from DPPC with bupivacaine.

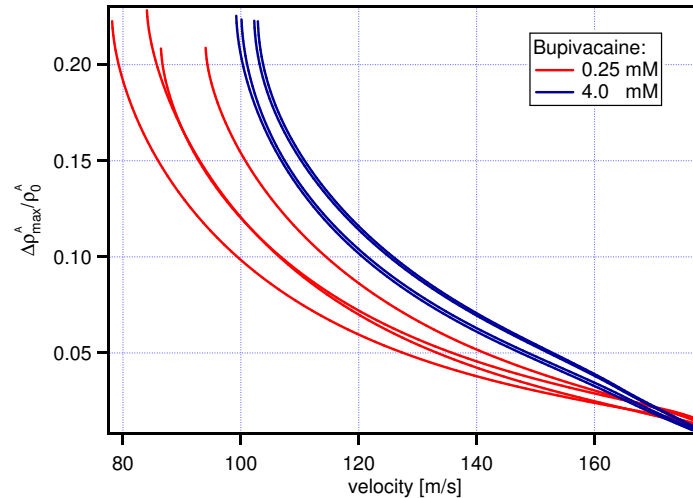


Figure A.11: Bupivacaine: Compression of solitons as functions of soliton velocity.

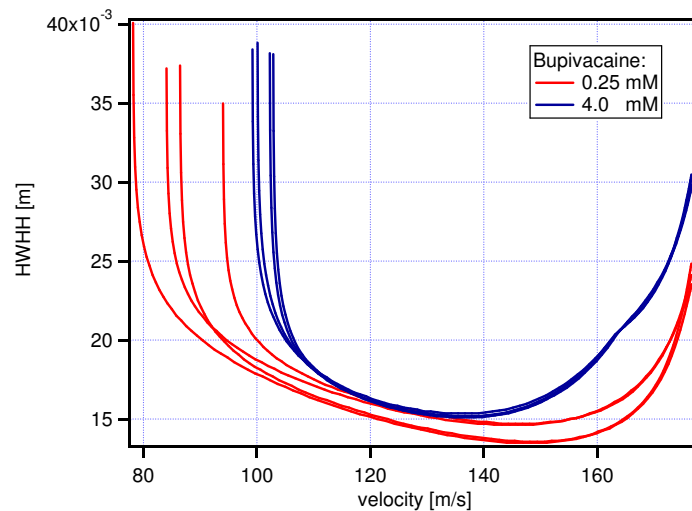


Figure A.12: Bupivacaine: Half Width at Half Height of solitons as function of soliton velocity.

### A.5.3 Propofol

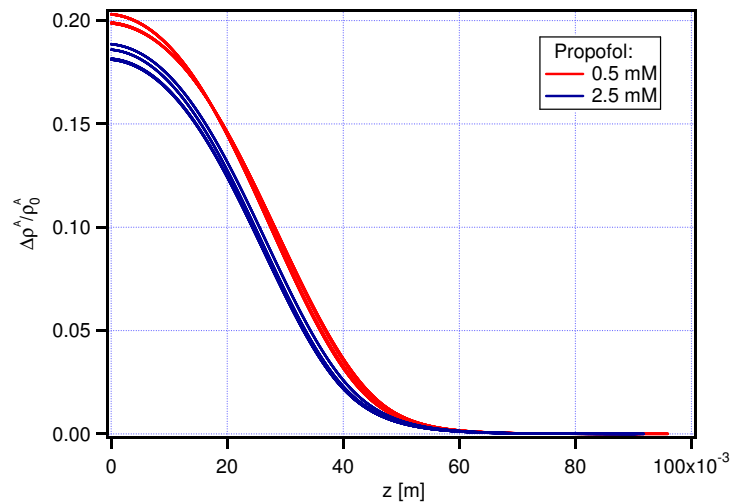


Figure A.13: Solitons from DPPC with propofol.

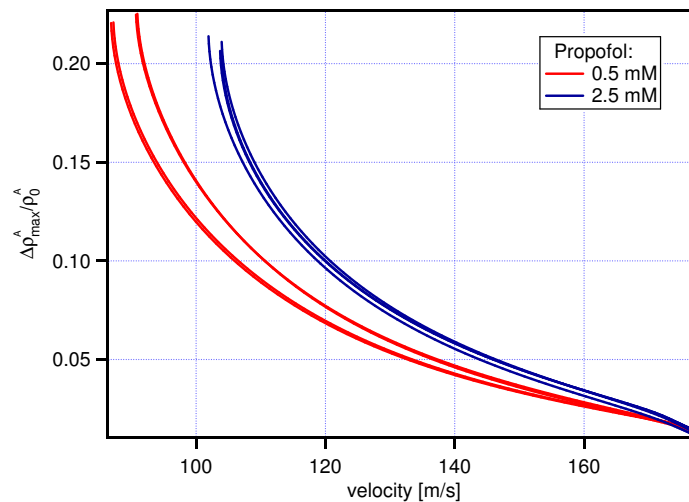


Figure A.14: Propofol: Compression of solitons as functions of soliton velocity.

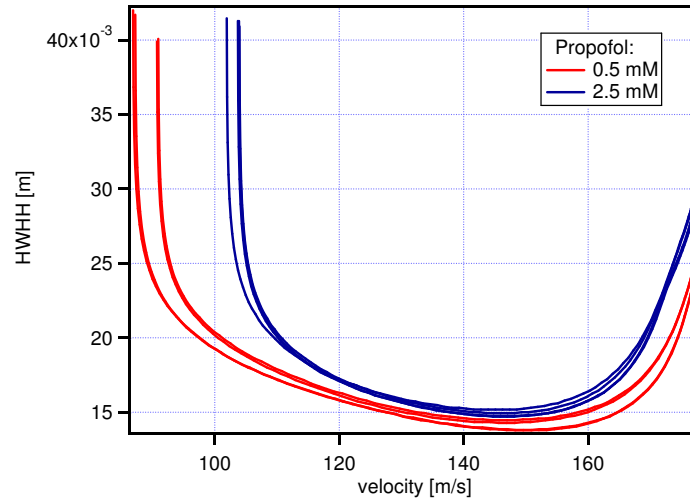


Figure A.15: Propofol: Half Width at Half Height of solitons as function of soliton velocity.

#### A.5.4 Pentobarbital

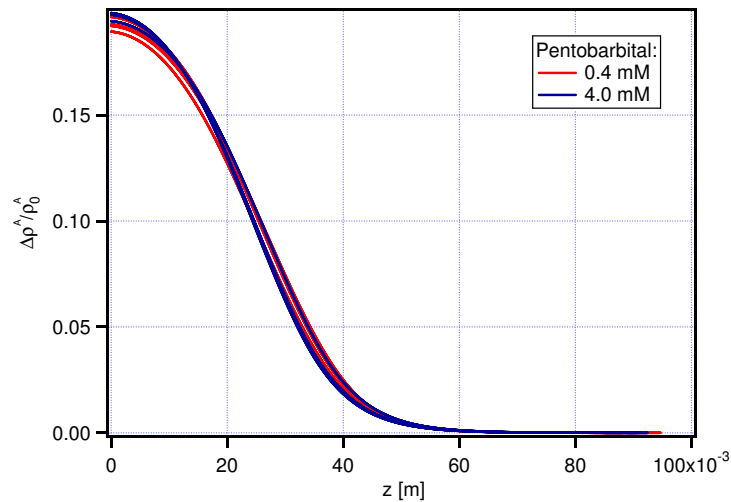


Figure A.16: Solitons from DPPC with pentobarbital

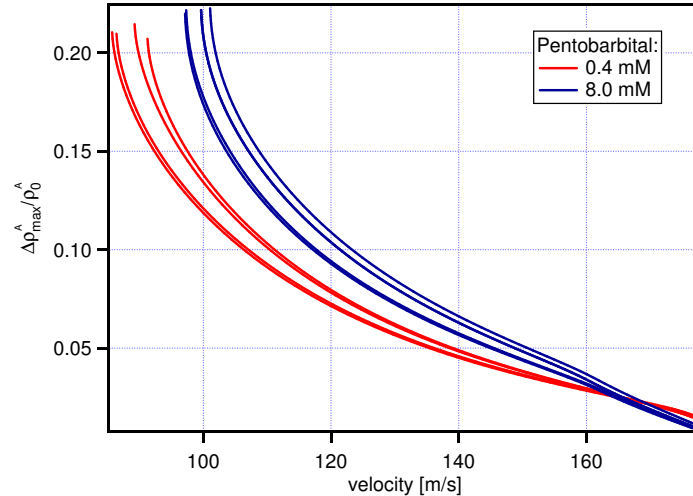


Figure A.17: Pentobarbital: Compression of solitons as functions of soliton velocity.

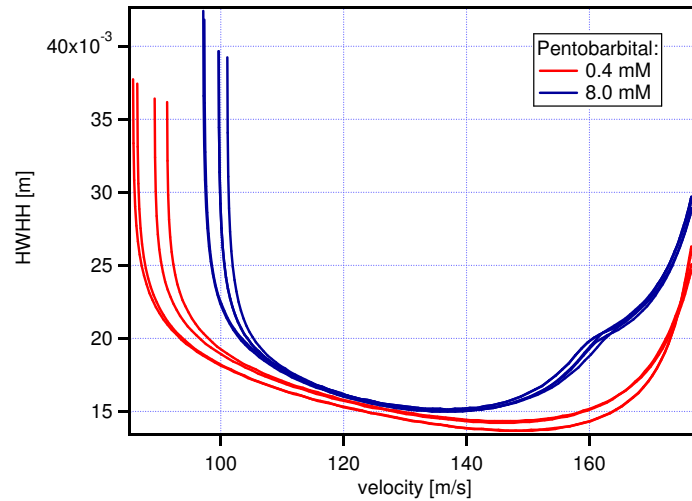


Figure A.18: Pentobarbital: Half Width at Half Height of solitons as function of soliton velocity.

# The End

*This is the end  
The only end, my friend.*

- In no way like the song made famous by 'The Doors'.